Utrecht University
Faculty of Geosciences
Department of Physical Geography

Arya Pamungkas Iwantoro – Morphodynamics of channel networks in tide-influenced deltas

USES 264

ISSN 2211-4335

Morphodynamics of channel networks in tide-influenced deltas

Arya Pamungkas Iwantoro

264 UTRECHT STUDIES IN EARTH SCIENCES

Morphodynamics of channel networks in tide-influenced deltas

Morfodynamiek van riviernetwerken in getij-gedomineerde delta's

(met een samenvatting in het Nederlands)

P R O E F S C H R I F T

ter verkrijging van de graad van doctor aan de Universiteit Utrecht
op gezag van de rector magnificus, prof. dr. H.R.B.M. Kummeling,
ingevolge het besluit van het college voor promoties in het openbaar te verdedigen op

maandag 7 november 2022 des middags te 12.15 uur

door

Arya Pamungkas Iwantoro
geboren op 28 Maart 1991 te Djakarta, Indonesië

Promotor:
Prof. dr. M.G. Kleinhans

Copromotor:
Dr. M. van der Vegt

Dit proefschrift werd mogelijk gemaakt met financiële steun van Indonesia Endowment Fund for Education (LPDP) nummer 20161222029838.

Morphodynamics of channel networks in tide-influenced deltas

Promotor:
Prof. dr. M.G. Kleinhans

Copromotor:
Dr. M. van der Vegt

Examination committee:
Prof. dr. ir. Z.B. Wang
Technische Universiteit Delft, The Netherlands

Prof. dr.eng. N.S. Ningsih
Institut Teknologi bandung, Indonesia

Dr.Ing. M. Bolla Pittaluga
Universitá di Genova, Italy

Prof. dr. ir. A.J.F. Hoitink
Wageningen University & Research, The Netherlands

Prof. dr. H.E. de Swart
Universiteit Utrecht, The Netherlands

ISBN 978-90-6266-633-1

DOI https://doi.org/10.33540/1537

Published by Faculty of Geosciences, Universiteit Utrecht, The Netherlands, in:
Utrecht Studies in Earth Sciences (USES 264), ISSN 2211-4335

Typeset using XeLaTeX

Cover: Mahakam River Delta, Kalimantan, Indonesia. Re-painted satellite image by Nadhila Codhel.

Printed by Ipskamp Printing, Enschede, The Netherlands

Correspondence to: Arya Pamungkas Iwantoro, aryaiwantoro@gmail.com

Utrecht Studies in Earth Sciences 258

Morphodynamics of channel networks in tide-influenced deltas

Arya Pamungkas Iwantoro

Utrecht 2022

Faculty of Geosciences, Utrecht University

Contents

Summary

River deltas and estuaries are transition zones where rivers debouch into the sea. Land, river and sea meet in these zones, making them very valuable, both economically and ecologically. Their morphodynamic development is modified by an interplay between external—river and sea—forcing and anthropogenic activities in the area. These processes could affect economic activity and the natural habitat in the delta. Understanding the morphodynamics of river deltas is therefore very important for delta management plans.

River deltas are formed by depositional processes driven by the interaction between upstream river forcing and downstream sea forcing. This interaction results in unique patterns based on the forcing's relative importance. Tide-influenced river deltas have a typical distributary-channel landscape with the number of channels increasing downstream. Here, the depositional processes are largely driven by the interaction between river flow conveyed from upstream and tides that come in from the sea along the channels. Most channel junctions in such systems are bifurcations: upstream channels that split into two downstream channels. The sediment distribution at bifurcations determines the sediment flux throughout the entire delta and hence the morphological development of the delta itself. Therefore to understand the morphodynamic development of the delta and its distributary channels, we need to understand the morphodynamics of bifurcations that connect the distributaries.

Unlike river-dominated deltas, tide-influenced deltas have a tidally modulated river flow that not only changes in magnitude but can also change in direction. This flow modulation can differ in different deltas, depending on the relative dominance of river discharge over tidal flow. The resulting sediment transport patterns are spatially and temporally complex and so are the morphodynamics. In addition, the morphodynamics of tide-influenced bifurcation are less well understood than those of river-dominated bifurcation. This thesis therefore aims to improve our understanding of the morphodynamics of tide-influenced bifurcations in river deltas.

To achieve this objective, a one-dimensional (1D) numerical model was developed to simulate morphodynamics in tide-influenced channel networks under a wide range of conditions. In this model, a novel approach was proposed to solve the sediment distribution at bifurcations under the changing flow conditions in tide-influenced deltas. To confirm the findings of the new 1D model I compared them with a well-established Delft3D model. With the help of these models, I systematically studied the critical factors in nature that influence the morphodynamics of bifurcations in tide-influenced deltas. The results are presented in Chapter 2 through 5 of this thesis, which are summarized in the next four paragraphs.

chapter 2 describes how I used the 1D model to study the effect of channel slopes and sediment grain size on the morphodynamics of river-dominated bifurcations in which only river discharge is imposed from upstream, while the downstream channels' sea boundary condition is a constant water level. I investigated how channel slopes and sediment grain size affect the morphological stability of river-dominated bifurcations. This study shows that besides larger width-to-depth ratio, as previous studies have suggested, finer sediment and lower channel slopes, which are typical of tide-influenced deltas, also result in a larger range of sediment mobility for asymmetric bifurcations and in downstream channel abandonment (avulsion). I conclude, therefore, that, without taking tidal influence into account, the typical landscape features in tide-influenced deltas are more likely to induce channel abandonment than in river-dominated channel networks.

chapter 3 describes how I applied a 2D model (Delft3D-flow) to study the asymmetry of tide-influenced bifurcations. I analysed the equilibrium asymmetry between downstream channels

for bifurcations with imposed asymmetric downstream channel geometries (depth or length) or asymmetric tidal conditions (tidal amplitude or phase difference). The forcing imposed on the bifurcations were river discharge from the upstream channel and tides from the sea boundary of the two downstream channels. I investigated the influence of tides on the asymmetry in the system by running a series of simulations with different river discharges and tidal properties. I found that a system with a larger tidal influence shows a less asymmetric bifurcation.

chapter 4 describes how the 1D model was applied to study the effect of tides on the morphological stability of tide-influenced bifurcations. I investigated the effect of tides on bifurcations for a wide range of natural conditions with varying sediment mobilities, tidal influences, and width-to-depth ratios. This study expanded the conditions investigated in chapter 3. A complex image of bifurcation morphodynamics emerged. For bifurcations with minor tidal influence, i.e. with low to no flood flows, increasing tidal influence results in a wider range of conditions where symmetric bifurcations are stable. However, in tide-dominated bifurcations with large flood flows, increasing tidal influence results in a more limited range of conditions where symmetric bifurcations stay stable. Despite this difference, for all tidal influences, the consistent pattern occurs. In conditions where symmetric bifurcations are unstable, greater tidal influence causes a less pronounced depth asymmetry between the two downstream channels. This confirms the findings in chapter 3. Therefore, compared to river-dominated bifurcations, tides reduce the avulsion tendency of downstream channels, either by reducing the conditions for asymmetric bifurcation or by reducing the asymmetry between downstream channels.

chapter 5 describes how the 1D model was applied to investigate the morphodynamic stability of deltaic channel networks with multiple bifurcations. This channel network setting was inspired by the Mahakam Delta, where the number of bifurcations and channels increases downstream. I studied the morphodynamic stability of the delta by exploring several distributary settings with increasing numbers of channels and bifurcations. This study shows that the morphological equilibrium of all channels with initially uniform depth is insensitive to the number of channels and bifurcations in the delta, as long as the summed width of all the channels stays the same and assuming negligible bank friction. However, an imposed depth asymmetry at a downstream bifurcation can induce asymmetry of the bifurcation apex and so reshape the morphological equilibrium of the entire delta. Compared to symmetric delta networks, this asymmetric depth will also increase the total cross-sectional area and therefore the tidal prism. I found that the morphological equilibrium of delta network systems strongly depends on their initial conditions, i.e. their history. The more channels there are in a delta, the more possible final equilibria. This is because perturbations in different channels can lead to different equilibria in the network.

Lastly, chapter 6 focuses on the main findings of this thesis in the context of the literature on this topic. The findings of this thesis provide insight into the key mechanisms underlying channel morphology in tide-influenced bifurcations. This chapter also includes ideas for follow-up studies, such as exploration of other factors that affect the morphological development of bifurcations in tide-influenced deltas. Four areas of research that deserve further exploration are: better representation of the complex natural flow structures and sediment transport processes; riverbank and tidal flat dynamics; the effects of climate change reflected in the boundary conditions; and anthropogenic interference in river deltas.

Samenvatting

Rivierdelta's en estuaria zijn overgangsgebieden waar rivieren uitmonden in zee. Land, rivier en zee ontmoeten elkaar in deze zones, waardoor zij zowel economisch als ecologisch zeer waardevol zijn. Hun morfodynamische ontwikkeling wordt bepaald door een samenspel van externe rivier- en oceaankrachten en antropogene activiteiten in het gebied. Deze processen kunnen de economische activiteit en de natuurlijke habitat in de delta beïnvloeden. Inzicht in de morfodynamiek van rivierdelta's is daarom van groot belang voor beheersplannen voor delta's.

Rivierdelta's worden gevormd door sedimentatieprocessen die worden aangedreven door de interactie tussen rivierforcering stroomopwaarts en golven en getij stroomafwaarts. Deze interactie leidt tot unieke patronen op basis van het relatieve belang van de forcering. Rivierdelta's onder invloed van getijden hebben een typisch vertakt geulenlandschap, waarbij het aantal riviertakken stroomafwaarts toeneemt. Hier worden de sedimentatieprocessen grotendeels gestuurd door de interactie tussen de rivierstroom van bovenaf en de getijden die via de riviertakken vanuit zee binnenkomen. De meeste geulsplitsingen in dergelijke systemen zijn bifurcaties: stroomopwaartse riviertakken die zich splitsen in twee stroomafwaartse takken. De sedimentverdeling bij bifurcaties bepaalt de sedimentstroom in de gehele delta en daarmee de morfologische ontwikkeling van de delta zelf. Om de morfodynamische ontwikkeling van de delta en haar verschillende riviertakken te begrijpen, moeten we de morfodynamiek begrijpen van de bifurcaties die de riviertakken met elkaar verbinden.

In tegenstelling tot rivier-gedomineerde delta's hebben door getijden beïnvloede delta's een door getijden gemoduleerd rivierdebiet dat niet alleen in grootte maar ook in richting kan veranderen. Deze modulatie van het debiet kan per delta verschillen, afhankelijk van de relatieve dominantie van de rivierafvoer ten opzichte van het getijdendebiet. De resulterende sedimenttransportpatronen zijn ruimtelijk en temporeel complex en dat geldt ook voor de morfodynamiek. Bovendien wordt de morfodynamiek van een door getijden beïnvloede bifurcatie minder goed begrepen dan die van door rivieren gedomineerde bifurcatie. Dit proefschrift heeft daarom tot doel ons begrip van de morfodynamiek van door getijden beïnvloede bifurcaties in rivierdelta's te verbeteren.

Om dit doel te bereiken is een eendimensionaal (1D) numeriek model ontwikkeld om de morfodynamiek van door getijden beïnvloede riviertakken te simuleren. In dit model werd een nieuwe methode toegepast om de sedimentverdeling op bifurcaties te bepalen, voor zowel rivier-gedomineerde als getij-gedomineerde omstandigheden. Om de bevindingen van het nieuwe 1D-model te bevestigen heb ik ze vergeleken met een de resultaten van een Delft3D-model. Met behulp van deze modellen heb ik systematisch de factoren bestudeerd die de morfodynamiek van bifurcaties in door getijden beïnvloede delta's bepalen. De resultaten worden gepresenteerd in hoofdstuk 2 tot en met 5 van dit proefschrift, die in de volgende vier paragrafen worden samengevat.

Hoofdstuk 2 beschrijft hoe ik het 1D-model heb gebruikt om het effect te bestuderen van steilheid van de rivierbodem en sedimentkorrelgrootte op de morfodynamiek van bifurcaties die alleen door rivierafvoer van bovenaf worden geforceerd. Deze studie toont aan dat fijner sediment en kleinere bodemhellingen, die typisch zijn voor door getijden beïnvloede delta's, resulteren in een groter bereik van sedimentmobiliteit waarvoor de bifurcatie asymmetrisch wordt en zelfs kan resulteren in het dichtslibben van één van de riviertakken (avulsie). Ik concludeer daarom dat, zonder rekening te houden met de invloed van het getij, de typische landschapskenmerken in door het getij beïnvloede delta's eerder leiden tot avulsie dan in rivier-gedomineerde delta's.

Hoofdstuk 3 beschrijft hoe ik een 2D-model (Delft3D-flow) heb toegepast om de asymmetrie van door getijden beïnvloede delta's te bestuderen. De geometrie bestond uit een bovenstroomse riviertak die bij de bifurcatie splitste in twee benedenstroomse takken. De forcering bestond uit rivierafvoer vanaf bovenstrooms en voorgeschreven waterstanden met getij vanaf benedenstrooms. De simulaties begonnen met een opgelegde asymmetrie in geometrie (diepte of lengte van de twee benedenstroomse takken) of in getij (getijamplitude of faseverschil) en de simulaties werden voortgezet totdat er een morfodynamisch evenwicht was gevonden. Ik analyseerde de asymmetrie in bodemligging tussen de twee benedenstroomse riviertakken en onderzocht de invloed van getijden op de asymmetrie in bodemligging door een reeks simulaties uit te voeren met verschillende rivierafvoeren en getijdeneigenschappen. Ik vond dat een systeem met een grotere getijdeninvloed minder asymmetrische bifurcaties vertoont.

Hoofdstuk 4 beschrijft hoe het 1D-model werd gebruikt om het effect van getijden op bifurcaties te bestuderen als functie van sedimentmobiliteit, getijdeninvloed en breedte-diepteverhouding. Deze studie breidde de in hoofdstuk 3 onderzochte omstandigheden uit en met een groot aantal nieuwe simulaties. Er ontstond een complex beeld van de morfodynamica van bifurcaties. Voor bifurcaties met weinig invloed van het getij, resulteert een toenemende invloed van het getij in een groter aantal omstandigheden waarin symmetrische bifurcaties stabiel zijn. Maar als het getij nog groter wordt en grotendeels bepaald wat stroomsnelheid en -richting is, resulteert een toenemende invloed van het getij in een beperkter scala van omstandigheden waarin symmetrische bifurcaties stabiel blijven. Echter, wanneer deze symmetrische bifurcaties onstabiel zijn, veroorzaakt een grotere invloed van het getij een minder uitgesproken diepte-asymmetrie tussen de twee stroomafwaarts gelegen riviertakken. Dit bevestigt de bevindingen in hoofdstuk 3. Vergeleken met rivier-gedomineerde bifurcaties verminderen getijden de neiging tot avulsie van benedenstroomse riviertakken, hetzij door de kansen op een symmetrische bifurcatie te vergroten, hetzij door de asymmetrie tussen benedenstroomse riviertakken te verminderen.

Hoofdstuk 5 beschrijft hoe het 1D-model werd toegepast om de morfodynamische stabiliteit van de Mahakam Delta te bestuderen. Deze delta bestaat uit een netwerk van bifurcaties en riviertakken, waar het aantal bifurcaties en takken stroomafwaarts toeneemt. Ik heb de morfologie en stabiliteit van de delta bestudeerd door de aantallen riviertakken en bifurcaties in opeenvolgede simulaties steeds verder te laten toenemen, beginnend bij een systeem zonder een bifurcatie. Deze studie toont aan dat het morfologisch evenwicht van een symmetrische delta ongevoelig is voor het aantal riviertakken en vertakkingen in de delta, zolang de totale gesommeerde breedte van alle riviertakken gelijk blijft, en de diepte nier vestoord wordt. Resultaten tonen echter ook aan dat de bifurcaties niet stabiel zijn en elke diepteverstoring tot een asymmetrische groei van de bodemligging leidt. Een opgelegde diepte-asymmetrie bij een benedenstroomse bifurcatie kan ook diepte-asymmetrie van de apex bifurcatie veroorzaken en zo het morfologisch evenwicht van de gehele delta veranderen. Bovendien resulteert de asymmetrische diepteontwikkeling in een toename van de totale doorstroomoppervlakte van de geulen in de delta en daarmee ook het getijprisma. Ik heb ontdekt dat het morfologisch evenwicht van de delta sterk afhangt van hun initiële omstandigheden, d.w.z. hun geschiedenis. Hoe meer bifurcaties en riviertakken er in een delta zijn, hoe meer mogelijke uiteindelijke evenwichten. Dit komt doordat verstoringen in verschillende takken kunnen leiden tot verschillende evenwichten in het netwerk.

Hoofdstuk 6 richt zich op de belangrijkste bevindingen van dit proefschrift en plaats dit in de context van de bestaande wetenschappelijke literatuur. De bevindingen van deze dissertatie verschaffen inzicht het effect van getij op de morfologie van door getijden beïnvloede delta's. Dit hoofdstuk bevat ook ideeën voor vervolgonderzoek naar andere factoren die de morfologische ontwikkeling van bifurcaties in door getijden beïnvloede delta's beïnvloeden. Vier aspecten die verder onderzoek verdienen zijn: betere weergave van de complexe natuurlijke stromings- en

sedimenttransportprocessen nabij bifurcaties; dynamiek van rivieroevers en intergetijdegebieden in het model incorporeren; de effecten van klimaatverandering; en antropogene verstoring van rivierdelta's.

Intisari

Delta sungai dan muara merupakan zona transisi yang mempertemukan aliran sungai dan laut. Wilayah tersebut memiliki nilai ekonomi dan ekologi yang sangat tinggi dikarenakan posisinya yang strategis, mempertemukan sungai, daratan dan lautan. Interaksi antara gaya-gaya yang dibangkitkan oleh gaya-gaya eksternal (aliran sungai dan hidrodinamika lautan) serta aktivitas manusia di wilayah tersebut mempengaruhi perubahan morfodinamika di delta sungai dan muara. Jika tidak dikelola dengan baik maka perubahan morfodinamika tersebut dapat berdampak negatif pada ekosistem dan kegiatan sosio-ekonomi di wilayah tersebut. Oleh karena itu, pemahaman mengenai perubahan morfodinamika sangatlah penting untuk perencanaan tata ruang di wilayah delta sungai dan muara.

Delta sungai terbentuk dari proses sedimentasi yang diakibatkan oleh interaksi antara gaya-gaya yang dibangkitkan oleh aliran sungai dari hulu dan gaya-gaya hidrodinamika yang berasal dari laut seperti gelombang, pasang surut dan badai. Perbedaan variasi, kuantitas serta rasio dari Interaksi antar gaya-gaya tersebut membentuk pola sedimentasi yang berbeda-beda di tiap delta sungai tergantung seberapa dominan pengaruh relatif dari tiap-tiap gaya tersebut. Delta sungai yang proses sedimentasinya didominasi oleh pengaruh gaya pasang surut yang berinteraksi dengan aliran sungai disebut *tide-influenced river delta*. *Tide-influenced river delta* identik dengan pola deposit/sedimentasi yang membentuk tipe sungai *distributary* dimana sungai utama akan bercabang-cabang dengan beberapa anak sungai yang jumlahnya bertambah ke arah hilir sebelum aliran sungai tersebut bermuara di laut. Bifurkasi, yang didefiniskan sebagai aliran sungai utama yang bercabang menjadi dua anak sungai ke arah hilir, banyak dijumpai di sistem delta sungai yang memiliki tipe *distributary*. Pada suatu sistem delta sungai, aliran sungai dari hulu yang membawa sedimen terdistribusi ke anak-anak sungai di bagian hilirnya melalui bifurkasi-bifurkasi di delta sungai tersebut. Maka distribusi sedimen pada bifurkasi juga mempengaruhi distribusi sedimen ke seluruh sistem delta dan oleh karena itu, mempengaruhi perubahan morfodinamika di sistem delta sungai tersebut. Oleh karena itu, untuk memahami perubahan morfodinamika pada suatu sistem delta sungai diperlukan pemahaman mengenai mekanisme distribusi sedimen pada suatu bifurkasi beserta perubahan morfodinamikanya.

Tidak seperti delta sungai yang proses sedimentasinya hanya didominasi oleh pengaruh arus yang berasal dari debit sungai (*river-dominated delta*), *tide-influenced river delta* memiliki arus sungai yang berubah-ubah setiap waktu, tidak hanya kecepatannya akan tetapi juga arah alirannya. Hal ini disebabkan oleh pengaruh propagasi gelombang pasang surut yang melalui anak-anak sungai di delta sungai tersebut. Dinamika pola arus ini dapat berbeda-beda di tiap delta sungai di dunia, tergantung dari perbedaan relative antara pengaruh gaya pasang surut dan debit sungai di delta sungai tersebut. Mekanisme dinamika arus sungai ini menghasilkan pola transportasi sedimen yang kompleks baik secara spasial maupun temporal, yang kemudian juga mengakibatkan terjadinya pola morfodinamika yang kompleks. Selain memiliki kompleksitas yang tinggi, pemahaman mengenai proses morfodinamika di *tide-influenced river delta* masihlah sangat terbatas jika dibandingkan dengan *river-dominated delta*. Maka penulisan disertasi ini bertujuan untuk meningkatkan pemahaman kita dalam konteks sains untuk menjelaskan fenomena dan proses morfodinamika pada bifurkasi di sistem delta sungai yang dipengaruhi pasang surut (*tide-influenced river delta*). Untuk mencapai tujuan ini, penulis mengembangkan model numerik satu dimensi (1D) yang dapat mensimulasikan morfodinamika pada sistem sungai bercabang yang kompleks dan memiliki aliran tak tunak seperti pada daerah delta sungai yang dipengaruhi gaya-gaya pasang surut. Pada penelitian ini, persamaan analitik termutakhir untuk menghitung distribusi sedimen di bifurkasi pada kondisi aliran tak tunak dikembangkan dan diaplikasikan dalam model numerik. Model yang dikembangkan pada penelitian

ini kemudian dibandingkan dan divalidasi dengan model numerik dua dimensi (2D) yang menyelesaikan seluruh perhitungan morfodinamika secara numerik (tanpa pendekatan analitik). Model 2D yang digunakan sebagai pembanding adalah model numerik yang dioperasikan dalam prangkat lunak Delft3D. Dengan menggunakan model numerik 1D ini, penulis secara sistematis mempelajari faktor-faktor alam yang terpenting dalam mempengaruhi proses morfodinamika dari bifurkasi-bifurkasi di *tide-influenced river delta*. Hasil dari penelitian ini disajikan pada Bab 2 hingga Bab 5 yang terangkum di dalam penjelasan di bawah ini.

Bab 2 berisi penelitian yang dilakukan oleh penulis untuk mempelajari efek dari kemiringan sungai dan ukuran butir sedimen terhadap proses morfodinamika sungai bercabang (bifurkasi) di sungai yang proses sedimentasinya didominasi oleh aliran debit sungai dari hulu tanpa adanya pengaruh pasang surut. Penulis melakukan penelitian untuk menjelaskan bagaimana perbedaan kemiringan sungai dan ukuran butir sedimen mempengaruhi kesetimbangan morfologi dari bifurkasi. Hasil penelitian ini menunjukkan bahwa selain sungai dengan nilai rasio antara lebar dan kedalaman sungai (*width-to-depth ratio*) yang lebih besar, seperti yang ditemukan pada-penelitian-penelitian sebelumnya, sungai dengan ukuran butir sedimen yang lebih halus dan kemiringan sungai yang lebih landai, seperti yang umumnya diamati di *tide-influenced river delta*, juga menghasilkan peluang kondisi yang lebih besar untuk menghasilkan: (1) bifurkasi yang asimetris dimana salah satu anak sungai lebih dangkal dari yang lain dan (2) penutupan salah satu anak sungai secara keseluruhan akibat sedimentasi (avulsi sungai). Maka dengan mengabaikan gaya pasang surut, tipikal konfigurasi dan ukuran butir sedimen di *tide-influenced delta* menghasilkan peluang yang lebih besar pada sebuah bifurkasi untuk terjadinya penutupan salah satu anak sungai secara keseluruhan akibat sedimentasi.

Pada Bab 3 penulis melakukan penelitian dengan mengaplikasikan model 2D pada perangkat lunak Delft3D untuk mempelajari proses evolusi dari ketidaksimetrisan batimetri dari sebuah bifurkasi di daerah pasang surut. Penelitian ini dilakukan dengan menganilisis derajat ketidaksimetrisan dari morfologi kedua anak sungai pada bifurkasi yang dipengaruhi oleh gaya pasang surut pada kondisi morfologi yang setimbang. Analisis dilakukan dengan mensimulasikan bifurkasi yang memiliki kondisi awal geometri atau pasang surut yang asimetris. Kondisi awal geometri yang asimetris yang dimaksud dalam penelitian ini adalah didefinisikannya kondisi awal bifurkasi yang memiliki perbedaan kedalaman atau panjang antara kedua anak sungai. Sementara kondisi pasang surut yang asimetris yang dimaksud adalah didefinisikannya perbedaan amplitudo atau fase pasang surut antara pasang surut di kedua muara dari anak-anak sungai pada sebuah bifurkasi. Gaya-gaya hidrodinamika eksternal yang diperhitungkan pada penelitian ini adalah debit sungai pada kondisi batas hulu dari sungai utama dan gelombang pasang surut dari kondisi batas laut pada muara kedua anak sungai dari bifurkasi yang dimodelkan. Pengaruh pasang surut terhadap ketidaksimetrisan morfologi antara kedua anak sungai dipelajari secara sistematis dengan melakukan beberapa simulasi yang memiliki perbedaan pengaruh pasang surut. Perbedaan ini diperoleh dengan memvariasikan debit sungai dan properti pasang surut untuk tiap kasus dengan definisi ketidaksimetrisan yang berbeda (geometri atau pasang surut yang asimetri). Pada penelitian ini ditemukan bahwa pada kondisi yang setimbang, derajat ketidaksimetrisan antara kedua anak sungai pada bifurkasi akan semakin kecil pada sistem bifurkasi yang memiliki pengaruh pasang surut yang lebih besar.

Pada bab 4 model numerik 1D yang dikembangkan pada penelitian doktoral ini diaplikasikan untuk menganalisis efek pasang surut terhadap stabilitas morfologi pada bifurkasi sungai di daerah pasang surut. Efek pasang surut terhadap bifurkasi di pelajari untuk kondisi seluas mungkin yang dapat ditemui di delta sungai dan muara. Kondisi yang dimaksud terkait dengan mobilitas sedimen, pengaruh pasang surut, dan rasio lebar-kedalaman sungai. Penelitian pada bab ini melanjutkan penelitian pada Bab 3 dengan memperluas kondisi alam yang dicakup dalam Bab 3. Pada penelitian ini, pola yang kompleks ditemukan terkait dengan morfodinamika bifurkasi di daerah pasang surut.

Pertama, untuk bifurkasi sungai dengan pengaruh pasang surut yang lemah dimana arus yang mengalir ke arah hulu (saat pasang) lemah atau tidak ditemukan, bifurkasi yang memiliki pengaruh pasang surut yang lebih besar akan memiliki kemungkinan kondisi yang lebih besar untuk sebuah bifurkasi memiliki morfologi yang simetris. Kedua, sebaliknya untuk bifurkasi yang memiliki pengaruh pasang surut yang besar yang menyebabkan perubahan arah arus (arus bolak-balik) pada tiap siklus pasang surut, pengaruh pasang surut yang lebih besar menyebabkan kondisi yang lebih kecil untuk bifurkasi memiliki morfologi yang simetris. Akan tetapi, secara keseluruhan untuk kedua kondisi pasang surut tersebut, pada situasi dimana bifurkasi memiliki morfologi yang asimetris, semakin besar pengaruh pasang surut menyebabkan semakin kecilnya derajat asimetri morfologi diantara dua anak sungai. Hasil ini mengkonfirmasi hasil yang ditemukan pada Bab 3. Maka dapat disimpulkan bahwa pengaruh pasang surut mengurangi tendensi untuk terjadinya penutupan salah satu anak sungai akibat sedimentasi (avulsi sungai) yang umumnya terjadi pada bifurkasi di daerah aliran sungai yang tidak dipengaruhi pasang surut. Kesimpulan ini terjadi melalui dua kemungkinan yakni dengan (1) semakin berkurangnya kondisi yang memungkinkan untuk bifurkasi memiliki ketidaksimetrisan morfologi atau (2) semakin kecilnya derajat ketidaksimetrisan antara kedua anak sungai pada kondisi dimana bifurkasi memiliki ketidaksimetrisan morfologi.

Di Bab 5, model numerik 1D diaplikasikan untuk mempelajari morfodinamika pada *distributary* yang memiliki lebih dari satu bifurkasi. *Distributary* yang disimulasikan pada studi ini diadopsi dari struktur *distributary* di Delta Mahakam. Kesetimbangan morfodinamika dari delta sungai dianalisis dengan mensimulasikan beberapa konfigurasi *distributary* yang memiliki jumlah bifurkasi yang berbeda. Hasil dari penelitian ini menunjukkan bahwa kesetimbangan morfologi pada *distributary* yang memiliki kedalaman yang seragam, tidak sensitif dengan jumlah anak sungai di dalam *distributary* tersebut. Selama total dari lebar sungai sepanjang *distributary* sama dan dengan mengasumsikan tidak adanya friksi pada dinding sungai. Akan tetapi, ketika perbedaan kedalaman didefinisikan pada kondisi awal dari setidaknya satu bifurkasi pada *distributary*, misalnya, dari satu bifurkasi yang paling hilir, perbedaan kedalaman ini dapat menyebabkan asimetri morfologi hingga ke bifurkasi yang paling hulu dari delta tersebut dan oleh karenanya, mengubah kesetimbangan morfologi pada keseluruhan delta. Perubahan kesetimbangan morfologi ini juga menyebabkan membesarnya total luas penampang keseluruhan anak sungai sepanjang delta dan menyebabkan kenaikan prisma pasang surut di delta tersebut. Dari hasil penelitian ini dapat disimpulkan bahwa kesetimbangan morfologi pada suatu delta sangatlah tergantung pada kondisi awal (*initial condition*) atau, dalam kondisi di lapangan, bergantung pada perubahan yang pernah terjadi baik yang diakibatkan oleh insiden alami maupun akibat campur tangan manusia. Semakin banyak anak sungai pada suatu delta, maka makin banyak pula posibilitas dari kesetimbangan morfologi delta tersebut. Hal ini terjadi karena perubahan pada anak sungai yang berbeda dapat menyebabkan perbedaan kesetimbangan morfologi pada tiap anak sungai.

Pada bab 6, hasil dari penelitian dalam disertasi ini didiskusikan dalam konteks hubungannya dengan literatur dan penelitian sebelumnya. Dipaparkan pula mengenai pentingnya hasil penelitian pada disertasi ini untuk memberikan fondasi dalam memahami mekanisme utama dalam proses morfodinamika pada sungai bercabang di daerah pasang surut. Selain itu, penulis menyadari adanya limitasi dalam penelitian ini serta perlunya penelitian lebih lanjut untuk meningkatkan pemahaman kita mengenai morfodinamika di *tide-influenced river delta*. Maka, penulis juga memberikan beberapa gagasan untuk penelitian lanjutan di masa depan. Gagasan yang dimaksud adalah untuk mengeksplorasi faktor-faktor lain yang mempengaruhi morfodinamika dari bifurkasi atau sungai bercabang di *tide-influenced river delta*. Penulis merekomendasikan empat penelitian lanjutan yang perlu mendapat perhatian lebih. Empat penelitian lanjutan tersebut adalah: (1) pengembangan model 1D untuk meningkatkan kompleksitas dalam mensimulasikan pola struktur arus sungai dan proses transportasi sedimen agar hasil yang diperoleh semakin merepresentasikan kondisi alam pada delta sungai dan muara, (2) menganalisis efek adanya evolusi dan morfodinamika bantaran sungai beserta

daerah basah-kering yang umumnya dapat di amati di daerah yang dipengaruhi pasang surut, (3) menganalisis efek perubahan iklim terhadap morfodinamika pada bifurkasi yang direfleksikan dengan mempertimbangkan kenaikan muka air laut, serta (4) mempelajari efek adanya pengembangan wilayah delta dan muara untuk aktivitas manusia.

Chapter 1 | Introduction

1.1 Background

River deltas are transition zones where rivers debouch into a large body of water, such as an ocean or a lake. This transition results in deposition of alluvial sediment transported from upstream. The depositional processes cause distributary channel networks to form in the deltas. Two mechanisms are involved in the shaping of deltaic channel networks: mouth bar depositions that form bifurcations (Edmonds and Slingerland, 2007; Jerolmack, 2009; Jerolmack and Swenson, 2007) and delta aggradation, which induces avulsion that relocates the flow to a different path, creates a new distributary and so expands the size of the delta (Ashworth et al., 2004; Jerolmack, 2009; Jerolmack and Mohrig, 2007). In case a river debouches into the ocean, the shape of the delta and the number of active channels is determined by the relative importance of river flow characteristics, wind-wave energy and tidal action, as shown in Figure 1.1 (Galloway, 1975; Rossi et al., 2016; Shaw and Mohrig, 2014). Other studies suggest more factors that determine the shape of deltas, such as sediment type and availability (Geleynse et al., 2011; Orton and Reading, 1993; Shaw and Mohrig, 2014), and sea level variability (Dalrymple et al., 1992; Leuven et al., 2019; Nienhuis and van de Wal, 2021; Postma, 1995).

River deltas are of great economic and ecological value because fluvial deposits are so rich in nutrients and because deltas are such strategic locations where rivers, land and sea meet (Ericson et al., 2006). This is why so many river deltas have become hubs of anthropogenic activity. Deltas are where megacities are built, where agricultural and aquacultural activities are concentrated, where navigable channels are dredged and where tourism flourishes (Ericson et al., 2006; Novico et al., 2018; Rahmawan et al., 2017; Setiawan et al., 2015; Syvitski and Saito, 2007). All these human activities require engineering works, such as the construction of river embankments for land reclamation and flood defence (Giosan et al., 2013), dredging and dumping activities (Jeuken and Wang, 2010; Luo et al., 2007; Pinter et al., 2004), land-use conversion for human activities (Ve et al., 2021) and the construction of dams(Yang et al., 2006). These engineering works have significantly influenced the morphological development of the deltas which has created new problems, such as increased vulnerability to flooding and delta subsidence (Syvitski et al., 2009; Syvitski and Kettner, 2011) and excessive sedimentation (Ve et al., 2021; Yuanita and Tingsanchali, 2008). These problems are the result of our lack of understanding of the morphodynamics of river deltas and morphodynamic responses to perturbation. Therefore, studying morphodynamic processes in river deltas is key to improving future delta management plans in a more sustainable way.

Many deltas consist of distributary channel networks. In such deltas, bifurcations—where a larger upstream channel splits into two smaller branches—are the main geomorphological feature that determines the delta's morphological fate. The bifurcations distribute the water and sediment across the entire delta and determine its morphological development (e.g. Jerolmack, 2009; Jerolmack and Swenson, 2007). Some efforts have been made to investigate how the sediment is distributed at bifurcations in bedload-dominated rivers (e.g. Bertoldi et al., 2009; Bertoldi and Tubino, 2007; Bolla Pittaluga et al., 2003; Kleinhans et al., 2008; Van der Mark and Mosselman, 2013), suspended-load dominated rivers (e.g. Edmonds and Slingerland, 2008; Slingerland and Smith, 1998) and tide-influenced deltas (e.g. Buschman et al., 2013; Kästner and Hoitink, 2019). Regarding the morphodynamics of bifurcations, previous studies have primarily explored the processes in river-dominated systems and have used various approaches, namely field observations (e.g. Aslan et al., 2005; Smith et al., 1989), physical modelling (e.g. Ashworth et al., 2004; Bertoldi and Tubino, 2007), and numerical modelling (e.g. Bolla Pittaluga et al., 2003; Kleinhans et al., 2008; Slingerland and Smith, 1998).

By contrast, research into the morphodynamics of tide-influenced river bifurcations—where river discharge flows from upstream and tides propagate into the downstream channels—is limited. We have a reasonable understanding of hydrodynamics (Friedrichs, 2010), sediment transport and

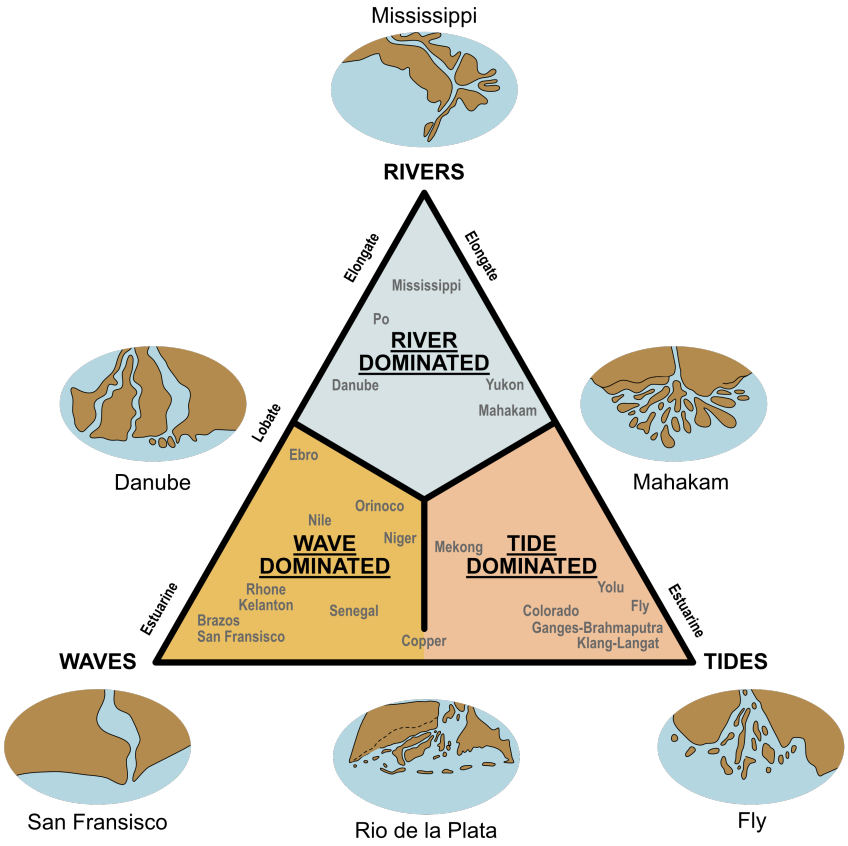

Figure 1.1 Delta classification and example of delta formation (after Galloway, 1975).

morphological change (Dronkers, 1986; Dyer, 1997; Dyer, 1995; Hibma et al., 2004) in single-channel tide-influenced estuaries. However, the dynamics of tide-influenced delta networks is less well understood. For example, the Yangtze estuary is strongly influenced by tides and most upstream bifurcation in this system is asymmetrical. Northern branches gradually silt up and become narrower, while southern branches deepen and widen (Chen et al., 1982). However, in other tide-influenced deltas, bifurcations have a near-symmetrical depth distribution, e.g. Berau River Delta (Buschman et al., 2013), and Kapuas River Delta (Kästner et al., 2017). Hoitink et al. (2017) also suggested that tide-influenced river deltas have more stable distributary channel networks with more limited occurrence of avulsion than river-dominated deltas. But again, we do not know exactly how the mechanisms that govern these phenomena work. Furthermore, morphological change in the delta networks affects the distribution of sediment and fresh water across the delta, which in turn affects the coastal seas and their important habitats. For example, the Berau River (Indonesia) debouches on the Berau shelf, which hosts a highly diverse coral reef area at its oceanic edge (Tarya et al., 2015). Due to land cover change, fresh water and nutrients are beginning to affect coral reef health (Tarya

et al., 2015; van Katwijk et al., 2011). For these reasons, this study focuses on research into the morphodynamics of tide-influenced river bifurcations.

1.2 Existing theoretical analysis of morphodynamics in fluvial-dominated river bifurcations

Over the last few decades, several efforts have been made to analyse the sediment division at bifurcations, because this process determines the morphological stability of bifurcations. Instability can lead to abandonment of one downstream channel, while stability enables the symmetrical or asymmetrical development of two open channels. This systematic analysis was pioneered by Wang et al. (1995) who concluded that the sediment division at bifurcation is a function of river discharge ratio between downstream channels and the power of velocity relationship in a generic sediment transport relationships. Slingerland and Smith (1998) studied the morphodynamics of river bifurcations in situations with a crevasse, i.e. a smaller branch that takes off from the main channel, and suggested that abandonment of a crevasse depends on (1) the depth difference between the main channel and the crevasse, and (2) the ratio of channel slope between the crevasse and the main channel. For broadly similar channel off-take systems, Van der Mark and Mosselman (2013) suggested that helical flow in sharp bends partly determines the morphodynamics of bifurcations and proposed a model for the sediment division for bifurcations in such conditions. Bolla Pittaluga et al. (2003) inferred that transverse sediment transport just upstream of the bifurcation enables stable bifurcations. Investigating bifurcations with fine-grained sediment, Edmonds and Slingerland (2008) suggested that the stability of bifurcations is controlled by the transverse water level difference at bifurcation.

Two analyses that have been widely implemented to study river bifurcation with the help of numerical and analytical models are Wang et al. (1995) and Bolla Pittaluga et al. (2003). Wang et al. (1995) pioneered a quantitative description of the mechanism behind the evolving morphology of bifurcations. Investigating the morphodynamics of sand bed rivers, they suggested that the morphological evolution of bifurcation depends on the sediment transport division at bifurcation. The morphological equilibrium of the bifurcations depends on the calibrated parameter k in the calculation of sediment transport division as follows:

$$\frac{Q_{s,2}}{Q_{s,3}} = \left(\frac{Q_2}{Q_3}\right)^k \left(\frac{w_2}{w_3}\right)^{1-k} \tag{1.1}$$

in which Q_s is the sediment supply to each downstream channel, Q is the river discharge and w is the width of the downstream channel. Subscripted notations indicate the downstream channel identity. Any depth difference between a bifurcation's downstream channels will decrease—resulting in a symmetric bifurcation—when $k>n/3$, and increase when $k<n/3$. Here, n is the power of flow velocity in the sediment transport relationship. Wang et al. (1995)'s research was applied and developed in several other studies. For example, Fokkink et al. (1995) applied this approach to gravel bed rivers, and Jeuken and Wang (2010) studied the sensitivity of bifurcation morphology to dredging-dumping activities in an estuary. Wang's pioneering study has some limitations. One is that the value of k in Eq. 1.1 significantly varies for different bifurcations as obtained by Wang et al. (1995) from field measurements and the physical model experiment. Another is that Wang's approach assumes a uniform distribution of water and sediment flux throughout the river cross-section. However, this distribution is not uniform if there is transverse asymmetry in the upstream channel at the bifurcation due to meandering or the presence of bars, for example, or if there is depth asymmetry between downstream channels (Kleinhans et al., 2008; Kleinhans et al., 2013).

An alternative approach to compute the sediment division at bifurcation was presented by Bolla Pittaluga et al. (2003), who focused on the morphological equilibrium of bifurcations in gravel-bed braided rivers. They proposed that the morphological development of bifurcations is not only determined by the division of along-channel sediment transport, but also by local transverse sediment transport just upstream of the bifurcation, as schematized in Figure 1.2. Transverse sediment transport is driven by two processes, as follows:

$$transverse\,transport = transverse\,flow\,induced\,sediment\,transport - transverse\,bedslope \tag{1.2}$$

The first process is the transverse river flow caused by unequal flow division. The second is the transverse bed slope effect caused by initially asymmetric morphology at bifurcation. These processes might be triggered by an initial asymmetry in morphology between downstream channels, e.g. depth or width differences. Using a one-dimensional model for their calculations, they suggested that the equilibrium morphology depends on sediment mobility and width-to-depth ratio in the upstream channel. Starting from a symmetrical condition, they found that a bifurcation's downstream branches will have an asymmetric morphology for the systems with lower sediment mobility. Additionally, the range of sediment mobility for the asymmetric morphology will be wider for bifurcations where the upstream channel has a larger width-to-depth ratio. Here, asymmetry can lead to channel abandonment. These findings were confirmed by Bertoldi and Tubino (2007)' s physical scale model. In this approach, the stability of bifurcations is independent of the calibrated parameter k in Wangs model. Bolla Pittaluga et al. (2003)'s approach to computing the sediment division at bifurcations has proven useful for studying the morphological evolution of river networks in various situations, for example to study the effect of a meandering upstream channel (Kleinhans et al., 2008); or the effect of upstream boundary change to the morphodynamics of an anastomosing river (Kleinhans et al., 2012); the effect of a downstream sink condition, similar to a delta, for bifurcations that are connected to the sea (Salter et al., 2017); and the morphodynamics of a delta with multiple bifurcations (Salter et al., 2020).

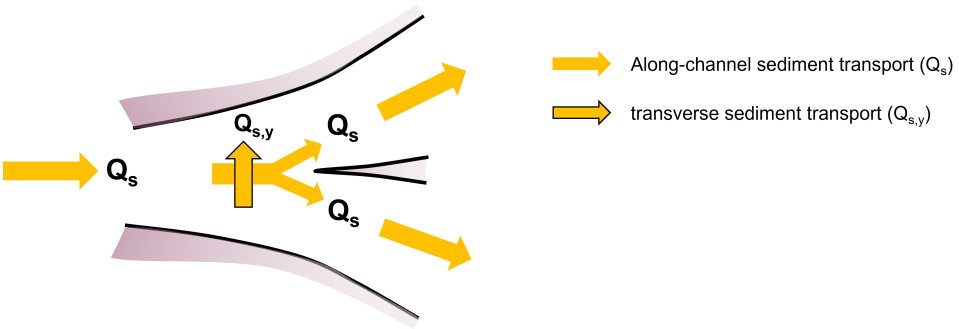

Figure 1.2 Sketch of along-channel sediment transport (Q_s) and transverse sediment transport ($Q_{s,y}$) at a bifurcation.

Bolla Pittaluga et al. (2015a) used Bolla Pittaluga et al. (2003)'s approach to compute river bifurcations' morphodynamic stability in both sand-bed rivers with high sediment mobility and gravel-bed rivers with low sediment mobility. They found that symmetric bifurcations are stable in a narrow range of intermediate mobility. This means that when bifurcations have a sediment mobility within this range, any perturbation that initially causes asymmetric bifurcation, such as a depth difference between the downstream channels, will ultimately reduce and result in a bifurcation with symmetric downstream channels. They also found that symmetric bifurcations are unstable in a wider range of low and high sediment mobility conditions. In this range, asymmetric bifurcations

occur, potentially leading to abandonment of one of the downstream channels. They also suggested that the parameter range for stable symmetric bifurcations is more limited in systems where the upstream channel has a wider width-to-depth ratio.

1.3 Morphodynamics in tide-influenced river bifurcations

The theory for fluvial-dominated river bifurcations might not be fully applicable to tide-influenced river bifurcations because of time-varying hydrodynamic conditions and typical coastal conditions such as a lower channel slope and finer sediment. In addition to the discharge that flows from the upstream river, tides propagate upstream from the sea into the downstream channels (Figure 1.3). Tide-influenced systems also have a gentler channel slope and finer sediment compositions than river-dominated systems. The river flow tends to be slower, and the sediment finer, which could make the importance of suspended load transport more important than bedload transport. This affects the transverse bed slope transport process at, and the stability of, the bifurcation. In addition, tidal propagation induces a bi-directional flow that changes in magnitude and direction in a tidal cycle, which significantly affects the time-averaged flow division at a bifurcation (Buschman et al., 2010; Sassi et al., 2011).

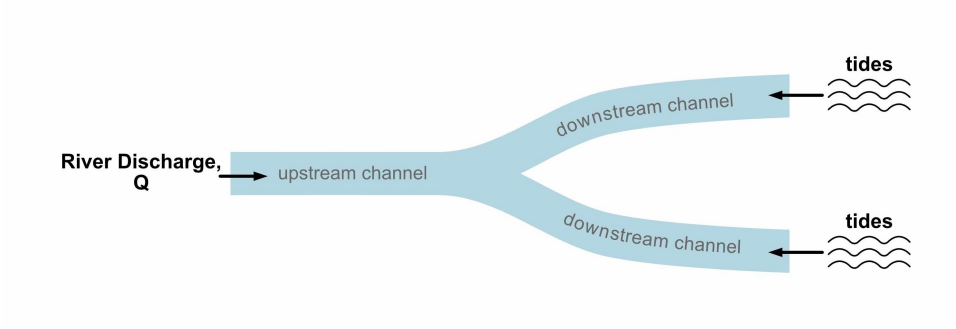

Figure 1.3 Schematization of a bifurcation imposed by discharge from the upstream river and tidal waves from the sea that propagate into the downstream channels.

Ragno et al. (2020) implemented Bolla Pittaluga et al. (2003)'s approach to investigate the stability of river bifurcations with limited tidal influence, i.e. where tides do not cause a change in flow direction. In a range of sediment mobility and width-to-depth ratio conditions, Ragno et al. (2020) found that tides increase the range of conditions where symmetric bifurcation is stable. They suggested that this is because tides cause a frequent flow fluctuation that deepens the downstream channels, which reduces the width-to-depth ratio. However, the tidal influence conditions studied by Ragno et al. (2020) are confined to limited tidal influence, where tides change the magnitude of the river flow but not the direction. Additionally, many bifurcations in tide-influenced river deltas appear to have an asymmetric geometry where one downstream channel is narrower and shallower while the other is deeper and wider (e.g. Kästner and Hoitink, 2019). Yet they also seem to have a stable morphology in which channel abandonment does not seem to occur as often as in fluvial-dominated river bifurcations. The underlying mechanism is still unknown. Another aspect of tide-influenced deltas concerns complexity of the distributary. Delta distributaries tend to consist of several, connected bifurcations. In the more tidally influenced Mahakam Delta, bifurcations located near the sea were found by Sassi et al. (2011) to have a less asymmetric river discharge division than bifurcations further upstream. However, Buschman et al. (2010) found the opposite behaviour. When they applied a flow model to a schematic bifurcation to study the sensitivity of river discharge

division to a range of tidal amplitudes, they suggested that the bigger the tidal influence, the larger the asymmetry in river discharge division. Since the morphological change in a bifurcation's downstream channels depends on the flow division at bifurcation, this indicates that there are processes at work in multiple network deltas that a single-bifurcation setup fails to capture. As many tide-influenced river deltas are important for human activities and our knowledge about tide-influenced bifurcations is still limited, it is imperative to learn how tides govern the morphological stability of river bifurcations.

1.4 Objectives

The objective of this study is to improve our understanding of the morphodynamics of tide-influenced bifurcations in river deltas. Before we can examine the effect of tides on the morphodynamics of bifurcations, we first need to establish how the characteristics of a typical river delta landscape affect these morphodynamics. Tide-influenced river deltas have lower channel slopes and finer grained sediment than river-dominated deltas, but it is not known what effect this has on the morphodynamics of bifurcations. As a first step, I will analyse the effect of channel slopes and sediment grain sizes on the morphological stability of bifurcations without taking tidal influence into account. My first research question therefore is:

1. *How do channel slope and sediment size affect the morphological stability of river bifurcations?*

Once I have established what effect these characteristics have, I will include the effect of tides in my research. I will then address the second and third research questions:

2. *How do tidal and fluvial influences affect the morphological asymmetry of bifurcations that have asymmetric downstream geometries or different tides in their downstream channels?*
3. *How does the relative importance of river and tidal influence affect the morphological stability of river bifurcations with a symmetric downstream geometry?*

Finally, tide-influenced river deltas often have multiple interconnected bifurcations. We do not know how the morphology of the entire delta evolves and how bifurcations in the system influence each other. Therefore, my fourth and final research question is:

4. *How do multiple bifurcations in tide-influenced delta networks affect the equilibrium of the entire deltaic channel network?*

1.5 Approach and thesis outline

To answer these research questions, I used two process-based numerical models to conduct morphodynamic simulations. The first model is a one-dimensional (1D) model developed in the Matlab environment. The second model applies the depth-averaged version (2D model) of the Delft3D model.

I built a one-dimensional numerical model to simulate the hydro- and morphodynamics in river network systems under unsteady flow condition. This makes the model suitable to study the morphodynamics in both fluvial-dominated and tidal-dominated rivers. Using 2D and 3D modelling techniques for morphodynamic modelling is computationally expensive because morphological development, especially in low-lying areas such as river deltas, is a long-term process that could take place on a millennial time scale. On such a long timescale, application of a 1D model is more efficient, especially when studying morphodynamics of a wide range of conditions in the spatial scale of river

network deltas. In other words, a 1D model is computationally more efficient for morphodynamic simulations than 2D and 3D models. To determine the morphological evolution in the river network channels, and hence the entire deltaic system, it is crucial to understand the sediment distribution, or division, at the junction. This study improves upon the sediment distribution calculation proposed by Bolla Pittaluga et al. (2003) by (1) separating suspended load and bedload transport to enable application to the suspended load-dominated river bifurcations (described in chapter 2) and (2) allowing the calculation for hydrodynamic condition with changing flow magnitude and direction that occur in tide-influenced junctions (described in chapter 4).

Subsequently, I used the depth-averaged version (two-dimensional model) of the Delft3D model suite to study the asymmetry of bifurcations imposed by the downstream channels' asymmetric geometry or tides. In the 2D model, a bifurcation is schematized using the approach of Kleinhans et al. (2008). The model setup is described in detail in chapter 3. The 2D model is applied to take into account the tide-induced 2D effect in the flow structures at the bifurcation that could significantly influence its morphodynamics. The 2D model results are also used to validate the 1D model developed.

These two models are used to conduct four studies, described in Chapters 2 through 5. chapter 2 describes and validates the 1D model development for river bifurcations. The study in this chapter is intended to answer the first research question. Hence, the model is applied to investigate how channel slopes and sediment grain sizes affect the stability of river-dominated bifurcations in a range of sediment mobilities from suspended load-dominated to bedload-dominated regimes and width-to-depth ratio of the upstream channel. The second research question is addressed in chapter 3 and chapter 4. In chapter 3, the 2D model is applied. The asymmetry of tide-influenced bifurcations is studied by analysing the equilibrium asymmetry for bifurcations with asymmetric geometries (depth or length) or asymmetric tides (tidal amplitude or phase difference) between downstream channels. The tidal influences are varied by running a series of simulations with different river discharges or tides to investigate the effect of tidal influence on the asymmetry. chapter 4 describes how the 1D model for tide-influenced bifurcations has been developed. This model is used to answer both the second and third research questions. The morphological stability of tide-influenced bifurcations is studied in a wide range of conditions of sediment mobility, width-to-depth ratio of the upstream channel and tidal influence at bifurcation. This study is conducted to analyse which settings and tidal influences make initially symmetric bifurcations stable or unstable, and to explain the intratidal mechanisms that drive the morphological development. The study in chapter 4 also confirms the findings in chapter 3 and expands the range of conditions of sediment mobility, width-to-depth ratio of upstream channel and tidal influence at bifurcations. In chapter 5, the 1D model is applied to investigate the morphodynamic stability of deltaic channel networks with multiple bifurcations (the fourth and final research question). The channel network setting is inspired by the Mahakam Delta, which has a distributary pattern characterized by an increasing number of downstream bifurcations and channels.

Chapter 2 | Effects of sediment grain size and channel slope on the stability of river bifurcations

Abstract

Channel bifurcations can be found in river network systems from high gradient gravel-bed rivers to fine-grained low gradient deltas. In these systems, bifurcations often evolve asymmetrically such that one downstream channel silts up and the other deepens and, in most cases, they eventually avulse. Past analytical and numerical studies showed that symmetric bifurcations are unstable in high and low Shields stress conditions resulting in asymmetric bifurcations and avulsion, while they can be stable in the mid-Shields range, but this range is smaller for larger width-to-depth ratio. Here, using a 1D numerical model, we show that effects of sediment grain size and of channel slope are much larger than expected for low-gradient systems when a sediment transport relation is used that separates between bedload and suspended load transport. We found that the range of Shields stress conditions with unstable symmetric bifurcations expanded for lower channel slopes and for finer sediment. In high sediment mobility, suspended load increasingly dominates the sediment transport, which increases the sediment transport nonlinearity and lowers the relative influence of the stabilizing transverse bed slope-driven flux. Contrary to previous works, we found another stable symmetric solution in high Shields stress, but this only occurs in the systems with small width-to-depth ratio. This indicates that suspended load-dominated bifurcations of lowland rivers are more likely to develop into highly asymmetric channels than previously thought. This explains the tendency of channel avulsion observed in many systems.

Published as: Iwantoro, A. P, van der Vegt, M., & Kleinhans, M. G. (2021). Effects of sediment grain size and channel slope on the stability of river bifurcations. *Earth Surface Processes and Landforms*, 46(10),pp. 2004–2018. https://doi.org/10.1002/esp.5141

2.1 Introduction

Various types of channel networks can be found in fluvio-deltaic environments, from tributary channel networks and braided rivers in the upstream to anastomosing rivers and river deltas in the downstream part (Kleinhans et al., 2013). Bifurcations are the locations in the channel network where a channel upstream splits into two downstream channels. At the bifurcations, river flow and sediment transport divide and control the morphodynamic evolution of the downstream channels (Wang et al., 1995). The sediment division processes are determined by many factors, such as a meandering upstream channel (Kleinhans et al., 2008), downstream sediment sinks (Salter et al., 2017), width-to-depth ratio of the upstream channel (Bolla Pittaluga et al., 2015a; Redolfi et al., 2019), and changing flow magnitude and direction induced by rivers and tides in tide-influenced deltas (chapter 3 and chapter 4). These factors determine whether the sediment transport division will increase the asymmetry of bifurcations and at high asymmetry, effectively lead to avulsion whereby one channel is abandoned.

Asymmetric bifurcations occur when bifurcations are unstable for symmetric conditions and any bed perturbation will result in aggradation in one downstream channel and erosion in the other. If the aggradation in the dwindling channel is sufficient for vegetation settling and floodplain formation processes to commence (Kleinhans et al., 2011; Smith et al., 1989), one downstream channel has been abandoned and an avulsion has occurred. Avulsions are common in various types of river networks such as in gravel-braided rivers (e.g. Burge, 2006; Lane et al., 2003), alluvial fans (e.g. Assine, 2005; North and Warwick, 2007) and lowland rivers (e.g. Hoyal and Sheets, 2009; Jones and Harper, 1998; Stouthamer and Berendsen, 2001). Bifurcations also occur in cases of flow diversion from a meandering channel into a chute cutoff, in braided rivers (Ashmore, 1982; Leddy et al., 1993) and in enlarging crevasses in anastomosing rivers and river deltas (Smith et al., 1989; Aslan et al., 2005). As such, high asymmetry of a bifurcation is a necessary condition for avulsion.

Efforts to understand the morphodynamic evolution of bifurcations have mainly been conducted using idealized mathematical models. Wang et al. (1995) introduced a nodal point relation to compute the sediment transport division at the bifurcation using a one-dimensional (1D) numerical model. They proposed that the asymmetry of bifurcations depends on the river discharge ratio to the power of a calibrated parameter k. Any depth asymmetry will decay in time resulting in a symmetric bifurcation when $k > n/3$ and will increase in time for $k < n/3$, where n is the velocity power in the sediment transport relation. While this work illuminated the importance of the sediment transport nonlinearly, it has some limitations. First, the stability of symmetric bifurcations depends on a non-physical calibrated parameter. Second, the estimated value of the calibrated parameter can be considerably different for different field and scale model conditions (Kleinhans et al., 2013).

Bolla Pittaluga et al. (2003) proposed an alternative nodal point relation. Their approach was designed for bifurcations in gravel braided rivers that have bedload dominated sediment transport. In their nodal point relation, they considered a transverse sediment transport at the bifurcation driven (1) by transverse river flow induced by unequal discharge division between the downstream channels and (2) by transverse bedslope effect (adopting the approach by Ikeda et al. (1981)). They showed that a symmetric bifurcation is unstable in low sediment mobility (low Shields number) and the Shields number range of unstable condition is wider for a larger width-to-depth ratio. Their results have been experimentally tested by Bertoldi and Tubino (2007) and developed further by including, for instance, evolving river banks (Miori et al., 2006; Kleinhans et al., 2011), the effect of meandering upstream channel (Kleinhans et al., 2008), and the effect of helical flow for offtake channel (Van der Mark and Mosselman, 2013).

Some studies have addressed the morphodynamic evolution of bifurcations in suspended load dominated rivers. Using a one-dimensional (1D) numerical model, Slingerland and Smith (1998) investigated the stability condition of crevasses to keep open and found that it depends on sand grain size, and the difference of channel slope ratio and depth between crevasse and the main channel.

Edmonds and Slingerland (2008) studied the stability of bifurcations for high sediment mobility conditions where the suspended load dominates the sediment transport. They suggested that in high sediment mobility symmetric bifurcations are unstable. Therefore, any perturbation in the downstream channels will cause the system to develop an asymmetric morphology.

Bolla Pittaluga et al. (2015a) proposed a general theory to predict stability of symmetric bifurcations for gravel and sand bed rivers (range of bedload to suspended load dominated conditions). They extended the nodal point relationship by Bolla Pittaluga et al. (2003) to suspended load and bedload transport conditions and found that symmetric bifurcations are unstable in high sediment mobility for sand bed rivers and for low sediment mobility for gravel bed rivers. Symmetric bifurcations can only be stable for intermediate sediment mobility. This range of sediment mobility for stable symmetric condition is narrower for rivers with higher width-to-depth ratio. Redolfi et al. (2019) further investigated the effect of width-to-depth ratio of upstream channel on the stability of bifurcations for sand and gravel bed rivers.

Generally, the stability of symmetric bifurcations depends on the ratio of sediment supply from the upstream channel and the sediment transport capacity in the downstream channels. When the morphology of the two downstream channels is asymmetric due to a small depth disturbance in one of the channels, a larger river discharge is conveyed into the deep channel than in the shallow channel. Due to this asymmetrical discharge division, the sediment transport capacity in the deep channel increases relatively fast due to the nonlinearity of sediment transport, while it decreases quickly in the shallow channel. However, because the sediment supply from upstream channel is also constant, this results in a lack of sediment supply to the deep channel but an over capacity to the shallow one. As a result, erosion occurs in the deep channel while the shallow channel has deposition, which increases the morphological asymmetry between the downstream channels and thereby results in unstable bifurcations. However, according to Bolla Pittaluga et al. (2003) there is a transverse sediment transport at the bifurcation induced by the transverse flow and transverse bedslope effect by which sediment is transported transversely, upstream of the bifurcation, from the side of shallow channel to the side of deep channel. This transverse sediment transport increases the sediment flux asymmetry between downstream channels and might be sufficient to change the system from unstable to stable. The stable symmetric bifurcations occur in the conditions when the combination of transverse sediment transport and the flow division driven asymmetry of sediment flux provides a sufficiently large sediment supply difference to exceed the difference of the sediment transport capacity between downstream channels.

Despite our understanding about the basic mechanisms that determines the stability of bifurcations, the dependence of the bifurcation stability on the mode of sediment transport raises new questions on how sensitive these mechanisms are to sediment grain size and to channel slope. Previous theoretical studies mainly focused on river settings with steep channel slope and coarse sediment (e.g. Bertoldi and Tubino, 2007; Bolla Pittaluga et al., 2003; Van der Mark and Mosselman, 2013). Though Edmonds and Slingerland (2008) studied the stability for high sediment mobility using a series of fine sand and cohesive sediment, it is unclear how channel slope affects the results. Ashworth et al. (2004) found in their experiments that the gentlest channel slope and thereby smallest flow resulted in highest occurrence of avulsion, suggesting that the effects of grain size and channel slope need more attention. Model results probably depend on the type of sediment transport predictor that is used. In a total load formula like Engelund-Hansen (Engelund and Hansen, 1967) (hereafter EH), no differentiation is made between bedload and suspended load. The total transport only depends on the Shields number and Shields number depends on flow velocity and the sediment grain size. In sediment transport predictors that differentiate between bedload and suspended load transport (e.g. van Rijn, 1984a; van Rijn, 1984b; Van Rijn, 1993), the ratio of the two not only depends on the Shields stress but also on the grain size and channel slope. Hence, for the same Shields stress

but different grain size and channel slope the ratio of bedload and suspended load will be different. This is further illustrated in Figure 2.1. For the same range of Shields stress, the systems with finer sediment result in a more suspended load dominated condition. Regarding the channel slope, the more suspended dominated condition occurs for the systems with lower channel slope.

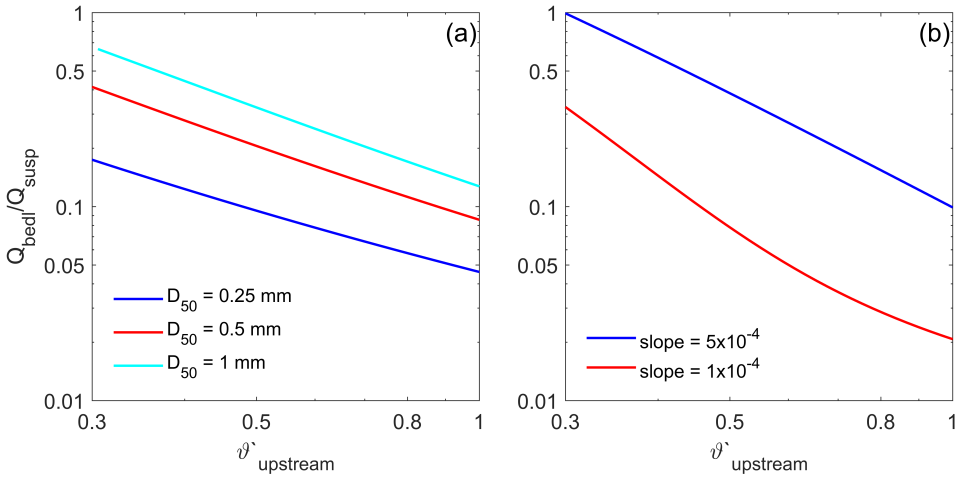

Figure 2.1 ratio of bedload over suspended load transport for (a) different grain size and (b) different channel slope as a function of Shields stress in an undivided channel (upstream of a bifurcation). The sediment transport is computed using sediment transport equation by van Rijn (1984a) and van Rijn (1984b)

Physically, the grain size and channel slope affect the relative quantity of suspended load and bedload, which then could affect the sediment division. If bedload transport dominates, transverse bedslope effect would have a significant contribution to the total transverse sediment transport. On the other hand, its contribution would be less significant if the system has a more dominant suspended load transport because it is not affected by the transverse bedslope effect. This remains untested as Bolla Pittaluga et al. (2015a) used a fixed grain size for both sand and gravel rivers to investigate the stability of bifurcations. In their results, stability of bifurcations is only affected by grain size through the Chézy friction parameter. Therefore, we aim to study the effect of grain size and channel slope on the morphological stability of river bifurcations in the range of sand and gravel bed. To address this objective, a one-dimensional model was developed to study the sensitivity of symmetric bifurcations to bed perturbations. In this study, we applied the sediment transport equations by van Rijn (1984a) and van Rijn (1984b) that separate the contribution of suspended load and bedload transport in the total sediment transport. Moreover, the contribution of those transports to the transverse sediment transport and therefore sediment division at bifurcations was also separated. This allowed us to investigate the effect of different channel slopes and sediment grain sizes to the ratio of bedload over suspended load and therefore stability of bifurcations. Finally, the sensitivity of results to channel slope and sediment grain size was studied in different sets of simulations.

The model description and model set-up are described in Section section 2.2, followed by the results in Section section 2.3. The physical mechanism behind the results and how this study contributes to the findings of the previous studies are discussed in Section section 2.4. Finally, the conclusions are provided in Section section 2.5.

2.2 Methodology

2.2.1 Model description

A bifurcating channel was studied using a 1D numerical model. Three channels connected at the bifurcation, where the upstream channel split in two downstream channels, as illustrated in Figure 2.2. The 1D model computed the hydrodynamics in each channel by numerically solving the Saint-Venant equations:

$$w\frac{\partial z}{\partial t} + \frac{\partial Q}{\partial x} = 0 \tag{2.1}$$

$$\frac{\partial Q}{\partial t} + \frac{\partial}{\partial x}\left(\frac{Q^2}{A}\right) + gA\frac{\partial z}{\partial x} + \frac{\mid Q \mid QPg}{C^2A^2} = 0. \tag{2.2}$$

Here, x and t are the spatial and temporal axes, z and Q are the water level and discharge, w is the channel width, g is the gravitational acceleration and C is Chézy coefficient as the roughness term calculated as follows

$$C = 18\log_{10}(12h/\xi) \tag{2.3}$$

where ξ is the Nikuradse roughness length related to the bedforms and h is water depth determined as

$$h = z - \eta \tag{2.4}$$

in which η is the bed level. Meanwhile, A and P are the cross-sectional area and wetted perimeter of the channel. We assume that the channels have a rectangular cross section where $A = wh$ and $P = w + 2h$.

In the model, two types of boundary nodes exist, namely open and junction boundary. Open boundaries are located at the upstream end of the upstream channel (upstream boundary in Figure 2.2) and at the downstream end of the downstream channels (downstream boundary in Figure 2.2). The junction boundary is shared by the three channels at the bifurcation, also known as nodal point. At upstream boundary, an equilibrium discharge condition was applied

$$Q_1 = w_1 C h_1 \sqrt{g h_1 S_1} \tag{2.5}$$

where the subscripted note indicates the channel identity as in Figure 2.2 and S is channel slope (m m^{-1}). At the downstream boundaries, since we neglected the presence of tides, a constant water level was prescribed. At the nodal point, to satisfy the conservation of mass, the discharge condition at the junction is

$$Q_1 = Q_2 + Q_3. \tag{2.6}$$

Meanwhile, the water level condition is

$$z_1 = z_2 = z_3. \tag{2.7}$$

The subscripted number in Eq. 2.5, 2.6 and 2.7 indicates the channel identity.

The sediment transport in the channels for the default setting was computed using van Rijn (1984a) and van Rijn (1984b) (hereafter vRijn), while the EH relation (Engelund and Hansen, 1967) was used to compare the model results with Bolla Pittaluga et al. (2015a). The advantage of using vRijn equation is that it can compute the bedload (van Rijn, 1984a) and suspended load (van Rijn, 1984b) separately

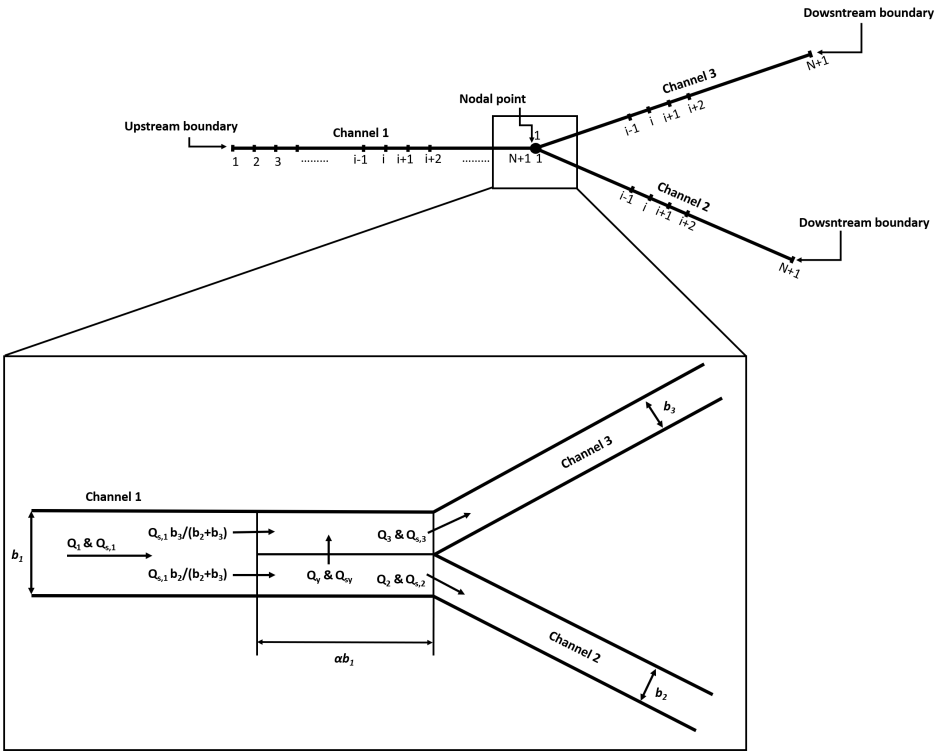

Figure 2.2 1D model discretization for bifurcation and sediment division scheme at the bifurcation point (inside the black box).

(see Appendix 2B for details). This is not possible in EH (See Appendix 2B for details on sediment transport). For the sediment division at the nodal point we adopted the approach of Bolla Pittaluga et al. (2003) and Bolla Pittaluga et al. (2015a) that includes transverse sediment transport at bifurcation in determining the distribution of sediment to downstream channels. At the nodal point, the conservation of sediment mass takes the following form

$$Q_{s,1} = Q_{s,2} + Q_{s,3}. \tag{2.8}$$

According to Bolla Pittaluga et al. (2003), the sediment that enters the downstream channels comes from the along-channel and transverse sediment transport at the junction (Figure 2.2). The transverse sediment transport occurs due to the transverse flow driven by asymmetric flow division and by the transverse bedslope effect driven by asymmetric bed levels across the channel at the bifurcation. This transverse sediment exchange effectively takes place over a distance αb_1 upstream from the bifurcation point, where constant α takes a typical value between 2 and 3 (Bolla Pittaluga et al., 2003). Unlike the approach of Bolla Pittaluga et al. (2003) and Bolla Pittaluga et al. (2015a), here the contribution of bedload and suspended load for the transverse sediment transport is separated because suspended sediment transport is not affected by transverse bedslope effect. The separation between those transport modes is as follows

$$Q_{s,y} = Q_{bedl,y} + Q_{susp,y}. \tag{2.9}$$

where $Q_{s,y}$, $Q_{bedl,y}$ and $Q_{susp,y}$ are the total, bedload part and suspended load part of the transverse sediment transport. $Q_{bedl,y}$ and $Q_{susp,y}$ are expressed by

$$Q_{bedl,y} = Q_{bedl,1}\left(\frac{Q_y h_1}{Q_1 \alpha h_{123}} - \frac{r}{\sqrt{\vartheta'}}\frac{\partial \eta}{\partial y}\right) \tag{2.10}$$

$$Q_{susp,y} = Q_{susp,1}\left(\frac{Q_y h_1}{Q_1 \alpha h_{123}}\right). \tag{2.11}$$

The first and the second term in the right-hand side of Eq. 2.10 account for the transverse sediment transport driven by transverse flow and the transverse bedslope, respectively, while transverse suspended load transport only has a transverse flow driven component. When EH sediment transport is used, the nodal point relationship becomes

$$Q_{bedl,y} = Q_{s,1}\left(\frac{Q_y h_1}{Q_1 \alpha h_{123}} - \frac{r}{\sqrt{\vartheta'}}\frac{\partial \eta}{\partial y}\right) \tag{2.12}$$

In Eq. 2.10 - Eq. 2.12, Q_y is the transverse water discharge calculated as

$$Q_y = \frac{1}{2}\left(Q_2 - Q_3 - Q_1\frac{w_2 - w_3}{w_2 + w_3}\right) \tag{2.13}$$

where $h_1 23$ is the average depth at the nodal point, expressed by

$$h_{123} = \frac{w_1 h_1 + w_2 h_2 + w_3 h_3}{w_1 + w_2 + w_3}. \tag{2.14}$$

The constant r in Eq. 2.10 and Eq. 2.12 is a calibration parameter for transverse bedslope effect (Ikeda et al., 1981; Talmon et al., 1995; Schuurman et al., 2013). Baar et al. (2018) experimentally determined the value of r to be in range of 0.2-1.5 depending on mobility and bedform characteristics. Moreover, unlike the previous works (e.g. Bolla Pittaluga et al., 2015a; Kleinhans et al., 2008; Talmon et al., 1995) grain-related Shields stress (ϑ') is applied to calculate the sediment mobility in the transverse bedslope effect term instead of total Shields stress that has been shown to be more represented to determine the transverse bedslope effect by Baar et al. (2018). Grain-related Shields stress is calculated as

$$\vartheta' = \mu\vartheta, \tag{2.15}$$

where μ is efficiency factor (van Rijn, 2007) defined as $\mu = (C/C')^2$ where C' is grain-related Chézy coefficient given by

$$C' = 18\log_{10}(12h/2.5D_{50}) \tag{2.16}$$

and ϑ is total Shields stress as follows

$$\vartheta = \frac{(Q_1/A_1)^2}{\left(\frac{\rho_s}{\rho_w} - 1\right)C^2 D_{50}} \tag{2.17}$$

where ρ_s and ρ_w are the density of sediment and water, respectively, and D_{50} is the median grain size of sediment. However, for EH, the sediment mobility term in transverse bedslope effect still applied

the total Shields stress (Eq. 2.12) because EH computes the total transport that is related to bedforms. Lastly $\frac{\partial \eta}{\partial y}$ in Eq. 2.10 and Eq. 2.12 is the transverse bed slope at the bifurcation calculated as

$$\frac{\partial \eta}{\partial y} = \frac{\eta_2 - \eta_3}{0.5 w_1}. \tag{2.18}$$

As a result, due to the presence of this transverse sediment transport, $Q_{s,2}$ in Eq. 2.8 becomes

$$Q_{s,2} = \frac{w_2}{w_2 + w_3} Q_{s,1} + Q_{s,y} \tag{2.19}$$

and therefore $Q_{s,3}$ is expressed by

$$Q_{s,3} = Q_{s,1} - Q_{s,2}. \tag{2.20}$$

Finally, the morphological change was computed using the sediment continuity equation (Exner equation),

$$w(1-p)\frac{\partial \eta}{\partial t} + \frac{\partial Q_s}{\partial x} = 0. \tag{2.21}$$

p is the sediment porosity and Q_s is the total sediment transport ($m^3 s^- 1$) obtained from the summation of bedload and suspended load transport (hereafter Q_{bedl} and Q_{susp}, respectively).

Meanwhile, two assumptions were made regarding the channel banks. First, fixed channel banks are defined. Although evolving channel banks also affect the stability of bifurcations (Miori et al., 2006; Kleinhans et al., 2011), we neglect this effect to keep the analysis as simple as possible. This assumption is reasonable because the adjustment of the hydraulic geometry to the hydrodynamic condition can still be accommodated by the morphodynamic changes of the riverbed. Second, the width of the downstream channels is half the value of the upstream channel. In nature, the summed width of downstream channels tends to be larger than the upstream width (see van den Berg (1995) for channel width and discharge relation). However, when applying such a condition the morphodynamic equilibrium would deviate from a linearly sloping bed (backwater effects expected) and we therefore chose to not take this into account. Using a wider downstream channel will increase the range of unstable conditions, but this effect is insignificant and can also be achieved by reducing the transverse bed slope effect.

2.2.2 Numerical methods

The mass and momentum balance in Eq. 2.1 and Eq. 2.2 were solved using an implicit Preissmann scheme according to Cunge et al. (1980) (see section 2.6). The advantage of this scheme is that it is unconditionally stable and allows for the computation of discharge and water level at the same node. Thus, the time step can be chosen freely to give sufficient accuracy or reduce the computational cost.

The Exner equation in Eq. 2.21 is solved in each channel using a modified FTCS (forward in time, central in space) scheme that solves the equation explicitly as follows

$$(1-p)w_i \left(\frac{\eta_i^{j+2} - \eta_i^{j+1}}{\Delta t^j} \right) + \frac{(1-\Phi)\left(Q_{s_{i+1}}{}^{j+1} - Q_{s_i}{}^{j+1}\right) + (1+\Phi)\left(Q_{s_i}{}^{j+1} - Q_{s_{i-1}}{}^{j+1}\right)}{2\Delta x_i} = 0 \tag{2.22}$$

where i and j are notations representing the node number in space and time, respectively. Φ is weighing factor for space derivatives that ranges between 0.5 and 1. The value of 1 may result in numerical oscillation. In this application we applied the value of 0.55.

Regarding the morphological change at the boundaries, a second-order upwind scheme was applied to solve the Exner equation:

$$(1-p)w_i\left(\frac{\eta_i^{j+2}-\eta_i^{j+1}}{\Delta t^j}\right)+\frac{-{Q_s}_{i+2}^{j+1}+4{Q_s}_{i+1}^{j+1}-3{Q_s}_i^{j+1}}{2\Delta x_i}=0. \tag{2.23}$$

Meanwhile, at the downstream boundaries, the following equation was solved

$$(1-p)w_i\left(\frac{\eta_i^{j+2}-\eta_i^{j+1}}{\Delta t^j}\right)+\frac{{Q_s}_{i+2}^{j+1}-4{Q_s}_{i+1}^{j+1}+3{Q_s}_i^{j+1}}{2\Delta x_i}=0. \tag{2.24}$$

Since we imposed an equilibrium discharge at the upstream boundary (Eq. 2.5), the morphological change at the upstream boundary is small.

Since morphological change is a slow process that requires a duration in centennial or even millennial time scale, the sediment transport Q_s is multiplied by a factor MorFac (Morphological acceleration factor) to accelerate the morphological process. This allows the model to simulate the morphological change in much shorter time scale than in the actual duration and thereby reduce the computational cost. MorFac was also applied and tested in Delft3D (see Lesser et al., 2004). Furthermore, since the scheme is explicit, the numerical scheme is conditionally stable. The application of MorFac affects the stability condition because it increases the quantity of simulated sediment transport. After the sensitivity test, the condition for numerical stability of the model was found to be

$$MorFac\frac{Q_s}{A}\frac{\Delta t}{\Delta x}\leq 1. \tag{2.25}$$

We chose the largest MorFac value for which the morphology had similar development as for value of 1 and numerical stability was satisfied. For high Shields stress condition, the Morfac value ranges between 18-100 while for low Shields stress condition it ranges between 1000-4000 depending on the time scale required to the morphological equilibrium. The high value for low Shields stress condition is still reasonable range for river systems with uni-directional flow (see Ranasinghe et al., 2011).

2.2.3 Set-up of simulations and determining bifurcation asymmetry

Simulations started with a symmetric condition, with equilibrium bed slope (changes between simulations) and water depth (10 m). To investigate whether this equilibrium condition is stable it was perturbed. We prescribed a depth difference between the downstream channels (which had a length of 1 km), where one downstream channel was slightly deepened (1 cm) and the other was shallowed (1 cm). We simulated the morphological evolution until the system reaches equilibrium again. The discharge asymmetry between downstream channels was calculated using the following equation

$$\Psi_Q=\frac{Q_2-Q_3}{Q_2+Q_3}. \tag{2.26}$$

When the final Ψ_Q equals to zero, both downstream channels have the same discharge, meaning that the perturbed bifurcation has returned to the initial condition and the symmetric bifurcation is stable. When the final Ψ_Q is unequal to zero, discharge in one of the channels is larger than the other, and a new asymmetric equilibrium is found. It means that the symmetric bifurcation is unstable. For the unstable symmetric bifurcations, complete avulsions are indicated by Ψ_Q equals to one (Bolla Pittaluga et al., 2015a; Wang et al., 1995), while approaching unity also indicates avulsion as floodplain processes can take over (Kleinhans et al., 2012).

Using this method, the effect of grain size and channel slope on the stability and asymmetry of bifurcations was investigated. To ensure that our model settings are in the reasonable range, we first

Table 2.1 Parameter settings for the simulations carried out in this study.

set of simulations	simulations	D_{50} (mm)	channel slope (m m^{-1})
Effect of D_{50}	Sand_0.25	0.25	4.5x10^{-5} - 7.2x10^{-4}
	Sand_0.5	0.5	8x10^{-5} - 1.35x10^{-3}
	Sand_1	1	1.4x10^{-4} - 2.3x10^{-3}
	Gravel_5	5	1x10^{-4} - 2.7x10^{-4}
	Gravel_10	10	2.4x10^{-4} - 5.1x10^{-4}
	Gravel_20	20	3.5x10^{-4} - 9x10^{-4}
Effect of channel slope	Slope_5e-4	0.25 - 32	5x10^{-4}
	Slope_1e-4	0.065 - 4	1x10^{-4}
	Slope_3e-5	0.065 - 0.9	3x10^{-5}

studied the variation of grain size and channel slope based on the dataset from 132 rivers worldwide collected by Kleinhans and van den Berg (2011) (Figure 2.3a). Three typical grain sizes for sand and gravel were chosen to represent the stability of bifurcations with fine, medium, and coarse sediment. Each grain size was run for different Shields stress conditions by varying channel slope and thereby river flow. The grain size values, and the range of channel slopes are shown in Table 2.1. Furthermore, to isolate the effect of channel slope, four typical channel slopes were used, and subsequently Shields stress was changed by varying the grain size (see Table 2.1). Both sets of simulation were repeated for a width-to-depth (w/h) ratio of 10 and 30 for the upstream channel. To keep the flow condition to be the same for both values of w/h, only the width of the channel was changed.

We kept all other parameters constant. For the roughness, we used a Chézy coefficient of 40 m$^{1/2}$s^{-1}. Thus, the roughness length ξ in Eq. 2.3 is 0.0656h. According to the dataset from Kleinhans and van den Berg (2011), only a weak relation between Chézy, sediment grain size and channel slope is present and the entire range of channel slope and sediment grain size considered in this study shows a similar Chézy value (Figure 2.3b and Figure 2.3c). Furthermore, for the other parameters, we used the value of 3 for α (in Eq. 2.10, Eq. 2.11 and Eq. 2.12) and 0.5 for r (in Eq. 2.10 and Eq. 2.12), respectively.

2.3 Results

2.3.1 Comparison of model results with nature and Bolla Pittaluga et al. (2015a)

To compare 1D model results with nature, we simulated the morphological development of bifurcations with the settings observed in Columbia River (Kleinhans et al., 2012) and Cumberland Marshes, Saskatchewan River, Canada (Bolla Pittaluga et al., 2015a). The results show that the bifurcations have asymmetric equilibrium configuration, both in the model and observed (Figure 2.4). For the Columbia River, the discharge asymmetry of the model and dataset are very similar. For the Cumberland marshes there is good correspondence between model and data for the bifurcations with large asymmetry, but significant difference for the intermediate values. For the cases that the model over-predicts the asymmetry (Delta 1 and Delta 3 in Figure 2.4), these differences can be caused by non-equilibrium morphology of the observed bifurcations and hardly erodible layers below the bed (as reported in Appendix 2 in Bolla Pittaluga et al. (2015a). However, for one observed bifurcation the model significantly underestimates the asymmetry (Smith1 Island in Figure 2.4). The discrepancies are due to meandering of the upstream channel or large angle between upstream and one of the downstream channels (close to 90 degrees), resulting in more asymmetric downstream channels.

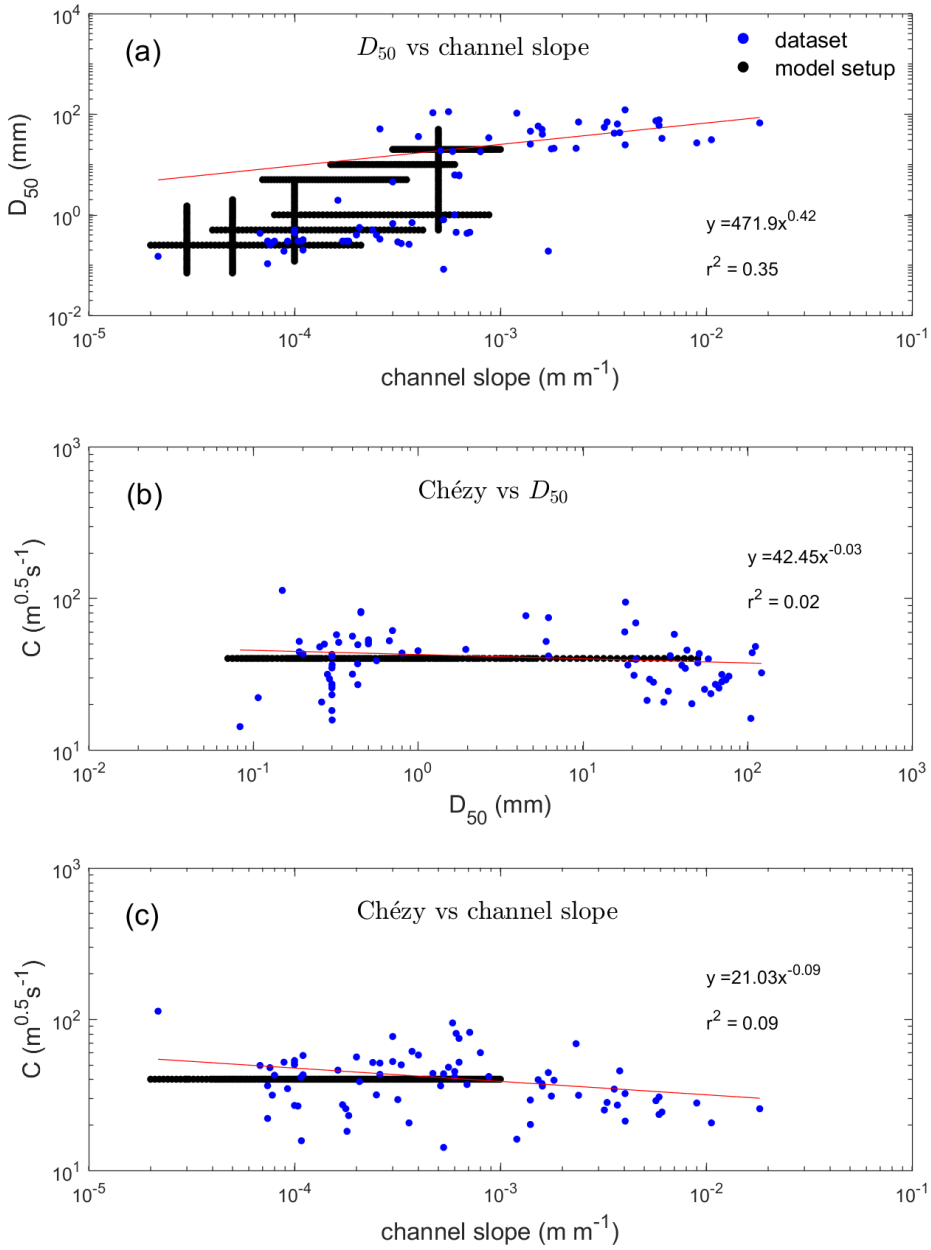

Figure 2.3 Scatter plot and fit between (a) Sediment grain size and channel slope, (b) Chézy coefficient and sediment grain size, and (c) Chézy coefficient and channel slope based on dataset from 132 rivers worldwide from Kleinhans and van den Berg (2011) overlaid by the model settings in Table 2.1 and Chézy coefficient.

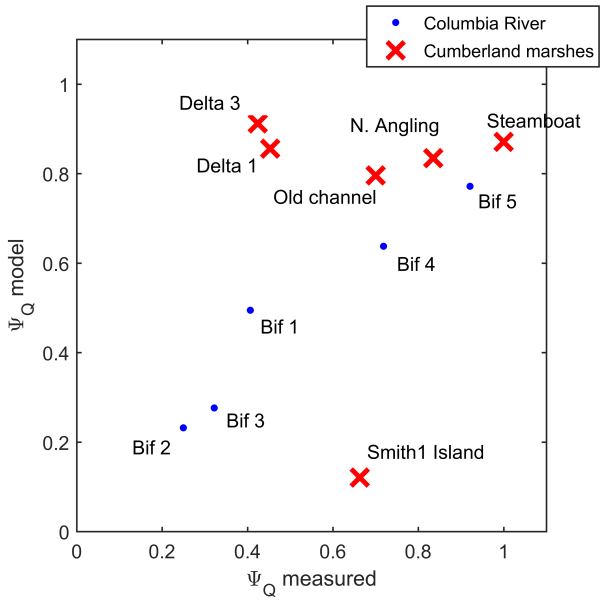

Figure 2.4 Discharge asymmetry from the model results and datasets obtained from Kleinhans et al. (2012) for Columbia River (blue dot) and Bolla Pittaluga et al. (2015a) for Cumberland marshes (red cross).

A series of simulations was run using the same settings as used in Bolla Pittaluga et al. (2015a) that applies EH for sediment transport to observe whether the developed 1D model can reproduce their results. We applied EH for this comparison because this sediment transport predictor depends on fewer parameterizations than vRijn reducing the model setup differences between our model and Bolla Pittaluga et al. (2015a) that may cause different results. As a result, the differences that occur between models is only due to numerical reasons. Bolla Pittaluga et al. (2015a) prescribed a single value of grain size (0.275 mm) and they varied the channel slope to simulate different Shields stress condition. Our 1D model shows similar results with Bolla Pittaluga et al. (2015a) regarding the transition between stable and unstable symmetric bifurcations (Figure 2.5). The differences between model are only in the discharge asymmetry value in high Shields stress but it is negligible. This shows that the 1D model is capable to confirm the previous findings regarding the stability of bifurcations.

2.3.2 Effect of grain size and channel slope

The stability of bifurcations clearly depicts a sensitivity to grain size (Figure 2.6a-d). Finer sands and gravels tend to have a smaller range of sediment mobility conditions for which symmetric bifurcations are stable. For sand and width-to-depth ratio of 10, the critical transition of the stability for the grain size of 0.25 mm occurs around Shields stress of 0.3 while it occurs around 0.5 and 0.8 for a grain size of 0.5 and 1 mm, respectively. With width-to-depth ratio of 30 only the set of simulations with grain size of 1 mm still has a limited range of stable symmetric conditions while the other grain sizes show that symmetric bifurcation is unstable for all Shields stress conditions. Meanwhile for gravel rivers, although the critical transition differences between grain sizes are small for width-to-depth ratio of 10, the same behaviour with sandy rivers occurs in which the finer gravels result in wider condition for unstable symmetric bifurcations. This behaviour is more obvious for the case of larger width-to-depth ratio (w/h 30).

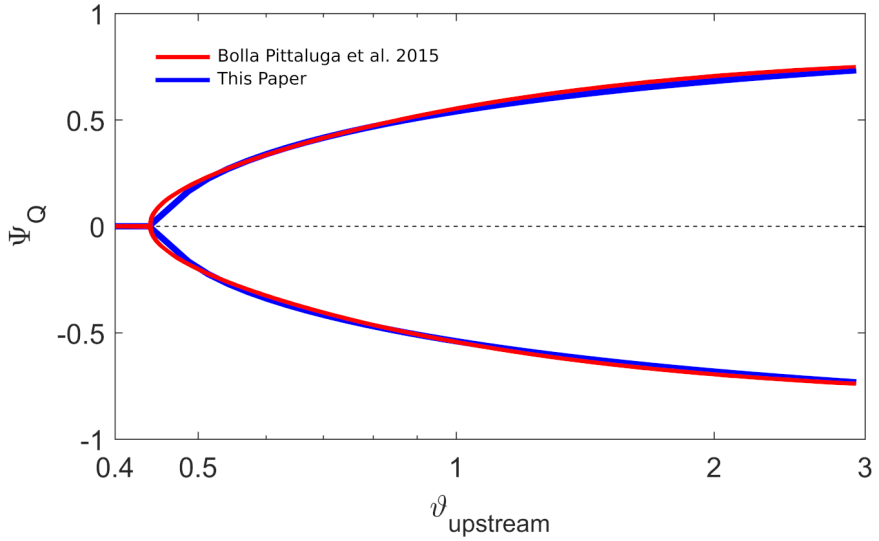

Figure 2.5 Stability of bifurcation as a function of total Shields stress from 1D model (solid red line) and from Bolla Pittaluga et al. (2015a) (solid blue line) using the same configuration for the width-to-depth ratio of 30, sediment transport by EH, $alpha$= 3 and r= 0.5.

There is also a clear effect of channel slope to the stability of bifurcations, as shown in Figure 2.6e and Figure 2.6f. The stable symmetric bifurcations in the intermediate range of Shields stress are more limited for gentler channel slope. In the most extreme case, for the width-to-depth ratio of 30, no stable symmetric bifurcations occur for the entire range of Shields stress. Surprisingly, we found another Shields stress range in which stable symmetric bifurcations occur in the high Shields stress regime. However, this condition only occurs for the systems with a small width-to-depth ratio on the very lower end of typical values found in nature, and for a more typical width-to-depth ratio of 30 this stable symmetric solution does not occur. For the set of simulations with channel slope of $1x10^{-4}$ and $3x10^{-5}$ the simulations are conducted until the finest sediment size for sand. Therefore, this results in a smaller maximum Shields stress than for the set of simulations with the steepest channel slope.

2.4 Discussion

2.4.1 Effect of suspended load transport on transverse sediment transport and bifurcation asymmetry

Symmetric bifurcations are stable for intermediate Shields stress as expected from Bolla Pittaluga et al. (2015a), but the transition from stable symmetric to asymmetric bifurcations differs considerably between runs. We found that the transition depends strongly on grain size and on slope (Figure 2.6), despite the fact that both are already incorporated in the dimensionless Shields stress.

The shift of stability transition for different sediment grain size and channel slope is caused by the different ratio of suspended load transport over the bedload transport for similar Shields stress (see Figure 2.1). A larger fraction of total load transport is caused by suspended load transport for finer sediments. For the effect of channel slope, a smaller channel slope requires finer sediment to have the same Shields stress and therefore results in a larger suspended load fraction. The stable symmetric bifurcation can occur when the transverse sediment transport is sufficient to increase the difference

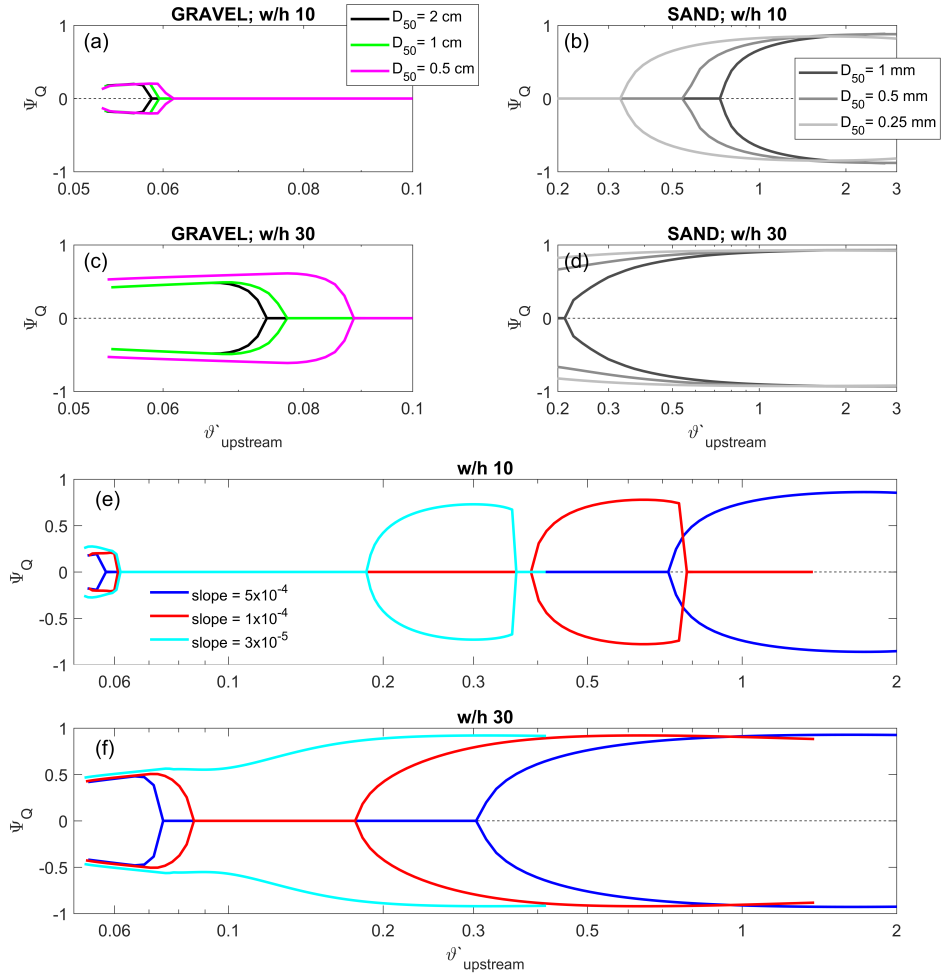

Figure 2.6 Stability of bifurcations as a function of grain-related Shields stress for sand and gravel bed river for a different grain size with width-to-depth ratio of 10 and 30 ((a) and (b)), and different channel slope with width-to-depth ratio of 10 and 30 ((c) and (d)). In panel (a)-(d), Shields stress was varied by changing the bed slope (and thereby flow velocity), while in panel (e) and (f) it was varied by changing the grain size.

of sediment supply to the downstream channels until it is larger than the difference of sediment transport capacity. In the intermediate range of Shields stress, where the bifurcations are stable in symmetric condition, the transverse sediment transport is smaller for the case with higher contribution of suspended load transport, because of the absence of a transverse bedslope effect for suspended load. As a result, the difference of sediment supplies between downstream channel decreases and therefore the Shields stress range where it can balance the difference of sediment transport capacity also decreases.

The stability that occurs in the high Shields stress range for small channel slopes is caused by the very fine sand required for high Shields stress. As a result, even though bedload transport drives a low transverse sediment transport, the suspended load is sufficiently large to drive a high transverse

sediment transport. This results in a higher sediment supply difference than the capacity (Figure 2.7), driving a stable bifurcation as shown in Figure 2.6.

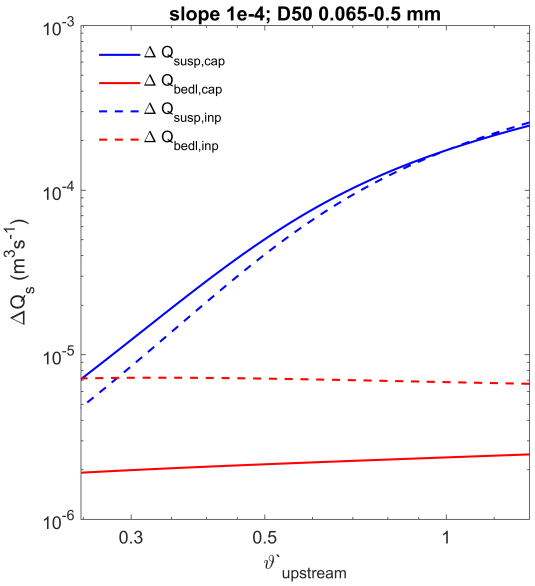

Figure 2.7 Sediment supply (dashed line) and capacity (solid line) difference for suspended load (blue) and bedload (red) transport between downstream channel in the initial condition for w/h= 10 and S= 1x10^{-4}.

2.4.2 Effect of sediment transport and nodal point relations

As argued in the introduction, the stability transition is also related to the sediment transport predictor used. We therefore also studied sensitivity of the results to grain size and bed slope using the EH sediment transport predictor. The results presented in Figure 2.8a,b show that results are insensitive to channel slopes and grain sizes when using the EH predictor. Irrespective of how Shields stress is changed, by either changing flow velocities through bed slope or by changing the grain size, it yields the same equilibrium and stability of the bifurcation. This is explained by the fact that EH sediment transport predictor is only a function of Shields stress, and not directly depends on grain size or bed slope.

By using the EH sediment transport predictor, also the nodal point relation is affected. For the transverse sediment transport, the suspended load and bedload transport are not treated separately. Therefore, both are subject to a transverse bed slope effect. When this approach is applied with vRijn, this makes symmetric bifurcations more stable for a wider range of Shields stress conditions (Figure 2.8c). We adapted the nodal point relation such that the transverse bed slope term also applied to the suspended load part (combined relation in Figure 2.8c). Hence, we used Eq. 2.12 together with the van Rijn sediment transport predictor. Applying the transverse bedslope effect in the nodal point relationship to the suspended load part results in the higher Shields stress for stability transition and less asymmetric equilibrium in the Shields stress range in which bifurcations are asymmetric. As the transverse bedslope effect opposes the asymmetric bed level development between downstream channel, applying the transverse bedslope effect to suspended load transport enhances the opposing mechanism against the asymmetry.

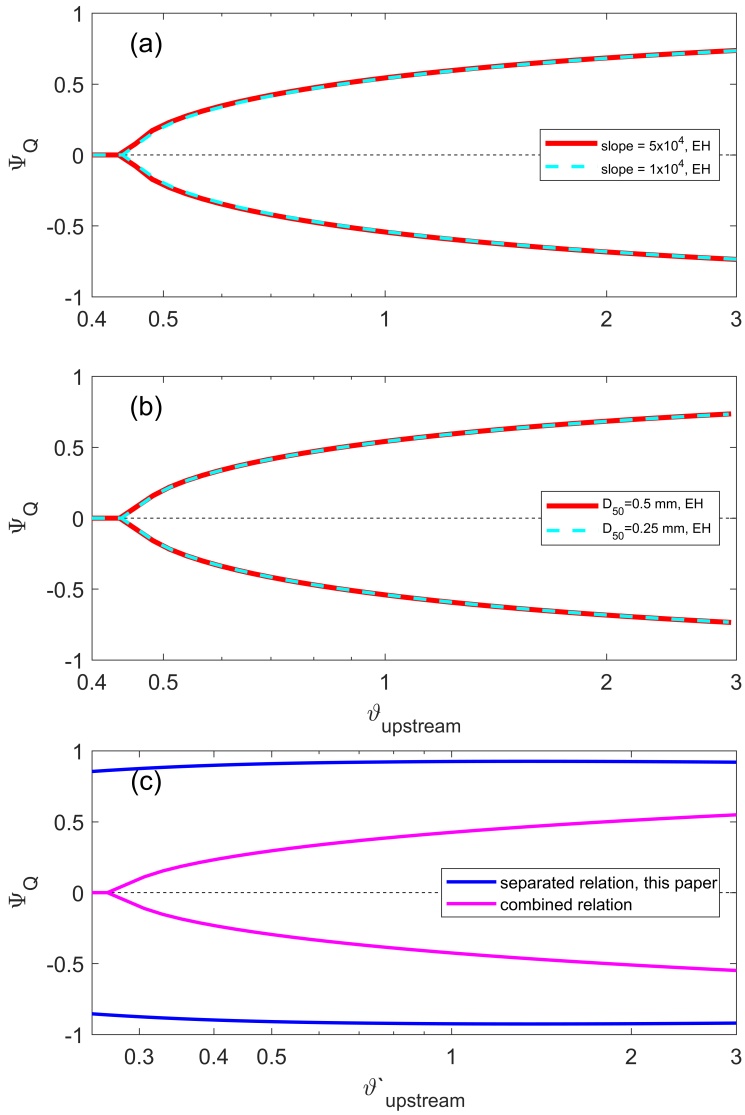

Figure 2.8 Stability of bifurcations using EH as a function of total Shields for (a) channel slope of 5x10^{-4} (red solid line) and 1x10^{-4} (cyan dashed line), (b) D_{50}=0.5 mm (red solid line) and D_{50}= 0.25 mm (cyan dashed line) (c) using vRijn as a function of grain-related Shields stress for the case D_{50}=0.25 mm that applies in this paper (separated relation, solid blue line) and applies the transverse bedslope effect to the suspended load transport (combined relation, solid magenta line).

Besides the dependence of the sediment transport, the stability transition is also related to the parameterization in the sediment transport. In vRijn, the quantity of suspended load transport depends on the reference height (see z_a in Eq. 2.49 in Appendix 2B) interpreted as the maximum height of bedload transport layer above the riverbed. The sediment transport above this height is defined as suspended load transport. It is related to the bedforms (van Rijn, 2007) but when it is not

known the minimum value is 0.01h (van Rijn, 1984b). The choice of the reference height affects the quantity of suspended load transport because it determines the suspended sediment transport quantity. Figure 2.9 shows the results using the default z_a (0.0656h) and z_a=0.01h as suggested for the minimum value by van Rijn (1984b). The result shows that a smaller reference height results in wider range of unstable symmetric bifurcation. This is because the suspended load is higher when smaller z_a is defined. The smaller z_a results in a larger predicted reference suspended load concentration at z_a and therefore higher suspended sediment transport.

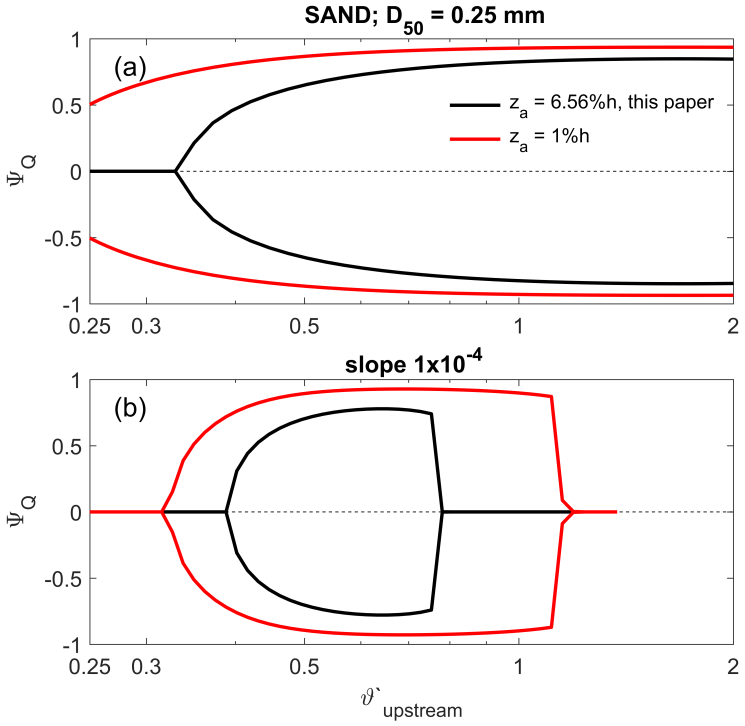

Figure 2.9 Stability of bifurcations as a function of grain-related Shields stress for different reference height (z_a) for suspended load transport for the case with (a) D_{50} = 0.25 mm and (b) channel slope of 1x10^{-4}. All parameters beside z_a had default values and w/h=10.

In this study, we applied grain-related Shields stress to determine the transverse bedslope effect in the nodal point relationship as suggested by Baar et al. (2018), while previous studies applied total Shields stress (e.g. Bolla Pittaluga et al., 2003; Bolla Pittaluga et al., 2015a; Kleinhans et al., 2008). These different approaches result in different stability transition because, for the systems with the same settings, grain-related Shields stress is always smaller than total Shields stress. As a result, when the total Shields stress was applied, the bedslope term is smaller than when the grain-related one was applied as shown in Figure 2.10. Furthermore, Baar et al. (2018) showed that for high Shields stress the power of sediment mobility in transverse bedslope effect is smaller than 0.5. This results in almost constant value of $r\sqrt{\vartheta'}$ in Eq. 2.10 where the value of 0.5 was applied in Figure 2.10. The stability of bifurcations with these three different approaches is compared in Figure 2.11. The smallest transverse bedslope term with total Shields stress induces the smallest transverse sediment transport compared to other approaches. This results in the smallest range of stable symmetric conditions, or even absence of it,

while our approach results in the widest range. With constant $r\sqrt{\vartheta'}$, this term becomes a callibrated parameter in which symmetric bifurcations will be stable in wider range of Shields stress when a higher constant is applied.

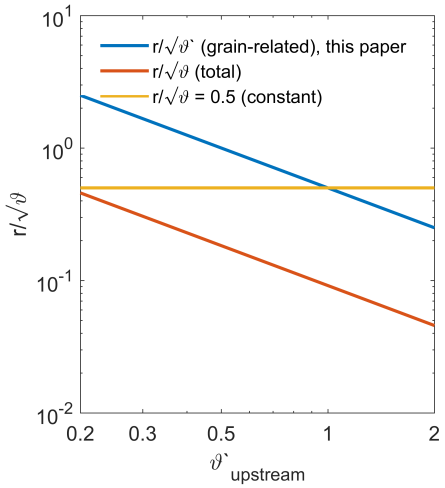

Figure 2.10 constant r over the square root of sediment mobility as a function of grain-related Shields stress for three different approaches to calculate transverse bedslope effect.

2.4.3 implications

Our findings show that beside the meandering of upstream channel (Kleinhans et al., 2008) and width-to-depth ratio of the channel (Bolla Pittaluga et al., 2015a; Redolfi et al., 2019), the typical landscapes and sediment properties in channel networks also considerably controls the stability of bifurcations. The effect of smaller sediment grain size and gentler channel slope to cause instability of symmetric bifurcations also implies that asymmetric bifurcations will occur for a larger range of conditions than previously suggested by Bolla Pittaluga et al. (2015a) and Redolfi et al. (2019). By implication, avulsion can also occur for a larger range of conditions. Lower channel slopes are found in the more downstream part of river systems (Pitlick and Cress, 2002) such as lowland rivers and deltas, which usually also have finer sediment (Figure 2.3). Therefore, the occurrence of asymmetric bifurcations and avulsion would be higher in the more downstream part of river systems.

In deltas where the rivers debouch in a lake or sea, several processes oppose the asymmetric development of bifurcations. First, the switching downstream channel lengthening could oppose the channel avulsions (Salter et al., 2017). The initial asymmetry between downstream channels results in the large amount of sediment transported in the dominant downstream channel to the sea or lake. The deposited sediment sinks results in delta progradation seaward and lengthens the dominant channel until it becomes longer than the other channel. Then the sediment transport capacity in the other channel becomes higher than in the lengthened channel. As a result, the other channel lengthens. This switching behaviour keeps both channels to remain open and convey the river flow. The process is more likely to occur when the channels lengthen fast without filling all the accommodation space (Salter et al., 2017). Second, tides may oppose the development towards asymmetry, such as obvious in the Berau River Delta (Buschman et al., 2013) and the Mahakam Delta (Sassi et al., 2013; Sassi et al., 2011). Even in the systems with small tides where tides only cause a

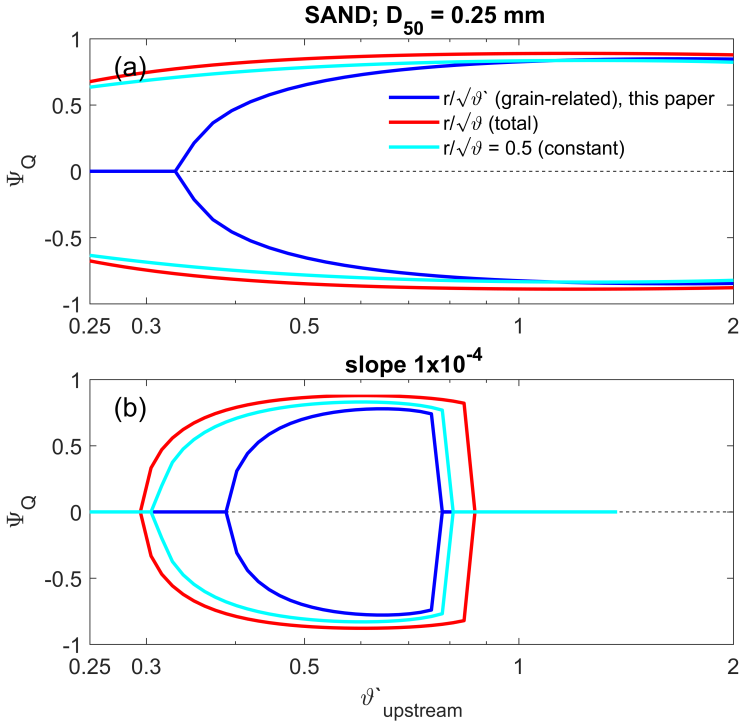

Figure 2.11 Stability of bifurcations for different sediment mobility for different choices of the transverse bedslope effect for the case with (a) D_{50}=0.25 mm and (b) channel slope of 1x10^{-4}.

change in flow magnitude and not direction, Ragno et al. (2020) found that the conditions of stable symmetric bifurcations are larger for the systems with larger tidal amplitude. Iwantoro et al. (2020) also found that the less asymmetric bifurcations occur in the more tide influence systems (presented in chapter 3).

2.4.4 Model limitations

Despite the general findings that explain the observed stability or instability of bifurcations in the various fluvial landscapes, the model neglects some physical processes. The model only accounts for the evolution of the river bed while in nature the river width also evolve to adjust the flow condition (Kleinhans et al., 2010). The evolving channel banks enlarge the range of conditions with instability of bifurcations and increases the possibility of avulsion (Miori et al., 2006; Kleinhans et al., 2011). Including the evolving banks in the model likely results in larger range of Shields stress conditions for which the bifurcation is unstable than in the present results. Another factor is the presence of transverse bedslope induced diffusive transport of suspended sediment (Biswas et al., 2015; Hepkema et al., 2019). In the model we assumed that the suspended load transverse transport at the bifurcation is only driven by the flow induced by asymmetrical discharge division. In nature, a diffusive cross-channel suspended load transport also occurs due to different depth in cross section at the bifurcation and difference in sediment concentration. This diffusion-induced sediment transport mechanism may lead to two opposed effects. First, since the deeper downstream channel receives higher river flow and therefore has higher sediment concentration, diffusion induces transverse

sediment transport from the deep channel to the shallow channel. As a result, this leads to asymmetric morphological development between downstream channels resulting in a wider Shields stress condition for asymmetric bifurcations because the sediment supply to both downstream channels becomes less asymmetric. Second, an opposing mechanism to the asymmetrical development of bifurcations may also occur due to the nonuniform distribution of sediment over the vertical. A transverse depth difference at an asymmetric bifurcation (as we imposed in the initial condition) will therefore result in a cross-channel concentration gradient. For the same vertical level, it is closer to the bed on the side of the shallower channel than on the side of the deeper channel, and combined with the vertical concentration profile, this will result in a diffusive sediment flux from the shallow to the deep side where lower concentration will occur on the deeper side. This induces transverse sediment transport to the side of deep channel resulting in the same effect as the transverse bedslope effect for bedload transport, as shown by Hepkema et al. (2019) for tidal bar formations in estuaries. Which of these effects dominates in lowland river bifurcations is presently unknown, but it is plausible that the range of stable bifurcations is closer to the model results in this paper than under the assumption of bed slope effects applied to the suspended load component. In other words, symmetrical bifurcations in lowland rivers with fine sand (without tides) are more likely to be unstable than hitherto thought.

2.5 Conclusions

In this study we applied a 1D model to investigate the stability of river bifurcations for different sediment size and channel slope conditions that represents various channel networks in different landscapes along the river stream. A significantly larger range of conditions for asymmetric bifurcations than previously thought was found for lowland rivers, which typically have fine sediment and gentle channel slope. Apart from Shields stress, sediment grain size and channel slope directly affect the quantity of sediment transport and determine the quantity of transverse sediment transport at bifurcation as a factor to compensate the asymmetrical sediment transport capacity in the downstream channels. Lastly, in high Shields stress conditions, suspended sediment transport induces asymmetric bifurcation by reducing the relative contribution of transverse bedslope effect to balance the sediment distribution to the downstream channels. However, when the suspended load is sufficiently large due to the existence of fine sand in the systems with small width-to-depth ratio, the transverse flow can compensate the instability to the symmetric bifurcation resulting in a stable symmetric bifurcation in high Shields stress condition.

2.6 Appendix 2A

2.6.1 Preissmann Scheme for hydrodynamic simulations

Eq. 2.1 and Eq. 2.2 were solved numerically using Preissmann scheme. The advantage of this scheme is that it allows the computation of discharge and water level at the same node. The scheme uses values from nodes (i,j),$(i+1,j)$,$(i,j+1)$ and $(i+1,j+1)$ to discretise the Saint-Vennant equations such that i and j are notations representing the node number in space and time, respectively.

Eq. 2.1 was modified to apply Preissmann scheme expressed by:

$$w_{i+1/2}\left(\frac{\left(z_{i+1}^{j+1}-z_{i+1}^{j}\right)+\left(z_{i}^{j+1}-z_{i}^{j}\right)}{2\Delta t^{j}}+\frac{\theta\left(Q_{i+1}^{j+1}-Q_{i}^{j+1}\right)+(1-\theta)\left(Q_{i+1}^{j}-z_{i}^{j}\right)}{2\Delta x_{i}}\right)=0$$

$$\leftrightarrow \frac{w_{i+1/2}}{2\Delta t^{j}}z_{i+1}^{j+1}+\frac{w_{i+1/2}}{2\Delta t^{j}}z_{i}^{j+1}+\frac{\theta}{\Delta x_{i}}Q_{i+1}^{j+1}-\frac{\theta}{\Delta x_{i}}Q_{i}^{j+1}=$$

$$\frac{w_{i+1/2}}{2\Delta t^{j}}z_{i+1}^{j}+\frac{w_{i+1/2}}{2\Delta t^{j}}z_{i}^{j}+\frac{1-\theta}{\Delta x_{i}}Q_{i}^{j}-\frac{1-\theta}{\Delta x_{i}}Q_{i+1}^{j} \tag{2.27}$$

i, j and i+1 are known while $j+1$ is at the next time step and therefore unknown. $\theta \geq 0.5$ is weighing coefficient for space derivatives. θ=0.5 is the solution for central approximation so called box scheme. If θ=1 the solution is fully implicit. The accuracy of Preissmann scheme decreases as the increasing θ from 0.5 to 1. However, θ=0.5 may result in numerical oscillation. Thus, the value 0.55$\leq \theta \leq$0.6 was often used (Islam et al., 2003). In this study, we use θ=0.56. Other advantage features of Preissmann scheme us the scheme are unconditionally stable as long as θ≥0.5 and the space interval between the x axes can be variable (Chau, 1990). Thus the time step can be chosen freely to give sufficient accuracy or reduce the computational cost, and, in terms of spatial axes, this scheme allows a more flexible placement of cross sections. Furthermore, width between nodes $\left(w_{i+1/2}\right)$ is computed as

$$w_{i+1/2}=\frac{w_{i}+w_{i+1}}{2}. \tag{2.28}$$

Thus Eq. 2.27 becomes

$$C1z_{i+1}^{j+1}+C1z_{i}^{j+1}+D1Q_{i+1}^{j+1}-D1Q_{i}^{j+1}=E1 \tag{2.29}$$

in which $C1$, $D1$ and $E1$ are known variables:

$$\begin{aligned} C1&=\frac{b_{i+1/2}}{2\Delta t^{j}}\\ D1&=\frac{\theta}{\Delta x_{i}}\\ E1&=\frac{b_{i+1/2}}{2\Delta t^{j}}z_{i+1}^{j}+\frac{b_{i+1/2}}{2\Delta t^{j}}z_{i}^{j}+\frac{1-\theta}{\Delta x_{i}}Q_{i}^{j}+\frac{1-\theta}{\Delta x_{i}}Q_{i+1}^{j}. \end{aligned} \tag{2.30}$$

The same rearrangement was also applied for Eq. 2.2

$$\frac{\left(Q_{i+1}^{j+1}-Q_{i+1}^{j}\right)+\left(Q_{i}^{j+1}-Q_{i}^{j}\right)}{2\Delta t^{j}}+\frac{1}{\Delta x_{i}}\theta\left(\frac{Q_{i+1}^{j}Q_{i+1}^{j+1}}{A_{i+1}^{j}}-\frac{Q_{i}^{j}Q_{i}^{j+1}}{A_{i}^{j}}\right)+\frac{1}{\Delta x_{i}}(1-\theta)\left(\frac{\left(Q_{i+1}^{j}\right)^{2}}{A_{i+1}^{j}}-\frac{\left(Q_{i}^{j}\right)^{2}}{A_{i}^{j}}\right)$$

$$+gA_{i+1/2}^{j+\theta}\frac{\theta\left(z_{i+1}^{j+1}-z_{i}^{j+1}\right)+(1-\theta)\left(z_{i+1}^{j}-z_{i}^{j}\right)}{\Delta x_{i}}$$

$$+\frac{1}{2}\frac{1}{C^{2}}\left(\frac{|\,Q_{i}^{j}\,|\,Q_{i}j+1P_{i}^{j}}{(A^{2})_{i}^{j+1/2}}+\frac{|\,Q_{i+1}^{j}\,|\,Q_{i+1}j+1P_{i+1}^{j}}{(A^{2})_{i+1}^{j+1/2}}\right)=0. \tag{2.31}$$

All multiplications in the equation with known variables are moved to the right hand side of the equation. Eq. 2.31 becomes

$$C2z_{i+1}^{j+1} + C2z_{i+1}^{j} + D2Q_{i+1}^{j+1} + E2Q_{i}^{j+1} = F2 \tag{2.32}$$

in which $C2$, $D2$, $E2$ and $F2$ is known variables as follow

$$\begin{aligned}
C2 &= \frac{gA_i^{j+\theta}\theta}{\Delta x_i} \\
D2 &= \frac{1}{2\Delta t^j} + \frac{\mid Q_{i+1}^j \mid P_{i+1}^j}{2\left(A^2\right)_{i+1}^{j+1/2}} \\
E2 &= \frac{1}{2\Delta t^j} + \frac{\mid Q_{i}^j \mid P_{i}^j}{2\left(A^2\right)_{i}^{j}} \\
F2 &= \frac{1}{2\Delta t^j}Q_{i+1}^j + \frac{1}{2\Delta t^j}Q_i^j - \frac{gA_i^{j+\theta}(1-\theta)}{\Delta x_i}\left(z_{i+1}^j - z_i^j\right) \\
&- \frac{1}{\Delta x_i}(1-\theta)\left(\frac{\left(Q_{i+1}^j\right)^2}{A_{i+1}^j} - \frac{\left(Q_i^j\right)^2}{A_i^j}\right).
\end{aligned} \tag{2.33}$$

To solve Eq. 2.29 and Eq. 2.32, the value of z and Q at the open and junction boundaries of each channel should be initially known. For open boundaries, the water level at downstream open boundaries and the discharge at upstream open boundaries for all time levels should be prescribed. in contrast, Q^{j+1} and z^{j+1} at the junction is unknown. Their value cannot be self-defined because their magnitude depends on the condition imposed from external boundary and therefore the condition at the node next to the junction. To overcome this problem, double sweep Thomas algorithm is applied. First, the substitution of Q_i and Q_{i+1} Eq. 2.29 and therefore Eq. 2.32 results in

$$\begin{aligned}
z_i^{j+1} &= MMQ_{i+1}^{j+1} + NN + MNz_{i+1}^{j+1} \\
z_{i+1}^{j+1} &= LLQ_i^{j+1} + ML + NLz_i^{j+1}.
\end{aligned} \tag{2.34}$$

The coefficients in Eq. 2.34 are

$$\begin{aligned}
MM &= \frac{1 + \frac{D2}{E2}}{\frac{C2}{E2} - \frac{C1}{D1}} \\
NN &= \frac{-\frac{F2}{E2} - \frac{E1}{D1}}{\frac{C2}{E2} - \frac{C1}{D1}} \\
MN &= \frac{\frac{C2}{E2} - \frac{C1}{D1}}{\frac{C2}{E2} - \frac{C1}{D1}} \\
LL &= \frac{-1 - \frac{E2}{D2}}{\frac{C2}{D2} - \frac{C1}{D1}} \\
ML &= \frac{\frac{F2}{D2} + \frac{E1}{D1}}{\frac{C2}{D2} - \frac{C1}{D1}} \\
NL &= \frac{\frac{C2}{D2} + \frac{C1}{D1}}{\frac{C2}{D2} - \frac{C1}{D1}}
\end{aligned} \tag{2.35}$$

.

To correlate the hydrodynamic condition at all nodes with the boundary conditions, Eq. 2.34 are rewritten as

$$
\begin{aligned}
Q_{i+1}^{j+1} &= K_{i+1} z_{i+1}^{j+1} + M_{i+1} + N_{i+1} z_1^{j+1} \\
Q_i^{j+1} &= KK_i z_i^{j+1} + MK_{i+1} + NK_i z_{N+1}^{j+1}
\end{aligned}
\tag{2.36}
$$

.

The coefficients in Eq. 2.36 are defined as follow

$$
\begin{aligned}
K_{i+1} &= \frac{-(C1 + C1MN - D1K_iMN)}{C1MM + D1 - D1K_iMM} \\
M_{i+1} &= \frac{-C1NN + D1K_iNN + D1M_i + E1}{C1MM + D1 - D1K_iMM} \\
N_{i+1} &= \frac{D1N_i}{C1MM + D1 - D1K_iMM} \\
KK_i &= \frac{C1NL + C1 + D1KK_{i+1}NL}{D1 - C1LL - D1KK_{i+1}LL} \\
MK_i &= \frac{C1ML + D1KK_iML + D1MK_{i+1} - E1}{D1 - C1LL - D1KK_{i+1}LL} \\
NK_i &= \frac{D1NK_{i+1}}{D1 - C1LL - D1KK_{i+1}LL}.
\end{aligned}
\tag{2.37}
$$

Finally, the relationship between upstream and downstream boundary of each channel is

$$
\begin{aligned}
Q_{N+1}^{j+1} &= K_{N+1} z_{N+1}^{j+1} + M_{N+1} + N_{N+1} z_1^{j+1} \\
Q_1^{j+1} &= KK_1 z_1^{j+1} + MK_{N+1} + NK_1 z_{N+1}^{j+1}
\end{aligned}
\tag{2.38}
$$

From the correlation among Eq. 2.5, Eq. 2.38, and water level prescribed at downstream open boundaries Q^{j+1} and z^{j+1} at the boundaries of all connected channels can be solved simultaneously using tridiagonal matrix system applied in Thomas Algorithm. Finally, after Q^{j+1} and z^{j+1} at all boundaries are known, Q^{j+1} and z^{j+1} at all in-channel nodes are calculated sequentially from downstream to upstream using Eq. 2.34 and Eq. 2.36.

2.7 Appendix 2B

2.7.1 Sediment transport equation by van Rijn (1984a) and van Rijn (1984b)

In vRijn, the non-dimensional bedload is calculated by

$$\phi_{bedl} = 0.1T^{1.5}D_*^{-0.3}. \tag{2.39}$$

D_* is Bonnefille number to express a non-dimensional sediment grain size given by

$$D_* = D_{50}\sqrt{\frac{\left(\frac{\rho_s}{\rho_w} - 1\right)g}{\nu^2}}. \tag{2.40}$$

ν is kinematic viscosity of water as 4x10^{-5}/(20+$temp$) where $temp$ is water temperature in ^{o}C. In Eq. 2.39, T is the Shields number fraction with respect to the Shields number threshold for incipient motion (ϑ_{crit} = 0.047) given by

$$T = \frac{\vartheta' - \vartheta_{crit}}{\vartheta_{crit}}. \tag{2.41}$$

ϑ' is grain-related Shields stress according to Eq. 2.15. Finally, bedload flux is calculated as

$$Q_{bedl} = \phi_{bedl} w\sqrt{\left(\frac{\rho_s}{\rho_w} - 1\right)gD_{50}}. \tag{2.42}$$

In van Rijn (1984b), the non-dimensional suspended load is calculated by

$$\phi_{susp} = \frac{f_{cs}uhC_a}{\sqrt{\left(\frac{\rho_s}{\rho_w} - 1\right)gD_{50}}}. \tag{2.43}$$

Thus, the suspended sediment flux is calculated as

$$Q_{susp} = f_{cs}uhC_a \tag{2.44}$$

where u is flow velocity and h is water depth. f_{cs} is a shape factor for the vertical distribution of suspended sediment concentration, parameterized by

$$\begin{aligned} f_{cs} &= \begin{cases} f_{cs,0}, & z_c \neq 1.2 \\ f_{cs,1}, & z_c = 1.2 \end{cases} \\ f_{cs,0} &= \frac{\left(\frac{z_a}{h}\right)^{z_c} - \left(\frac{z_a}{h}\right)^{1.2}}{(1.2 - z_c)\left(1 - \frac{z_a}{h}\right)^{1.2}} \\ f_{cs,1} &= \left(\frac{\frac{z_a}{h}}{1 - \frac{z_a}{h}}\right)^{1.2} \ln\frac{z_a}{h}. \end{aligned} \tag{2.45}$$

Here, z_a is the reference height for suspended load transport measured from the bed. It is interpreted as the threshold to distinguish bedload and suspended load transport where sediment transport above this height is defined as suspended load transport while below this height is defined as bedload transport. Meanwhile, z_c is interpreted as the Rouse suspension number

$$z_c = \min\left(20, \frac{w_s}{\beta\kappa u_*}\right) \tag{2.46}$$

where w_s is sediment settling velocity. The Van Rijn settling velocity predictor consists of three separate functions depending on the grain size with breaks between them. Here we used the similar but continuous settling velocity predictor by Soulsby (1997) to keep the settling velocity continuous for different D_{50} and thereby Shields stresses in the results. The equation is given as

$$w_s = \frac{\nu}{D_{50}}\left(\sqrt{10.36^2 + 1.01D_*^3} + 10.36\right) \tag{2.47}$$

β is coefficient to represent the ratio between the sediment water diffusion with the value of 1, κ is von Karman constant with the value of 0.4 and u_* is bed-shear velocity given as

$$u_* = uC. \tag{2.48}$$

C is nondimensionalized total Chézy coefficient. In Eq. 2.43 and Eq. 2.44, C_a is the reference concentration at elevation z_a calculated by

$$C_a = 0.015\frac{D_{50}}{z_a}\frac{T^{1.5}}{D_*^{0.3}}. \tag{2.49}$$

2.7.2 Sediment transport equation by Engelund and Hansen (1967)

EH directly compute total transport where its non-dimensional value is calculated by

$$\psi_s = \frac{0.05C^2}{g}\vartheta^{2.5} \tag{2.50}$$

and the total sediment flux is

$$Q_s = \phi_s w\sqrt{\left(\frac{\rho_s}{\rho_w} - 1\right)gD_{50}}. \tag{2.51}$$

2.7.3 Notation

A	cross section area of the channel
C_a	reference concentration
D_*	Bonnefille number for sediment grain size
C	Total Chézy coefficient
C	grain-related Chézy coefficient
D_{50}	median diameter of sediment
f_{cs}	vertical distribution of suspended load for sediment transport equation
g	gravitational acceleration
h	water depth
i	notation for spatial node number
j	notation for temporal node number
P	wetted perimeter of the channel cross section
p	sediment porosity
Q	water discharge
Q_{bedl}	bedload flux
$Q_{bedl,y}$	transverse bedload flux at bifurcation
Q_s	total sediment load
Q_{susp}	suspended load flux
$Q_{susp,y}$	transverse suspended load flux at bifurcation
Q_y	transverse water discharge
r	empirical constant for transverse bed slope effect
S	channel slope
T	dimensionless bed shear stress parameter
t	time
$temp$	water temperature in ^{o}C
u	flow velocity
u_*	bed-shear velocity
w	channel width
w_s	sediment settling velocity
x	spatial coordinate in streamwise direction
y	spatial coordinate in transverse direction
z	water level
z_a	reference height from the riverbed to indicate bedload layer thickness
z_c	Rouse number
α	dimensionless length of the downstream end of upstream channel
β	ratio of sediment and fluid diffusion coefficient for sediment transport equation
ΔQ_s	sediment transport difference between downstream channels
Δx	space interval
Δt	time interval
η	bed level
ϑ	total Shields stress
ϑ'	grain-related Shields stress
ϑ_{crit}	critical Shields stress for incipient of sediment motion
κ	von Karman constant
μ	efficiency factor for grain-related Shields stress
ν	kinematic viscosity of water
ξ	Nikuradse roughness length related to the bedform
ρ_s	sediment density
ρ_w	water density
Φ	weighing factor for upwind and downwind space derivatives for the calculation of morphology
ϕ_{bedl}	nondimensional bedload transport
ϕ_s	nondimensional total sediment transport
ϕ_{susp}	nondimensional suspended load transport
Ψ_Q	discharge ratio between downstream channels

Chapter 3 | Morphological asymmetry of bifurcations in tide-influenced deltas

Abstract

In river-dominated deltas, bifurcations often develop an asymmetrical morphology; i.e. one of the downstream channels silts up, while the other becomes the dominant one. In tide-influenced systems, bifurcations are thought to be less asymmetric and both downstream channels of the bifurcation remain open. The main aim of this study is to understand how tides influence the morphological development of bifurcations. By using a depth-averaged (2DH, two-dimensional horizontal) morphodynamic model (Delft3D), we simulated the morphological development of tide-influenced bifurcations on millennial timescales. The schematized bifurcation consists of an upstream channel forced by river discharge and two downstream channels forced by tides. Two different cases were examined. In the first case, the downstream channels started with unequal depth or length but had equal tidal forcing, while in the second case the morphology was initially symmetric, but the downstream channels were forced with unequal tides. Furthermore, we studied the sensitivity of results to the relative role of river flow and tides. We find that with increasing influence of tides over river, the morphology of the downstream channels becomes less asymmetric. Increasing tidal influence can be achieved by either reduced river flow with respect to the tidal flow or by asymmetrical tidal forcing of the downstream channels. The main reason for this behaviour is that tidal flows tend to be less unequal than river flows when geometry is asymmetric. For increasing tidal influence, this causes less asymmetric sediment mobility and therefore transport in both downstream channels. Furthermore, our results show that bedload tends to divide less asymmetrically compared to suspended load and confirm the stabilizing effect of lateral bed slopes on morphological evolution as was also found in previous studies. We show that the more tide-dominated systems tend to have a larger ratio of bedload-to-suspended-load transport due to periodic low sediment mobility conditions during a transition between ebb and flood. Our results explain why distributary channel networks on deltas with strong tidal influence are more stable than river-dominated ones.

Published as: Iwantoro, A.P., van der Vegt, M., & Kleinhans, M. G. (2020). Morphological evolution of bifurcations in tide-influenced deltas. *Earth Surface Dynamics*, 8(2), pp. 413-429. https://doi.org/10.5194/esurf-8-413-2020

3.1 Introduction

Deltas often consist of distributary channel networks. In these systems, water and sediment are divided at the bifurcations and distributed over the delta. The shape of the delta and the number of active channels depends on many factors like the forcing by rivers, tides and waves (Galloway, 1975; Rossi et al., 2016; Shaw and Mohrig, 2014), sediment availability and sediment type (Geleynse et al., 2011). Bifurcations tend to develop differently in river- than in tide-dominated systems, because tides influence the mouth bar formation processes of active river-dominated deltas (Edmonds and Slingerland, 2007; Leonardi et al., 2013; Shaw and Mohrig, 2014). In tidal deltas tides propagate upstream and can induce bi-directional flows. This unique characteristic may lead to a different morphological evolution of the bifurcations than would occur in the river-dominated zone (Frings and Kleinhans, 2008; Hoitink et al., 2017), but this has not been proven yet and the underlying mechanisms have not been studied. The focus of this paper is on the stability and depth asymmetry of bifurcations in tidally influenced deltas. We do not focus on the morphological evolution of the entire delta or the formation process of mouth bars, but consider a single bifurcation consisting of one upstream and two downstream channels. These are the building blocks of deltas and the hydro- and morphodynamics of such a system has been studied before by many others (Wang et al., 1995; Bolla Pittaluga et al., 2003; Kleinhans et al., 2008; Buschman et al., 2010; Sassi et al., 2011; Buschman et al., 2013).

In river-dominated systems, the morphology of the downstream channels of bifurcations often develops asymmetrically, such that one downstream channel deepens while the other silts up (Kleinhans et al., 2008). In many cases this condition develops into an avulsion. This asymmetric development can be triggered by a small perturbation such as a different bed elevation at the junction (Bolla Pittaluga et al., 2003), by a meandering upstream channel nearby the bifurcation or by the geometry of the downstream channels such as different length of the downstream branches (Kleinhans et al., 2008). The study of this morphological evolution in river-dominated bifurcations was pioneered by Wang et al. (1995). They applied an analytical model to predict the stability of river bifurcations. They found that bifurcations can be stable if any tendency for a downstream branch to become more dominant is counteracted by a relatively large share of the sediment input. Bolla Pittaluga et al. (2003) improved the model of Wang et al. (1995) by taking into account the cross-channel flow that can be induced by an asymmetric cross-sectional profile at the bifurcation. This effect induces a lateral bedload transport, which affects the asymmetric sediment division to the downstream branches. Using this approach, they found that the asymmetry of depth of the two downstream branches depends on the Shields number and on the width-to-depth ratio of the upstream channel at the bifurcation. Bifurcations with high width-to-depth ratio and low Shields number will be unstable and develop asymmetrical depths. Bertoldi and Tubino (2007) confirmed the results of Bolla Pittaluga et al. (2003) using a physical-scale model. Kleinhans et al. (2008) proposed that this asymmetrical depth development is also influenced by meandering of the upstream channel. The meandering bend induces an asymmetrical cross-sectional bed profile, and thereby influences the division of sediment at the junction. Bolla Pittaluga et al. (2015a) continued the work of Bolla Pittaluga et al. (2003) for a wider range of sediment mobility conditions. They found a range of sediment mobility numbers that result in stable symmetric bifurcations. Meanwhile, bifurcations with sediment mobility higher or lower than this range will grow asymmetrically and avulse. Applying the concept of Bolla Pittaluga et al. (2003), Salter et al. (2017) showed that deposition of sediment at a relatively shallow shelf causes the shorter channel to lengthen and reduce in gradient, thereby balancing the sediment transport division between downstream channels with unequal lengths. Redolfi et al. (2016) eliminated the need for a calibrated parameter in the lateral bedload transport of Bolla Pittaluga et al. (2015a) and by using that approach, Redolfi et al. (2019) showed that stable symmetric bifurcations can only occur when the width-to-depth ratio of the upstream channel

is below the critical limit originally defined in the theory of meandering rivers by Blondeaux and Seminara (1985) where the critical limit value depends on the friction and Shields stress at bifurcation.

In contrast to our knowledge of morphological development of bifurcations in river-dominated systems, our knowledge of this particular area in tide-influenced systems is still limited. Observations suggest that a similar development as in river-dominated systems can occur, as for example found in the most upstream bifurcation of the Yangtze Estuary that divides the main channel into North Branch and South Branch. According to Chen et al. (1982), the North Branch has evolved to be narrower and shallower while the South Branch has deepened. However, bifurcations in other tide-influenced deltas have downstream channels that seem to have a less asymmetric depth distribution, for example the Berau River Delta (Buschman et al., 2013) and Kapuas River Delta (Kästner et al., 2017). It has been suggested that tidal deltas have more stable distributary channel networks than their river-dominated counterparts (Hoitink et al., 2017), but the underlying mechanisms are unknown. Furthermore, several studies have investigated tidal characteristics at tidal bifurcations. Despite a general understanding on tides and subtidal water division at tidally influenced bifurcations (Buschman et al., 2010; Sassi et al., 2011; Zhang et al., 2012; Buschman et al., 2013; Alebregtse and de Swart, 2016), the effect of tides on the morphological evolution of tidal bifurcations has not been fully understood yet. From previous studies it is clear that tides influence the subtidal flow (Buschman et al., 2010; Sassi et al., 2011) and sediment division (Buschman et al., 2013), induce tidal currents that influence the sediment mobility, and can cause cross-channel currents at the junction (Buschman et al., 2013; Kleinhans et al., 2013). In river systems, all these factors are important for the morphological development of the downstream channels and it is expected that this is also the case for tide-influenced systems.

Therefore, the main aim of this paper is to study the effect of tides on the morphological evolution of bifurcations with the focus on how tides contribute to the asymmetrical development. For this purpose, an idealized bifurcating channel was set-up in Delft3D. We simulated the morphological evolution of a system consisting of two downstream channels (branches) forced by tides and an upstream channel forced by river discharge. We consider this system as a building block of each delta system. We studied two cases, i.e. asymmetric geometry of downstream channels, and asymmetric tides between the downstream channels. In the former case, the asymmetric downstream geometry was initially prescribed to see how tides affect the asymmetrical development of the downstream channels. The relative effect of tides was investigated by imposing equal tides at downstream boundary of each downstream branch and by using different values for the river discharge in a series of simulations. In the latter case, we imposed unequal tidal forcing at the two downstream boundaries that had a symmetric geometry. In tide-influenced deltas, the asymmetric tides between downstream channels can occur because the downstream channels are connected to other channels with different complexity, which may dissipate the tidal range or slow down the tides unequally before the tides propagate into the downstream channels of the bifurcation.

This paper is organized as follows. The model setup and methodology are described in Section section 3.2. In Section section 3.3, the results of the simulated morphological development are presented. Section section 3.4 presents a discussion on the findings. Finally, the conclusions of this study are provided in Section section 3.5.

3.2 Methodology

3.2.1 Model set-up

An idealized bifurcating channel was set up and its morphological development was simulated using the depth-averaged version (2DH) of Delft3D. This 2D approach is suitable for long-term and large scale

morphodynamic modelling because it is computationally lighter than a 3D approach. Even though a 3D approach allows for vertical flow patterns (Lane et al., 1999) such as curvature induced flow, which might be important for the sediment transport process (Daniel et al., 1999), the 2D approach is sufficient for this study since we focus on large scale morphodynamic evolution and therefore simulating detail 3D features of flow and morphology is not our goal. Furthermore, the reason to prefer the 2D above the 1D approach is to explicitly simulate cross-channel flow induced by tidal propagation from one branch to another at the junction as observed in Buschman et al. (2010) and Buschman et al. (2013) and as being identified by Bolla Pittaluga et al. (2003) as an important process for sediment division at the junction.

The model solved the 2DH unsteady shallow water equations using an semi-implicit Alternating Direction Implicit (ADI) scheme on a staggered grid (see Lesser et al., 2004). For bed friction the Chézy formulation was used with a value of 60 $m^{0.5}s^{-1}$. Meanwhile the horizontal eddy viscosity was set to 10 m^2s^{-1}. This value was chosen because applying a smaller value for horizontal eddy viscosity will cause a numerical instability near the bifurcation as flow magnitude and direction rapidly change in this location and applying a larger value will not significantly affect the results. Bedload and suspended load sediment transport were calculated by the Van Rijn (1993) method. We used medium sand with a single grain size of 0.25 mm with a dry bed density of 1600 kg m^{-3}. This sediment size is in the range of observed grain size in tide-influenced deltas, as for example by Buschman et al. (2013) in Berau River Delta (0.125-0.25 mm), Kästner et al. (2017) in Kapuas Delta (0.22-0.3 mm), Sassi et al. (2011) in Mahakam Delta (0.25-0.4 mm), and Stephens et al. (2017) in Mekong Delta (0.074-0.385 mm). Transverse bed slope effects for bedload transport were accounted for by the approach of Ikeda (1982) and we used a value of 10 for α_{bn}. This value is much higher than Delft3D default value (1.5) and that suggested by Bolla Pittaluga et al. (2003) (0.3-1) because a low value of this parameter in Delft3D leads to unrealistic and grid size-dependent channel incision as well as bar formations (Baar et al., 2019). Even though we prescribed a high α_{bn}, this value is still in the range of what other studies used for Delft3D modelling work e.g. Dissanayake et al., 2009; van der Wegen and Roelvink, 2012; Van Der Wegen and Roelvink, 2008. For streamwise bed slope effects the Bagnold (1966) approach was used with a Delft3D default value of α_{bs} =1. For morphology the MorFac approach was used (Lesser et al., 2004; Roelvink, 2006) with an acceleration factor of 400. We tested several values between 1 and 1000 and chose the largest value for which morphology had similar development as for value of 1 and numerical stability was satisfied. This allows for long-term morphodynamic simulation at time scales of decades (Lesser et al., 2004) and centuries (van der Wegen et al., 2008) in much shorter duration. Furthermore, in this study, non-erodible channel banks were used. This limitation was acceptable since changes in width-depth ratio could still be accommodated by the bed level change, and using erodible banks is not realistic as long as the model is not able to allow for channel bank growth.

The spatial domain consisted of an upstream channel that bifurcates in two downstream channels. The two downstream channels had a default length of 30 km, although in one series of simulations the length of one channel was 15 km. The upstream channel had a length of 220 km to ensure that upstream propagating tides decay smoothly. The downstream channels and the first 20 km of the upstream channel had a convergent width profile, while the upstream 200 km had a constant width. The channel width was configured by:

$$W_{upstream}(x) = \begin{cases} W_0 e^{x/L_w}, & \text{for} -20km \leq x \leq 0 \\ W_0 e^{-20km/L_w}, & \text{for} x \leq -20km \end{cases}$$
$$W_{downstream}(x) = 0.5 W_0 e^{x/L_w}, \tag{3.1}$$

in which $W(x)$ is the channel width, x the longitudinal distance from the junction (i.e. positive in upstream direction, $x = 0$ is at bifurcation, hence negative x in downstream channels), W_0 =480 m is the width at the junction and L_w =50 km is the e-folding length scale. Further, in a region within 800

m near the junction an additional widening was applied (Figure 3.1b) to overcome the loss of two grid cells (see grid description in Kleinhans et al. (2008)). This widening is a typical feature of bifurcations found in delta systems (Kleinhans et al., 2008). After the additional widening, W_0 becomes 750 m.

The spatial domain of the model was discretized in a curvilinear grid and followed the same method as in Kleinhans et al. (2008) and Buschman et al. (2010). At the bifurcation two grid cells had to be removed in the middle of the channel for numerical reasons (Kleinhans et al., 2008), as illustrated in Figure 3.1. The grid cell length in along channel direction was 80 m. The upstream channel had 12 grid cells across the channel whereas in both downstream channels 5 grid cells were used. Therefore, the grid cell size in across channel direction was spatially varying in order to adapt the funnelling shape of the channel and the additional widening near the bifurcation. Near the junction this resulted in typical grid cell width of 62.5 m. Based on grid size and channel depth a time step of 6 seconds was used in all simulations to have Courant Number smaller than $4\sqrt{2}$ as required for the ADI scheme. The domain had three open boundaries where boundary conditions for flow and sediment transport were prescribed. At the upstream end of the upstream channel river discharge was prescribed while at the ends of the two downstream channels M_2 tidal water levels were imposed. At all open boundaries, equilibrium sediment transport was computed during inflow while during outflow the sediment transport was assumed to be just flushed out from the domain. As a result, no morphological change occurred during inflow but the bed is free to evolve during outflow.

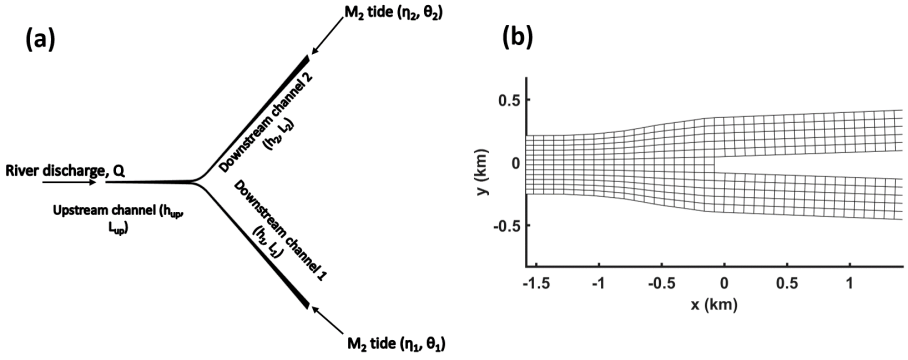

Figure 3.1 (a) Illustration of bifurcation model setup from the upstream channel forced by river discharge Q to the downstream boundaries which are forced by tidal water levels. Here, h indicates the depth and L indicates the length of each channel. Meanwhile, η and θ indicates amplitude and phase of tidal water levels at each downstream boundary. (b) Zoom of model grid near the junction, showing the additional widening near the junction and the disappearance of two grid cells downstream of the junction.

Because the formation of alternating bars will affect flow and sediment division at the junction, the channel depth and upstream prescribed river discharge were chosen such that the system was in the overdamped bar regime (Struiksma et al., 1985). To this end, we conservatively followed the empirical classification proposed by Kleinhans and van den Berg (2011). Therefore, the three connected channels had an initial depth of 15 m and a constant along-channel bed slope of $3\text{x}10^{-5}$. The prescribed discharge ranged between 500 and 2,800 m^3s^{-1}.

3.2.2 Description of model scenarios and boundary conditions

Depth, width and length of the downstream channels of bifurcations in deltas can be unequal. Hence, in Case 1 we started the simulations with an unequal geometry, either being a difference in depth or length between the two downstream channels. We simulated the morphological evolution of the

Table 3.1 Summary of simulations undertaken in the present study and their boundary conditions (river discharge and tidal properties), and geometry differences between the downstream channels.

scenario	simulation name	Q (m^3s^{-1})	η_{M_2} (m)		$\Delta\theta_{M_2}$ (°)	ΔL (km)	Δh (m)
			branch 1	branch 2			
Control simulation	Control_Q2800	2,800	1	1	0	0	0
	Control_Q1596	1,596	1	1	0	0	0
Depth difference	Depth1_Q2800	2,800	1	1	0	0	7.5
	Depth1_Q1596	1,596	1	1	0	0	7.5
	Depth1_Q500	500	1	1	0	0	7.5
	Depth2_Q2800	2,800	1	1	0	0	1
	Depth2_Q1596	1,596	1	1	0	0	1
Length difference	Length_Q2800	2,800	1	1	0	15	0
	Length_Q1596	1,596	1	1	0	15	0
Amplitude difference	Amp_0.75	2,800	0.75	1	0	0	0
	Amp_0.5		0.5	1	0	0	0
	Amp_0.25		0.25	1	0	0	0
Phase difference	Phase_10	2,800	1	1	10	0	0
	Phase_22.5		1	1	22.5	0	0
	Phase_35		1	1	35	0	0

bifurcation until it approximately reached morphodynamic equilibrium (discussed later on). Note that length of the branches was fixed in time, while an initial depth difference does not necessarily result in an asymmetric equilibrium depth because it can adapt. All simulations belonging to Case 1 were forced by equal tides from downstream and river discharge from upstream (settings summarized in Table 3.1). The depth difference scenarios were performed in two different ways. First, simulations were started from a system in which the upstream channel and one downstream channel were 15 m deep, while the other branch was 7.5 m deep (called Depth1). The upstream 2 km of the shallow downstream channel was gradually changed over 2 km to avoid a sudden depth change near the bifurcation. In a second type of simulation, we started with uniform bathymetry of 15 m depth and simulated till morphodynamic equilibrium was reached (called Depth2). Next, one downstream channel was made 0.5 m deeper and the other 0.5 m shallower. We studied the sensitivity of the results to the relative magnitude of tides over river discharge by changing the prescribed upstream discharge. The simulation with largest river discharge (2,800 m^3s^{-1}) represents a river dominated system while the simulations with lower river discharge (500 m^3s^{-1}) represent the more tide-influenced systems.

In Case 2 the effect of unequal tidal forcing on morphological development was studied. In natural systems tides in the two downstream branches can be unequally forced. For example, when the two branches end in a shelf sea, amplitude and phase in the two channels can be different because they have a different position with respect to the amphidromic system in the shelf sea. Furthermore, in deltas with multiple bifurcations and unequal depths and channel lengths, tidal amplitude and phase differences will be present in the channels because propagation speeds and times in the channels are different. Hence, in Case 2 we started simulations with a symmetric geometry but with asymmetric tidal forcing, either being a tidal water level amplitude difference or a tidal phase difference. The corresponding settings of the simulations can be found in Table 3.1. The difference in downstream tidal forcing between the two channels was studied for values between zero and 0.75 m (η_1 in Figure 3.1 was 0.75, 0.5 or 0.25 m while η_2 was 1 m) where η_1 and η_2 are tidal water level amplitude imposed at the downstream end of downstream channel 1 and 2, respectively. Meanwhile for another set of simulation the tides had equal amplitude, but the phase difference was 10, 22.5, or 35 degrees (for M_2 tide this means one channel had delayed tides of 20, 46 or 72 minutes).

We also performed two control simulations with different discharge, symmetric geometry, and equal tides (see Table 3.1) to study the equilibrium bed profiles in absence of any initial asymmetry. The

morphology change simulated for Case 1 and Case 2 were caused by the asymmetric forcing/geometry and by the adaptation to the initial conditions. Therefore, the results of the control simulations can be used to better interpret the simulations of Case 1 and Case 2.

3.2.3 Methods to evaluate model simulations

The morphological development of the bifurcation was observed by evaluating for each downstream channel the tidally and spatially averaged depth of the first 2 km from the bifurcation (Figure 3.2, called h_1 and h_2 from hereon). This region was chosen because it determined the morphological development of the entire downstream channel. The development of the downstream channels starts from upstream and develops downstream. Therefore, analysing the most upstream end of the downstream channels is sufficient to determine the growth in asymmetry between them. After analysing all cases, it was found that a distance shorter than 2 km cannot be representative due to the presence of local morphological features near the bifurcation such as bar formation or small incisions in the downstream channel that is silting up. However, a longer distance cannot be representative because even though one downstream channel almost avulses upstream, tides can cause a deepening of that same channel near the downstream boundary. To determine whether the system was in morphodynamic equilibrium we analysed the evolution in time of h1 and h2. We stopped the simulation when the changes in h_1 and h_2 were small. A true morphodynamic equilibrium, in the sense that no bed level change occurred in the entire domain, was never achieved. This is very common for morphodynamic simulations of estuaries (Van Der Wegen and Roelvink, 2008; Nnafie et al., 2018). Typical simulated period was between 1,200 and 2,400 years, depending on the prescribed river discharge.

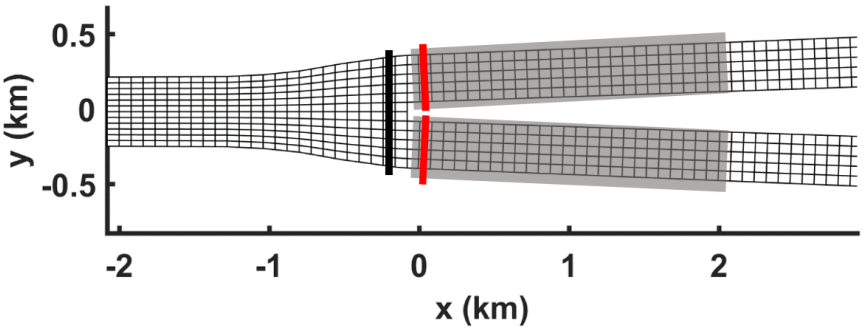

Figure 3.2 The grids in surrounding of the bifurcation overlaid by the areas where the bed level changes were evaluated (grey boxes), the grids where the asymmetry indices (red lines) and upstream channel flow (black line) were calculated.

To compare the depth of the two downstream channels, the depth asymmetry parameter Ψ_h was calculated as:

$$\Psi_h = \frac{|\, h_2 - h_1 \,|}{h_2 + h_1}. \tag{3.2}$$

A larger Ψ_h indicates a more asymmetric morphology. When Ψ_h is close to one this indicates an avulsion, given that the widths are fixed, while a zero value indicates equal depth of the downstream channels.

The sediment mobility was evaluated by calculating the width-averaged value of the Shields number two grid cells away from the bifurcation, as illustrated in Figure 3.2. The Shields number at each grid point was calculated as:

$$\tau_* = \frac{\tau_b}{(\rho_s - \rho_w)\, g D_{50}} \tag{3.3}$$

where $\rho_s - \rho_w$=1650 kg m^{-3}, g is gravitational acceleration (9.81 m^{2}s$^-$1) and τ_b is the bed shear stress magnitude expressed by

$$\tau_b = \frac{\rho_w g u^2}{C^2}, \tag{3.4}$$

in which C is the Chézy coefficient and u is instantaneous flow velocity. In tide-influenced systems, tides cause a temporal change of bed shear stress and we calculated both the peak and the tide-averaged value of the Shields number. A Shields asymmetry parameter Ψ_{τ_*} was defined and calculated by:

$$\Psi_{\tau_*} = \frac{\mid \Delta\overline{\tau_{*;1,2}} \mid}{\overline{\tau_{*,2}} + \overline{\tau_{*,1}}}. \tag{3.5}$$

where $\overline{\tau_{*,1}}$ and $\overline{\tau_{*,2}}$ are the width-averaged Shields number in each downstream channel and $\Delta\overline{\tau_{*;1,2}}$ is the difference between both. A higher value of Ψ_{τ_*} indicates a more asymmetric sediment mobility condition while Ψ_{τ_*}=0 indicates a symmetric sediment mobility. When Ψ_{τ_*} was based on peak bed shear stresses it is denoted by $\Psi_{\tau_{*max}}$ while $\Psi_{<\tau_*>}$ is used when it is based on tidally averaged bed shear stresses.

At the grid locations where we determined the Shields number, we also determined the tidally averaged (U_0) and the M_2 tidal (U_{M_2}) flow magnitudes, in a similar way as for the Shields number. Furthermore, we calculated the width-integrated and tidally averaged bedload and suspended load transport at the cross-sections shown in Figure 3.2.

3.3 Results

3.3.1 Evolution of control runs

Results of the two control simulations show that bed levels were initially not in morphodynamic equilibrium. The time-stack diagram of width-averaged depth as a function of space is shown in Figure 3.3. The morphology changed over time until an approximate equilibrium was reached, which took about 1,200 years. There are two time-scales involved. First, there are deposition fronts from the upstream channel that migrate downstream. Second, there is a slower adaptation to the equilibrium condition. The results also show that true morphodynamic equilibrium, in the sense that bed levels are steady, was not achieved after 1,200 years. However, bed level changes were small at the end of the simulation. The lowest discharge resulted in the smallest depth for the upstream channel, but the river discharge does not significantly affect the depth of the two downstream channels. This is because both control simulations were imposed by the same tidal forcing and the morphology of the downstream channels is mainly controlled by the tides. Typical depths are around 8 - 10 m for the downstream channels, and 10–12 m for the upstream one.

3.3.2 Geometry difference case

When simulations started with unequal channel depth, a similar evolution as the control simulations occurred. The morphological evolution was characterized by three typical time scales. First, there was erosion near the bifurcation, mainly because of the decrease in the cross-sectional area directly seaward of the bifurcation. Second, this erosion was followed by deposition fronts that migrated downstream during the simulation. This deposition front can be identified by a rapid decrease of the depth in the downstream channels at the beginning or halfway the simulation (Figure 3.4). It is

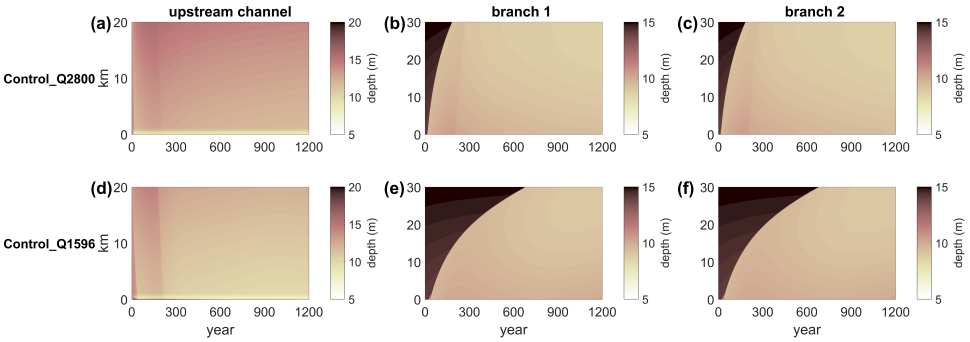

Figure 3.3 Time-stack diagram of width- and tide-averaged depth (colour) of the upstream channel (left panels; km 0 is junction, km 20 upstream) and downstream channels (middle and right panels; km 0 is junction, km 30 near sea) as a function of distance from the bifurcation (vertical axis) for the two control simulations. The top panels ((a), (b), and (c)) are the result from the high discharge simulation (Control_Q2800) while the bottom panels ((d), (e), and (f)) are for the low discharge simulation (Control_Q1596).

similar to the evolution of Control_Q2800 and Control_Q1596, but this depositional front was not necessarily similar in the two downstream channels because of the imposed differences in the initial bed level. Furthermore, in the lowest discharge simulations (Q=500 m^3s^{-1}) it takes much longer for the deposition front to reach downstream boundary and therefore it takes much longer before the system is in the steady state. Third, after the initial adaptation phase, the morphology of the channels started to change gradually. Some simulations took 2,400 years (Q=500 m^3s^{-1}) until the morphological changes near the junction were small. Furthermore, the results show that at the end of the simulation the depth of the shallow branch depends on the discharge (Figure 3.4). The higher the discharge, the shallower the shallowest branch is. For the deepest branch it is the other way around. The deepest branch is shallowest for the lowest discharge.

The simulations that were based on perturbed equilibrium depth (Depth2) had a different morphological evolution and final equilibrium than the ones that started with 7.5 m depth difference (results not shown). The Depth2 simulation did not show the fast, initial depth response, but was mainly characterized by a slow adaptation to a new equilibrium because the system was still close to equilibrium at the start of the simulation. It took relatively long to achieve the new equilibrium and total simulation time was 2,400 years in this case. Interestingly, although the external forcing for the Depth1 and Depth2 simulation were the same, the final equilibria were different. Because the depth in the channels influences the tidal dynamics (by for example the relative importance of friction and by difference in tidal propagation speed due to the different initial depths), the tide-induced flows were different at the junction and stayed different during the entire simulation. Hence, the equilibrium not only depends on external forcing but also on initial conditions. The initial and final morphology near the bifurcation for all Depth1 and Depth2 simulations can be seen in Figure 3.14 in Appendix 3A.

The simulations with Length difference show that the shortest branch developed to be the deepest, while the longest became very shallow (Figure 3.5). The longest branch becomes so shallow that it becomes morphologically inactive. This occurred for both the highest and for the medium discharge scenario and is also independent of the initial conditions (starting with equilibrium bathymetry and shortened channel, or with 15 m deep channels). Meanwhile, the shortest channel was deepest for the highest discharge condition. The final morphology near the bifurcation for the simulations in $Length\ difference$ scenario is provided in Figure 3.14 in Appendix 3A.

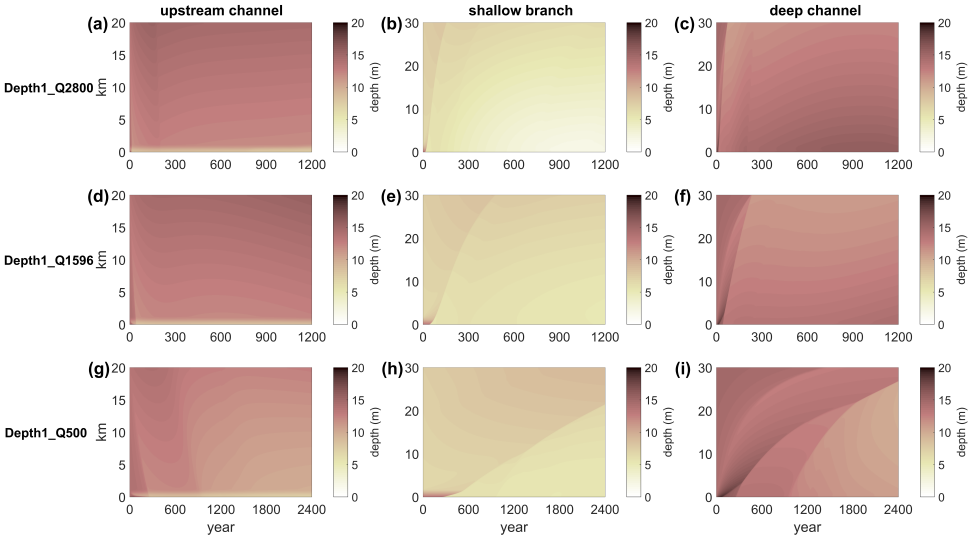

Figure 3.4 Same plot as Figure 3.3 but for simulations of Depth1. The panels from top to bottom show the results from different simulation (Depth1_Q2800, Depth1_Q1596, Depth1_Q500, respectively) while from left to right show the upstream channel, shallow branch, and deep branch, respectively.

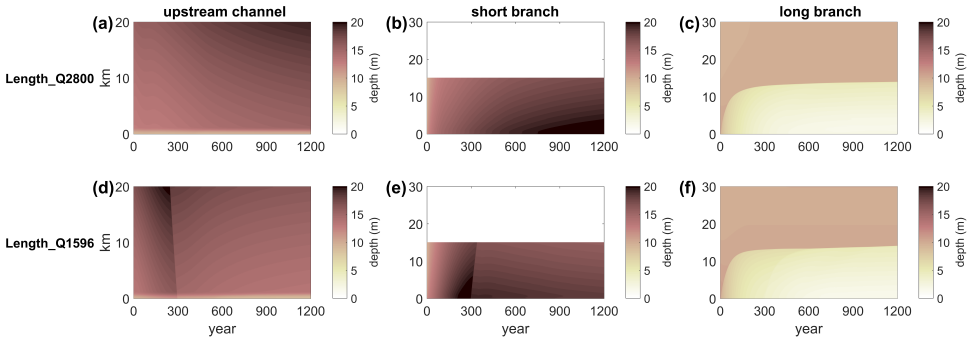

Figure 3.5 Time-stack diagram of width- and tide-averaged depth as a function of space for the simulations in $Length\ difference$ scenario with the same order as Figure 3.4 but with short (panel (b) and (e)) and long (panel (c) and (f)) downstream branch.

3.3.3 Tide difference case

Asymmetric forcing of tides resulted in asymmetric morphological evolution. Because the system started out of equilibrium, the morphological evolution is again characterized by a quick adaptation followed by a slow evolution to the equilibrium. When forced by different tidal amplitude, the downstream branch with the smallest downstream tidal forcing evolved into the shallowest branch (Figure 3.6). Interestingly, when tidal amplitude in Branch 1 was decreased from 0.75 m to 0.5 m or even 0.25 m the bifurcation evolved into a less asymmetric system. Furthermore, when the two downstream channels were forced by equal amplitudes, but with different phase, this also resulted in the development of an asymmetric morphology of the bifurcation (Figure 3.7). In general, the channel with delayed tides developed smallest channel depth while the channel with earlier tides developed deeper channels. Interestingly, the deposition front in the shallowest branch became

stagnant for the largest imposed phase differences, suggesting that the flow magnitude was below the threshold for erosion (static equilibrium). However, the depth around the bifurcation did not become zero and still evolved. The larger the difference in tidal phase at the two downstream boundaries the shallower the delayed branch became, while the other branch was deeper. The final morphology near the bifurcation for all simulations of this case is provided in Figure 3.15 in Appendix 3A.

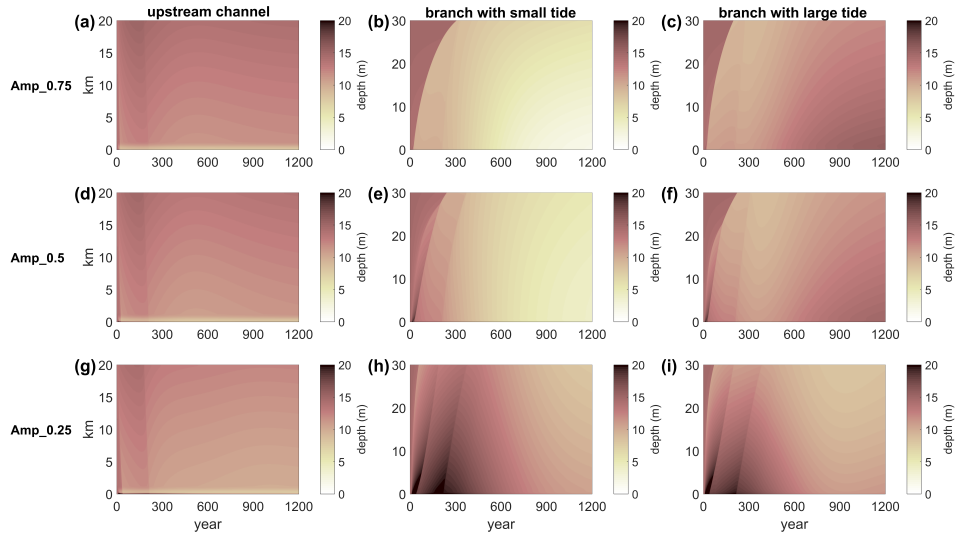

Figure 3.6 Time-stack diagram of width- and tide-averaged depth as a function of space for *Amplitude difference* scenario.

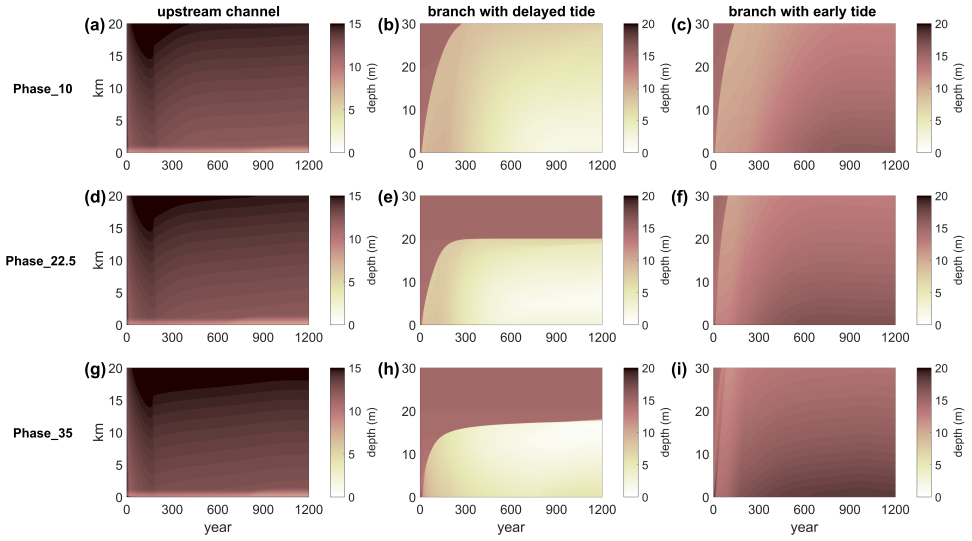

Figure 3.7 Time-stack diagram of width- and tide-averaged depth as a function of space for *Phase difference* scenario.

3.4 Discussion

3.4.1 Relation between tides and the morphological evolution of bifurcations

The results suggest that tides cause less asymmetric bifurcations. To quantify how tides affect the morphology, the results from all scenarios were correlated. Figure 3.8 shows a scatter plot and linear fit between the final Ψ_h (dimensionless depth asymmetry) and Ψ_{τ_*} (dimensionless Shields asymmetry) for all model simulations. As can be seen, Ψ_h is linearly correlated with $\Psi_{<\tau_*>}$ and $\Psi_{\tau_* max}$. Hence, the degree of asymmetry in the morphology is directly related to the degree of asymmetry in the sediment transport capacity. From the comparison of $\Psi_{<\tau_*>}$ and $\Psi_{\tau_* max}$ against Ψ_h (Figure 3.8a and Figure 3.8b), the latter comparison shows the strongest relation and therefore the maximum mobility, which occurred during the peak ebb flow in our simulations, is the most representative to determine the morphological asymmetry of the downstream channels.

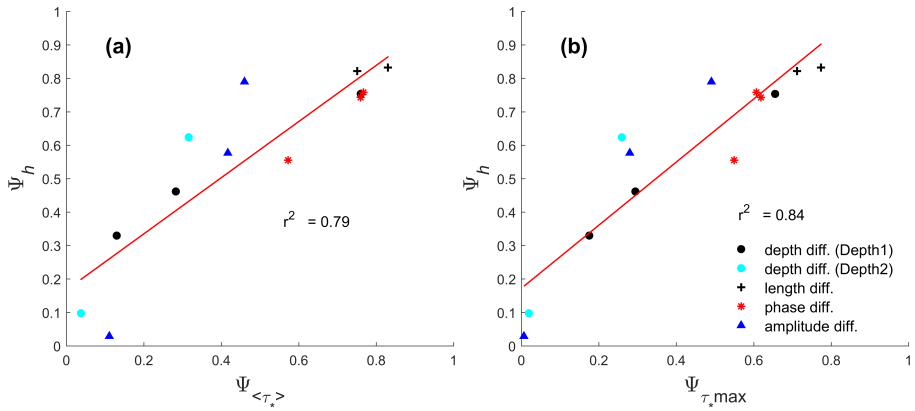

Figure 3.8 Relation between depth asymmetry number Ψ_h and: (a) the asymmetry in tidally averaged Shields number ($\Psi_{<\tau_*>}$), and (b) the asymmetry in peak Shields number ($\Psi_{\tau_* max}$) at the equilibrium condition for all simulations from scenarios described in Table 3.1. Note that in panel (a), two simulations of $Phase\,difference$ scenario and a simulation of Depth1 scenario is slightly overlapping.

According to Eq. 3.3, in a system with uniform sediment properties and water density, the sediment mobility in the downstream channels only depends on the total bed shear stress τ_b. Because in the downstream channels the flows are mainly in along-channel direction, the instantaneous flow velocity to calculate the total bed shear stress τ_b in Eq. 3.4 can be represented by the along-channel flow velocity. Based on a harmonic analysis, it became clear that the mean flow (U_0) and M2 component (U_{M_2}) were the main tidal constituents and higher harmonics like M_4 were relatively small. Therefore, the maximum sediment mobility scales very well with the square of summation of U_{M_2} and U_0 ($\Psi_{\tau_* max} \approx (U_{M_2} + U_0)^2$). The sediment mobility and flow conditions near the bifurcation for all simulations is provided in Table 3.2 in Appendix 3A.

The relatively strong river discharge in the simulations performed causes the ratios of U_0 to U_{M_2} in the upstream channel cross section near the junction to be in the range between 0.2 and values slightly larger than 1 (see Figure 3.16a in Appendix 3A). This similar importance between those components indicates that our model is a mixed river- tide-influenced system. For most simulations, U_0, dominated by the river flow, in the two downstream branches was more asymmetric than U_{M_2} (see Figure 3.16b in Appendix 3A). In river-dominated systems, bifurcations with higher flow division asymmetry will also develop a more asymmetric morphology (Kleinhans et al., 2008). Interestingly, the tidal flows oppose the asymmetry induced by U_0. U_{M_2} becomes less asymmetric

with the increase of tidal influence, shown by the decreasing trend in $\Psi_{U_{M_2}}$ for increasing sum of U_{M_2} ($\sum U_{M_2}$) in the two downstream channels (Figure 3.9a), in which the summed U_{M_2} was measured from the width-averaged U_{M_2} at U_{M_2} section in the downstream channels shown in Figure 3.2. This explains why the increased tidal influence, indicated by larger sum of U_{M_2} in Figure 3.9a and Figure 3.9b, causes less asymmetric bifurcations. Due to tides, the sediment mobility in both channels is closer to each other than without tides (Figure 3.9b). A more tide influenced condition is not only achieved by decreasing river discharge, but also by inducing an asymmetry in the tidal forcing in the downstream channels. For either increased difference in amplitude or phase, the sum of U_{M_2} in both downstream channels also increased and became similar in magnitude. The scatter in the results shown in Figure 3.9 is caused by the different imposed asymmetries for different scenarios. The asymmetry is not only controlled by external forcing, but also determined by internal dynamics when the depth of the branches develop, and because we have different types of initial asymmetries (forcing, depth, length), there is quite some scatter in Figure 3.9. Still, we found that all simulations have a similar behaviour, i.e. more tidal influence drives less morphological asymmetry between downstream channels.

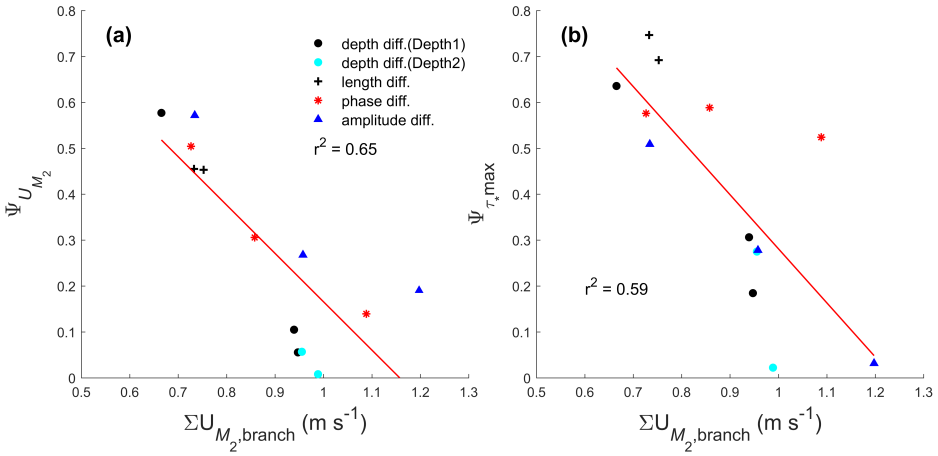

Figure 3.9 Comparison between: (a) tidal flow asymmetry and (b) Peak Shields number asymmetry in the two downstream branches against the total tidal flow magnitude from the two downstream channels.

There are two processes that drive a less asymmetric tidal flow in the more tide-influenced condition. First, the propagation of tides from the dominant downstream channel to the other downstream channel balances the tidal flow in the two downstream channels. This process mainly rules in tide difference case. Tidal forcing asymmetry between downstream channels drives tidal propagation from one downstream channel to the other and results in phase lags of tidal flow inducing strong cross-channel flow at the junction (similarly as discussed in Buschman et al., 2013). This can be seen by a larger cross-channel flow in the upstream channel near the bifurcations for larger asymmetry between the prescribed tides in Figure 3.10. This cross-channel flow is dominated by the tides V_{M_2} while its mean flow value (V_0) was close to zero. Strong cross-channel flows caused erosion at the bifurcation, resulting in a trench-like scour connecting the downstream channels. This scour can be found in the $Amplitude\ difference$ and $Phase\ difference$ scenarios and is most pronounced in the simulation Amp_0.25 (see Figure 3.15c-f in Appendix 3A). Although a bar developed in the upstream channel on the side of the downstream channel imposed with lower tidal amplitude, the cross-channel flows deepened the bed at bifurcation and maintained the connection between both downstream channels and the upstream channel. The development of the trench-like

scour at the bifurcations is also observed in the Berau River Delta (Buschman et al., 2013) and Mahakam Delta (Sassi et al., 2011). This deepening at the bifurcation can be also affected by the angle of the bifurcation, something we did not study here. Second, with equal tides imposed in the two downstream channels for $Depth\ difference$ and $Length\ difference$ scenario, the larger river discharge in the dominant downstream channel dampens the tides in this channel while the shallowing bed level in the other downstream channel increase the tidal flow in this channel. As a result, this combining effect induces a less asymmetric tidal flow in the downstream channels.

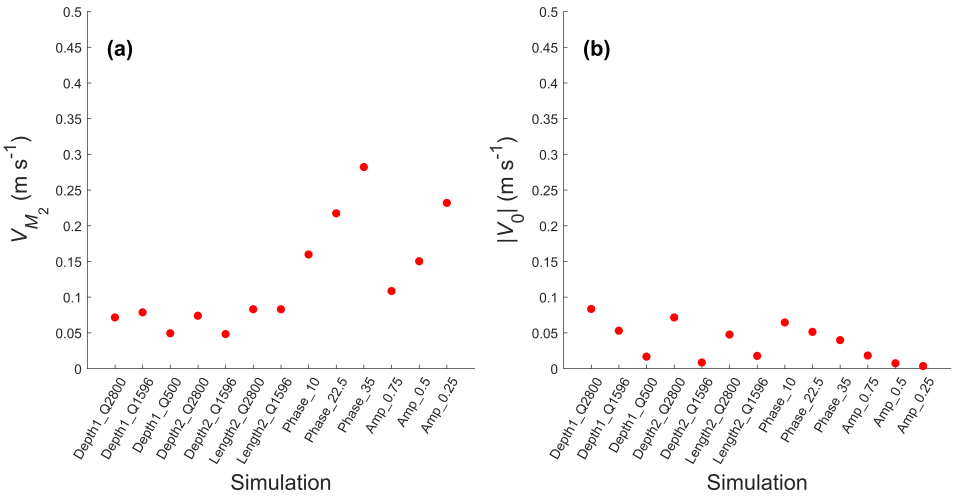

Figure 3.10 Cross channel flow of: (a) tidal current amplitude and (b) mean current at bifurcation in the upstream channel for all simulations.

3.4.2 Role of bedload versus suspended load

In the theory of Bolla Pittaluga et al. (2003) and Bolla Pittaluga et al. (2015a) the lateral bed slope causes additional sediment transport into the dominant channel, thereby having a stabilizing effect on the bifurcation. Here, we used the Van Rijn (1993) sediment transport formulations in which bed slope only affects the bedload transport and not the suspended load transport. Based on this, we expected that bedload transport will be divided less asymmetrically than suspended load transport. To check this hypothesis, the tidally averaged and width-integrated sediment transport at the cross-sections shown in Figure 3.2 were calculated. We calculated an asymmetry index similar as we did for the Shields number and depth. The results of the scatter plot of suspended load asymmetry versus bedload asymmetry index clearly show that suspended load tends to be divided more asymmetrically at the bifurcation (Figure 3.11a). Only when the system is fully symmetric or asymmetric is there no difference in asymmetry of bedload and suspended load transport because the downstream channels receive an equal amount of sediment when the downstream channels are symmetric, while only one downstream channel receives all sediment when an avulsion occurs (both bedload and suspended load asymmetry are 1). Furthermore, from a scatter plot of depth asymmetry (Ψ_h) versus the ratio of bedload to suspended load transport in the upstream channel, it becomes clear that systems that have more asymmetric bed levels have a smaller contribution of bedload transport to the total transport, and vice versa (Figure 3.11b). However, there is also some considerable scatter due to the sensitivity to the initially imposed asymmetry. Lastly, a scatter plot of the ratio of mean flow and M_2 flow magnitude versus ratio of bedload and suspended load transport

in the upstream channel (Figure 3.11c) suggest that when river flow is relatively important, the system is suspended load dominated, while for more tide-dominated conditions bedload plays a more important role. This further explains why the more tide-dominated conditions result in less asymmetric morphology.

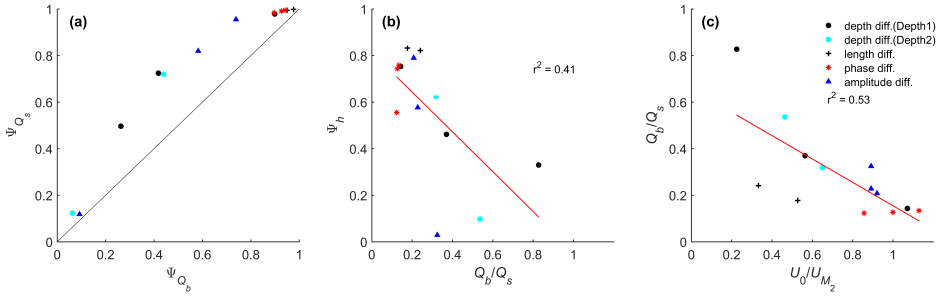

Figure 3.11 Comparison of: (a) Suspended load asymmetry (Ψ_{Q_s}) against bedload asymmetry (Ψ_{Q_b}) overlaid by the line of equality (black line), (b) Scatter plot of morphology asymmetry (Ψ_h) against ratio of bedload and suspended load transport in the upstream channel, and (c) Scatter plot ratio of bedload and suspended load transport in the upstream channel against the dominance of river flow over tidal flows in the upstream channels. The legend for all panels is provided in panel (c).

3.4.3 Sensitivity to sediment grain size and transverse bedslope effect

Defining a different sediment grain size would change the sediment mobility and drive a different ratio of bedload to suspended load transport. These would affect the sediment transport division and therefore the morphological development in the downstream channels. When using finer sediment this results in a more asymmetric development of the downstream channels, as is shown in Figure 3.12. The finer sand induces a larger contribution of suspended load transport to total sediment transport and therefore counteracts the stabilizing effect by the transverse bedslope effect on the bedload. As a result, the depth asymmetry between downstream channels increases. Similarly, a coarser sediment results in smaller depth asymmetry between the downstream channels.

The importance of the effect of transverse bedslope to oppose the asymmetrical morphological development between downstream channels causes the model results to be sensitive to the parameter α_{bn}. Using physical scale models, previous studies have suggested that αbn value should take values between 0.2-1.5 (Baar et al., 2018; Ikeda, 1982; Schuurman et al., 2013; Talmon et al., 1995). However, Delft3D shows unrealistic morphological development when small values of α_{bn} are used, as shown in Figure 3.13. Simulation Depth1_Q2800 with small α_{bn} (α_{bn}=1) showed the development of an elongated bar upstream on the side of shallow downstream channel and a large incision occurred on the other side. This unrealistic behaviour has also been evaluated by Baar et al. (2019). The use of small value of α_{bn} causes the morphological development to be dependent on the grid size (Baar et al., 2019). Several studies have used much higher value to overcome this issue (Dissanayake et al., 2009; van der Wegen and Roelvink, 2012; Van Der Wegen and Roelvink, 2008, e.g.). Using our model set-up, the model results started to be insensitive to the value of αbn when α_{bn} is 10. Using this value the transverse slope developing upstream of the bifurcation is less than threefold of upstream channel width as also suggested by Bolla Pittaluga et al. (2003) and Kleinhans et al. (2008) for river-dominated bifurcations.

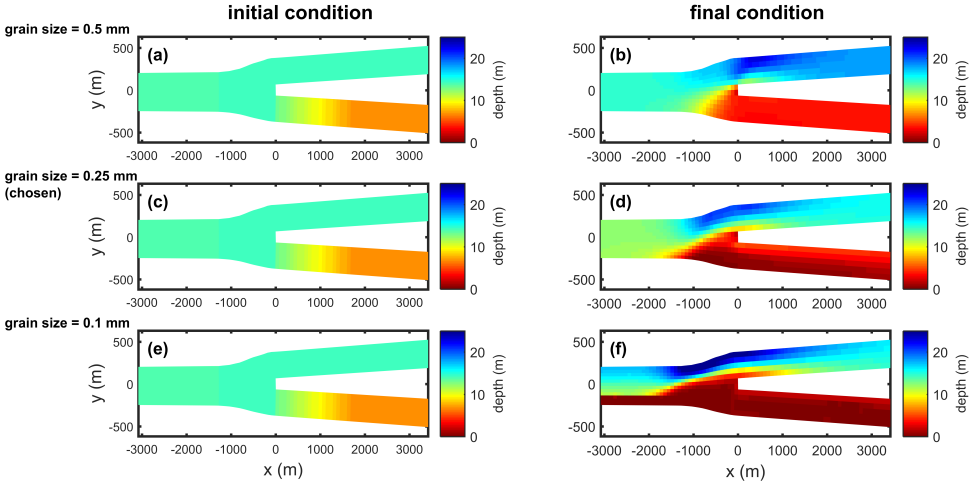

Figure 3.12 Initial ((a), (c), and (e)) and final (b, d, and f) depth near the bifurcation for coarser sand ((a) and (b)), applied sand ((c) and (d)), and finer sand ((e) and (f)) using the set-up of simulation Depth1_Q2800.

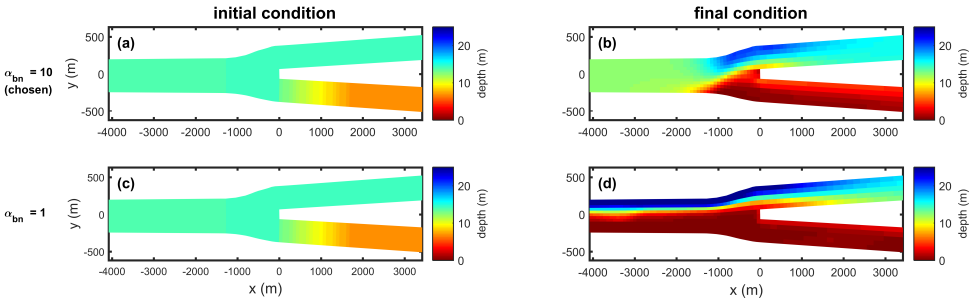

Figure 3.13 Initial ((a) and (c)) and final ((b) and (d)) depth near the bifurcation for large ((a) and (b)) and small ((c) and (d)) αbn using the set-up of simulation Depth1_Q2800.

3.5 Conclusions

In this manuscript, the effect of tides on the morphological development of bifurcations was investigated using a numerical modelling approach in Delft3D. An idealized bifurcation was built by splitting an upstream channel into two downstream branches. The idealized bifurcations were forced by river discharge from upstream and tides from downstream. To identify the effect of tides, two cases were studied, namely geometry difference (length and depth of channels) and tide difference (difference in prescribed tides at the two downstream channels).

The results show that increased tidal influence compared to river influence, results in a less asymmetric morphology of the bifurcation. This increased tidal influence can either be achieved by smaller river discharge or by asymmetric tides from downstream. The main mechanism is that tidal flows tend to be less asymmetric in the two downstream channels than tidally averaged flows. This causes the peak Shields number in the branches to be closer to each other with increasing influence of tides. Furthermore, we have shown that bedload transport tends to be divided less asymmetrically than suspended load due to the influence of lateral bed slopes, which tends to stabilize the system. In our simulations, bifurcations with increased tidal influence had a relatively high ratio of bedload over

suspended load transport and therefore developed a less asymmetric morphology than in river-dominated systems. Our results can explain why tides tend to stabilize the bifurcations in deltas.

3.6 Appendix 3A

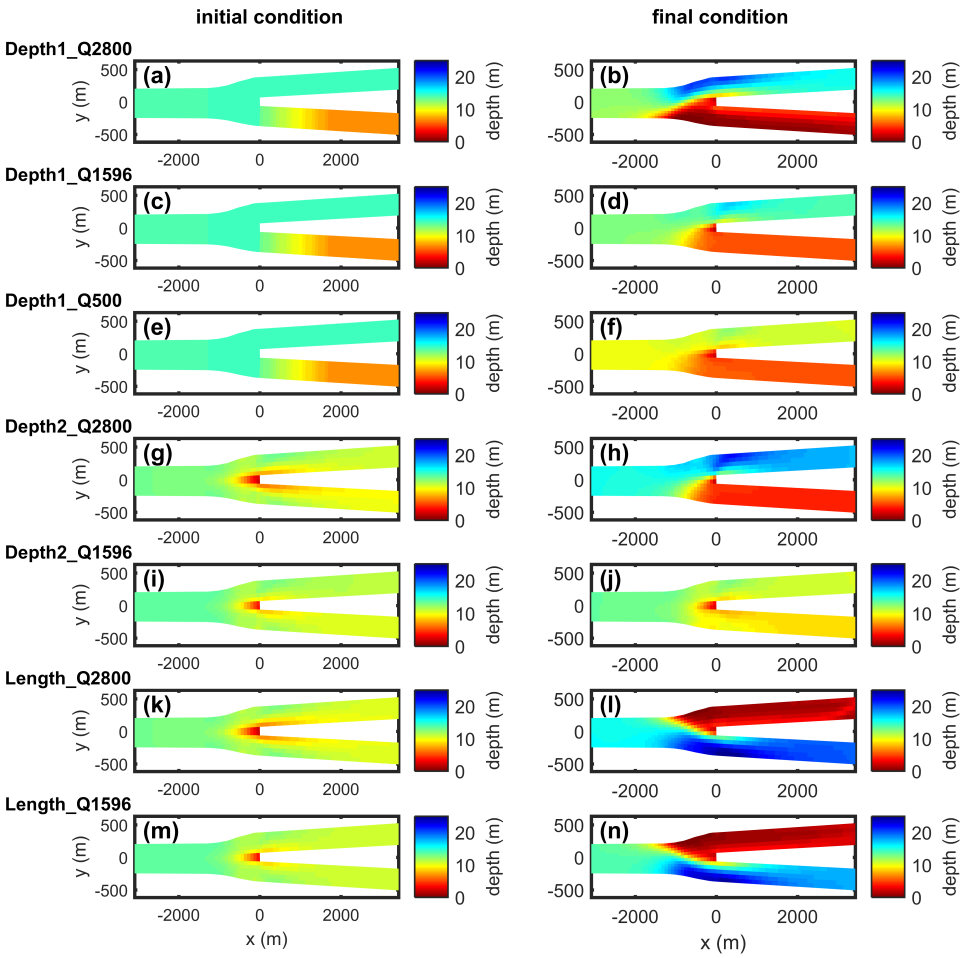

Figure 3.14 Initial (left panels) and final (right panels) depth near the bifurcation for all simulations in Case 1. For $Depth\ difference$ scenario (panel (a)-(j)), the top branch in each panel is the deep downstream branch and the bottom one is the shallow downstream branch. For $Length\ difference$ scenario (panel (k)-(n)) the top branch in each panel is the long downstream branch and the bottom branch is the short downstream branch.

Table 3.2 Sediment mobility (tide-averaged and maximum), mean flow and tidal flow amplitude at the cross sections near the bifurcation as shown in Figure 3.2 for all simulations. Main channel is the upstream channel, minor channel is the downstream channel that tend to be shallower, and major channel is the deepened downstream channel.

simulation	$< \tau_* >$			τ_{*max}			U_0			U_{M_2}		
	main channel	minor branch	major branch	main channel	minor branch	major branch	main channel	minor branch	major branch	main channel	minor branch	major branch
Depth1_Q2800	0.76	0.04	0.28	0.66	0.14	0.67	0.30	0.16	0.54	0.28	0.14	0.52
Depth1_Q1596	0.28	0.09	0.16	0.29	0.24	0.44	0.22	0.20	0.32	0.39	0.42	0.52
Depth1_Q500	0.07	0.07	0.09	0.20	0.18	0.26	0.09	0.09	0.13	0.40	0.45	0.50
Depth2_Q2800	0.13	0.10	0.19	0.37	0.29	0.50	0.26	0.21	0.40	0.40	0.45	0.50
Depth2_Q1596	0.10	0.11	0.12	0.27	0.30	0.31	0.19	0.22	0.24	0.41	0.49	0.50
Length2_Q2800	0.11	0.02	0.22	0.31	0.08	0.60	0.19	0.00	0.44	0.31	0.20	0.53
Length2_Q1596	0.08	0.02	0.15	0.24	0.08	0.45	0.12	-0.01	0.29	0.32	0.21	0.55
Phase_10	0.15	0.04	0.28	0.40	0.16	0.67	0.30	0.18	0.53	0.31	0.17	0.55
Phase_22.5	0.15	0.04	0.28	0.38	0.16	0.66	0.26	0.10	0.51	0.36	0.30	0.56
Phase_35	0.17	0.07	0.27	0.41	0.20	0.68	0.22	0.05	0.47	0.45	0.47	0.61
Amp_0.75	0.17	0.10	0.26	0.42	0.23	0.66	0.35	0.35	0.47	0.31	0.16	0.58
Amp_0.5	0.19	0.11	0.26	0.49	0.37	0.66	0.33	0.31	0.46	0.40	0.35	0.61
Amp_0.25	0.23	0.20	0.25	0.54	0.58	0.59	0.33	0.42	0.35	0.51	0.49	0.71

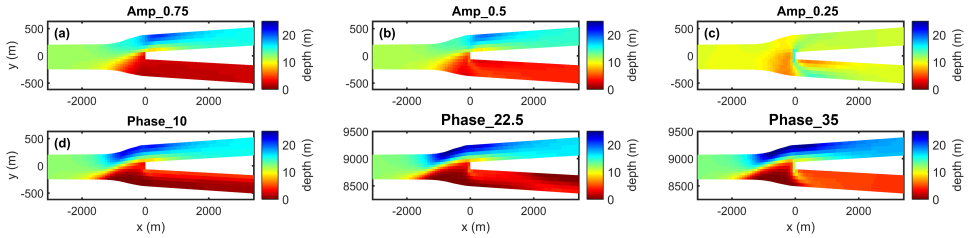

Figure 3.15 Final depth for Case 2. For $Amplitude\ difference$ scenario (panel (a)-(c)) the downstream branch imposed by low tides is the bottom branch while for $Phase\ difference$ scenario (panel (d)-(f)) the bottom branch is the downstream branch imposed by delayed tides.

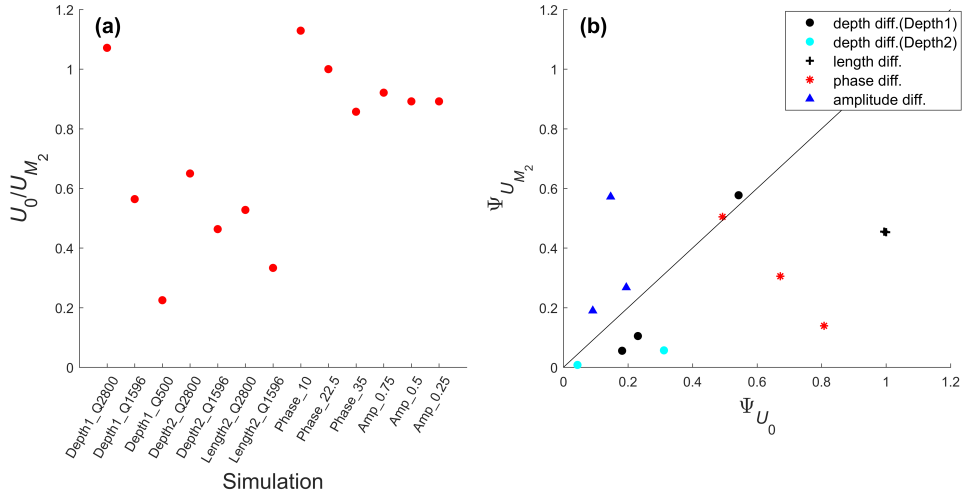

Figure 3.16 (a) Ratio of U_0 and U_{M_2} for all simulations and (b) Comparison of asymmetry of U_{M_2} against asymmetry of U_0.

Chapter 4 | Stability of tide-Influenced river bifurcations

Abstract

Bifurcations are important geomorphological features in tide-influenced deltas. At bifurcations, river flow and tides distribute sediment over the channel network and determine the morphodynamic evolution of the entire delta. Using a one-dimensional numerical model, we study the effects of tides on the morphological evolution of bifurcations from river-dominated to tide-dominated systems. In accordance with previous studies, bifurcations with small tidal influence, in which the flood flow hardly drives morphological change, have a larger range of Shields stress and width-to-depth ratio conditions for which symmetric bifurcations are stable to depth perturbations, compared to their river-dominated counterparts. We extended the existing studies to tide-dominated conditions. When bifurcations become increasingly tide-dominated, the range of conditions under which balance discharge partition (symmetric morphology) can exist, shrinks. Under these conditions, the bed can also change during the flood phase and growth of the bed asymmetry is larger than the decay during ebb. However, the bed asymmetry in equilibrium becomes less pronounced with increasing tidal dominance. We conclude that tides reduce the tendency of closure and abandonment of one of the downstream channels compared to river-dominated bifurcations, either by inhibiting the instability or by reducing asymmetry.

Published as: Iwantoro, A.P., van der Vegt, M., & Kleinhans, M. G. (2022). Stability and Asymmetry of Tide-Influenced River Bifurcations. *Journal of Geophysical Research: Earth Surface*, 127 (6), pp. e2021JF006282. https://doi.org/10.1029/2021JF006282

4.1 Introduction

Bifurcations are common features in fluvial systems, where a larger upstream channel splits into two smaller downstream channels and can be found in steep slope rivers as well as in lowland rivers and deltas. In the fluvial-dominated channel networks, river flow divides at bifurcations and determines the sediment distribution as well as the morphodynamics of the downstream channels. In these systems, one of the downstream channels of a bifurcation is often abandoned, resulting in one dominant downstream channel that conveys the river discharge (Bolla Pittaluga et al., 2015a; Kleinhans et al., 2008). In the tide-influenced systems, tides cause a change in flow magnitude during ebb and even change the system into a confluence during flood if tides are large enough, suggesting that bifurcations in these systems may develop differently. Hoitink et al. (2017) suggested that such channel abandonment rarely occurs in tide-influenced systems, keeping both downstream channels open to convey the water. In this paper we investigate the effect of tides on the stability and asymmetry of bifurcations as found in tide-influenced river deltas.

Morphodynamics of river-dominated bifurcations have been thoroughly studied for a range of settings in river systems, from low sediment mobility in gravel bed rivers (Bertoldi and Tubino, 2007; Bolla Pittaluga et al., 2003; Bolla Pittaluga et al., 2015a) to high sediment mobility rivers (Bolla Pittaluga et al., 2015a; Edmonds and Slingerland, 2008; Slingerland and Smith, 1998). It was found that symmetric bifurcations are unstable in high and low sediment mobility (Shields stress), resulting in asymmetric bifurcations and abandonment of one of the downstream channels. Only a limited mid-range of sediment mobility conditions exists that results in stable symmetric bifurcations. The stability of symmetric bifurcations also depends on width-to-depth ratio of the upstream channel. Bifurcations with larger width-to-depth ratio have a more limited range of sediment mobility for which stable symmetric bifurcations can exist (Bolla Pittaluga et al., 2015a; Redolfi et al., 2016; Redolfi et al., 2019). Some studies have addressed effects of different geomorphological features in river systems. Meandering of the upstream channel enhances the asymmetry between downstream channels (Kleinhans et al., 2008; Slingerland and Smith, 1998), migrating bars increases the dynamics of bed level of bifurcations (Bertoldi et al., 2009), and evolving river banks increase the conditions for asymmetric downstream channels (Kleinhans et al., 2011; Miori et al., 2006). Furthermore, Salter et al. (2017) showed that the asymmetric morphological development of bifurcations in river-dominated deltas can be controlled by the presence of downstream sediment sinks. Sediment deposition at a shallow estuary-shelf boundary will result in channel lengthening. This will shift the asymmetry evolution of the bifurcation, where the lengthened channel will silt up and the shallow channel will deepen, whereupon this channel will lengthen. This shifting asymmetry evolution will continue until the estuary-shelf transition is in very deep water.

The stability and morphodynamics of tide-influenced bifurcations are much less clear. Though observations demonstrate the existence of seemingly stable, nearly symmetric bifurcations in tide-influenced deltas such as in Mahakam Delta (Sassi et al., 2013) and Berau River Delta (Buschman et al., 2013), some observations also found highly asymmetric bifurcations (e.g. Chen et al., 1982; Kästner and Hoitink, 2019). Based on a two-dimensional (2DH) modeling study, Iwantoro et al. (2020) found that bifurcations are less asymmetric for tide-dominated rivers because tide-induced flows tend to partition less asymmetrically than river-induced flow velocities (see chapter 3). However, they only simulated a small range of sediment mobility, tidal influence and width-to-depth ratio conditions applied in 13 simulations and in many cases the asymmetry was externally forced by differences in either channel length or tidal forcing. They were also not able to find stable symmetric bifurcations. Simulating a full deltaic channel network by using a 2DH numerical model, Rossi et al. (2016) found that delta systems with stronger tidal influence have a more stable morphology resulting in a less frequent avulsion. Using physical laboratory experiments, Lentsch et al. (2018) confirmed the finding of Rossi et al. (2016) and suggested that the same results will occur under sea level rise

conditions. However, they only simulated a limited range of tidal amplitudes and sediment sizes, and did not systematically vary the sediment mobility and width-to-depth ratio that were shown to be important parameters for the morphodynamics of bifurcations in river dominated systems (e.g. Bolla Pittaluga et al., 2015a; Redolfi et al., 2019). In a recent study, Ragno et al. (2020) showed that symmetric bifurcations are stable to bed perturbations for a wider range of Shields stress and width-to-depth ratio values when tides are added to a river system. This is caused by the increased flow velocity in a tidal cycle, which deepens both downstream channels, reduces the width-to-depth ratio, and reduces the asymmetry between them. However, Ragno et al. (2020) studied small tide conditions in which tides only cause a fluctuation in river flow magnitude but no flow reversal during a tidal cycle. Besides, they also applied a straight channel while in tidal systems a converging channel width is more common (e.g. Davies and Woodroffe, 2010; Fagherazzi and Furbish, 2001; Langbein, 1963; Lanzoni and Seminara, 1998; Savenije, 2015). As a result, it is still unclear how tides affect the asymmetry of tide-dominated bifurcations for a wide range of Shields stress conditions and width-to-depth ratios.

To extend our knowledge about the morphodynamics of tide-influenced bifurcations, in this study we aim to determine the effects of tides on 1) the stability and 2) the asymmetry in morphodynamic equilibrium of tide-influenced bifurcations, from small tidal influence that results in a changing flow magnitude, to tide-dominated conditions at which the flow is bi-directional. To achieve this objective, the one-dimensional (1D) morphodynamic numerical model in Chapter 2 was applied to tidal systems. The model was adapted such that flow and sediment transport at the bifurcation can change in magnitude and direction. Though a 1D model is not as capable to simulate the detailed flow conditions and morphology as 2D or 3D models (e.g. Edmonds and Slingerland, 2007; Edmonds and Slingerland, 2008; Kleinhans et al., 2008; Rossi et al., 2016) or physical models (e.g. Bertoldi et al., 2009; Bertoldi and Tubino, 2007; Lentsch et al., 2018), 1D models have been widely applied to study long-term morphodynamic evolution of rivers, estuaries and deltas (e.g. Bolla Pittaluga et al., 2015b; Salter et al., 2017; Salter et al., 2020). The advantage of the 1D approach is that it is computationally less expensive than 2D and 3D approaches, but still capable to explain the important processes that drive the morphodynamic evolution of bifurcations (e.g. Bolla Pittaluga et al., 2015a; Iwantoro et al., 2021; Ragno et al., 2020; Redolfi et al., 2019). As a result, a broader range of conditions that exists in nature could be studied in a much shorter computational time than with the other approaches. We limit our study to deltas that have a sandy bed, thereby ruling out muddy systems, which need a different approach to model sediment transport.

A single bifurcation was studied at which three channels connect (Figure 4 1). The two downstream channels were forced by tides from the downstream boundary, while at the upstream channel a steady river discharge was prescribed. Sets of simulations were prepared to simulate the morphodynamics of bifurcations with different tidal influence. This was achieved by changing discharge, tidal range, and the geometry of the system (width profile). The detailed approach is described in Section 4.2. Then the results and the explanation of the basic mechanisms that drive the morphodynamic evolution tide-influenced bifurcation are provided in Section 4.3. The results, limitations and future studies are discussed in Section 4.4, and finally the conclusions of this study are presented in Section 4.5.

4.2 methodology

4.2.1 Model description

Hydrodynamics

The Saint Venant equations were solved to compute the hydrodynamics (Cunge et al., 1980). This approach is more suitable for this study than other approaches, such as locally uniform flow (Salter

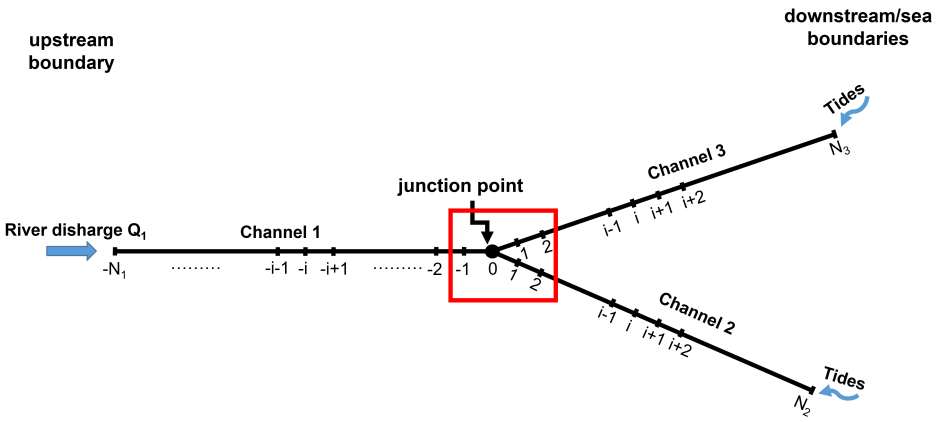

Figure 4.1 Illustration of bifurcation model domain and boundary conditions. Channel 1 is the upstream channel and is forced by river discharge from upstream boundary, while Channel 2 and Channel 3 are the downstream channels that are forced by time-varying water levels at the downstream boundary. The three channels are connected at the junction point/boundary.

et al., 2017) or the backwater equations (Kleinhans et al., 2008) because tides cause unsteady flow. The following equations were solved:

$$w\frac{\partial z}{\partial t} + \frac{\partial Q}{\partial x} = 0 \tag{4.1}$$

$$\frac{\partial Q}{\partial t} + \frac{\partial}{\partial x}\left(\frac{Q^2}{A}\right) + gA\frac{\partial z}{\partial x} + \frac{|\,Q\,|\,QPg}{C^2A^2} = 0. \tag{4.2}$$

in which x and t are the spatial and temporal axes and Q is the discharge caused by river flow and tides. Furthermore, w is the channel width and A and P in Eq. 4.2 are the cross-sectional area and wetted perimeter of the channel, respectively. The model assumes that the presence of tidal flats is negligible. Therefore, w is constant in the entire tidal cycle. This assumption is considered plausible because many tidal systems has limited tidal flat that are insignificant to the flow dynamics in the channel such as in Mahakam Delta, Berau River Delta and Mekong River Delta. By assuming that the channels have a rectangular cross section, A is calculated by $A = w(z - \eta) = wh$, where η is the bed level, z is water level and h is water depth. Meanwhile, we approximate here that $P = w$, therefore P/A in the friction term in Eq. 4.2 equals $1/h$, and the friction term does not depend on the width-to-depth ratio. By doing this the hydrodynamics and morphodynamics of the system are independent of the width as long as the prescribed specific discharge upstream is not changed between simulations. This allows for studying the sensitivity of the results to the width-to-depth ratio without changing the equilibrium bathymetry. Finally, g is the gravitational acceleration and C is Chézy coefficient, related to roughness by

$$C = 18\log_{10}(12h/\xi) \tag{4.3}$$

where ξ is the Nikuradse roughness length related to the presence bedforms (van Rijn, 1984a).

Two kinds of boundary nodes are present, namely open boundaries and junction boundaries. Open boundaries are located at the upstream node of the upstream channel (upstream boundary in Figure 4.1) and at the downstream node of the downstream channels (downstream boundary in

Figure 4.1). The junction boundary is a node shared by three connected channels at the bifurcation, known as nodal point. At the upstream boundary, equilibrium river discharge was prescribed as follows

$$Q_{1;ub} = w_{1;ub} C h_1 \sqrt{g h_1 S_1} \tag{4.4}$$

where the subscripted number defines the channel identity as in Figure 4.1, $w_{1;ub}$ is the channel width at upstream boundary and S is channel slope (m m^{-}1).

At the downstream boundaries, water level is prescribed as

$$z = z_0 + \sum_{k=1}^{N} a_k \cos\left(\omega_k t + \varphi_k\right) \tag{4.5}$$

where z_0 is the mean water level (z_0=0 here), a_k and φ_k are amplitude and phase of the tidal constituent k, and $\omega_k = 2\pi/T_k$, in which T_k is tidal period of constituent k. Here, we only prescribed one tidal constituent at the seaward boundary, but in principle multiple constituents can be prescribed.

Defining the junction boundary to be located at x=0, and positive x in downstream direction, the discharge at the junction satisfies the conservation of mass as follows

$$Q_1(0,t) = Q_2(0,t) + Q_3(0,t) \tag{4.6}$$

while the water level was assumed to be equal, neglecting the effect of dynamic pressure:

$$z_1(0,t) = z_2(0,t) = z_3(0,t) \tag{4.7}$$

Because the dynamic pressure was neglected, the water level difference between the channels at the junction due to energy dissipation by turbulence as used, for example, in Edmonds and Slingerland (2008), Gurram et al. (1997), Ragno et al. (2021), is neglected. The hydrodynamic calculations were solved using an implicit Preissmann scheme (see Cunge et al. (1980) for details). The scheme is unconditionally stable. Therefore, the time steps can be independently defined to optimize the spatial accuracy and computational capacity.

Sediment transport and morphodynamics

The sediment transport is based on van Rijn (1984a) and van Rijn (1984b) and is applicable in the range of sand and gravel. It computes the bedload and suspended load separately. The details of the sediment transport equations applied in the 1D model can be found in chapter 2. The applied sediment transport model assumes local flow and transport are in equilibrium and neglects time lags that may occur between peak flow and sediment transport (Groen, 1967) as well as a spatial settling lag (Postma, 1961) that typically occurs in tide-influenced systems. We applied this simplification because of two reasons. First, we would like to keep the computation in the model as simple as possible and focus on how tides can affect the morphological evolution of bifurcations. Second, the time and spatial settling lag are mainly important for fine-grained sediment like mud (e.g. van Straaten and Kuenen, 1958; Pritchard and Hogg, 2003), while in this study we use sand. For very fine sand of 70 microns (smallest value used in this study) the settling velocity (w_s) is around 0.4 cm/s and for the water depth of 5 m the settling time scale (h/w_s) is around 20 minutes, which, although not very small, is considerably less than the semidiurnal time scale. Therefore, the assumption to neglect these lag effects are plausible for sandy systems as studied here.

Compared to chapter 2 the main difference is the calculation of sediment transport at the junction. For tide-influenced conditions, the sediment transport direction depends on the phase of tidal currents

in the branches (it can be ebb or flood flow in each channel and timing of ebb and flood is not necessarily the same in each channel) and the junction can behave as a bifurcation or as a confluence. There are three possible conditions under which the junction behaves as a bifurcation and three for which the junction is a confluence, as illustrated in Figure 4.2. The conditions depicted in the lower two rows of Figure 4.2 can occur because of different phase of the flow at the junction, causing a timing difference in ebb and flood at the junction. This can itself have many reasons, like a difference in bed level between the downstream channels, different channel lengths, difference in amplitude or phase at the seaward boundaries (see chapter 3) and these time differences have been observed in deltas, such as in Berau River Delta (Buschman et al., 2013) and Wax Lake Delta (Wagner and Mohrig, 2019). When the flow merges the system is a confluence and the sediment transport to the channel that receives the sediment (sink channel) is calculated by adding the sediment transport from the other two channels:

$$Q_{s,out} = Q_{s,inp1} + Q_{s,inp2}. \tag{4.8}$$

$Q_{s,out}$ is sediment transport in sink channel while $Q_{s,inp1}$ and $Q_{s,inp2}$ is sediment transport from the channels that distribute the sediment transport (source channels). Meanwhile, when the flow bifurcates, the sediment transport from one source channel distributes to two sink channels:

$$Q_{s,inp} = Q_{s,out1} + Q_{s,out2}. \tag{4.9}$$

Hence, during bifurcation conditions an expression is needed that describes how the sediment of the source channel is distributed over the two sink channels. This is the so-called nodal point relationship and previous studies have shown that results critically depend on it (Wang et al., 1995).

Here, we applied the same nodal point relationship as used in chapter 2, which was based on the nodal point relationship of Bolla Pittaluga et al. (2003). The main difference here is that, depending on the flow condition, the input channel is different. This is also depicted in Figure 4.2 by the splitting of the last cells in the source channel. In this area a transverse sediment transport is calculated. Basically, the along channel sediment transport divides according to the width of each sink channel, plus a correction term $Q_(s, y)$ caused by transverse suspended load transport ($Q_{susp,y}$) and transverse bedslope driven bedload transport ($Q_{bedl,y}$):

$$Q_{s,y} = Q_{bedl,y} + Q_{susp,y}. \tag{4.10}$$

where

$$Q_{bedl,y} = Q_{bedl,x}\left(\frac{Q_y h_{inp}}{Q_{inp}\alpha h_{123}} - \frac{r}{\sqrt{\vartheta'_{inp}}}\frac{\partial \eta}{\partial y}\right) \tag{4.11}$$

while $Q_{susp,y}$ is expressed by

$$Q_{susp,y} = Q_{susp,x}\left(\frac{Q_y h_{inp}}{Q_{inp}\alpha h_{123}}\right). \tag{4.12}$$

Here, $Q_{bedl,y}$ and $Q_{susp,y}$ are along-channel bedload and suspended load transport from the source channel at the junction, respectively. The transverse bedload transport is affected by both transverse flow (first term on the right-hand side), which occurs because one of the two sink channels receives relatively more water than the other, and by transverse bedslope effect (second term on the right-hand side). The transverse suspended load transport is only affected by the transverse flow. In Eq. 4.11 and Eq. 4.12, Q_{inp} is discharge in the source channel and Q_y is transverse discharge computed by

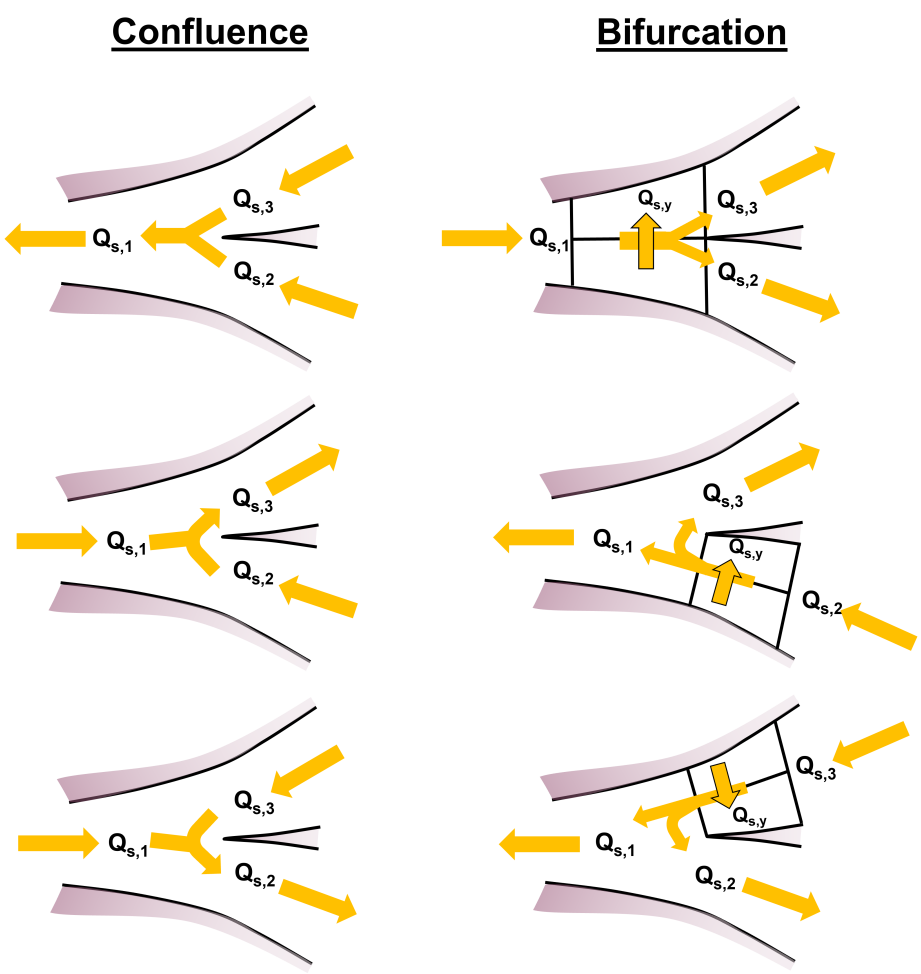

Figure 4.2 All six possible flow-induced sediment transport conditions for a tide-influence bifurcating channel. The arrow indicates the sediment transport direction for each condition. The left conditions are for the confluence conditions and the right conditions are for the bifurcation conditions.

$$Q_y = \frac{1}{2}\left(Q_{out1} - Q_{out2} - Q_{inp}\frac{w_{out1} - w_{out2}}{w_{out1} + w_{out2}}\right) \tag{4.13}$$

where Q_{out1} and Q_{out2} are the water discharge in the two sink channels. Note that when the discharge divides at the bifurcation proportional to the respective widths of the sink channels, Q_y=0. In Eq. 4.11 and Eq. 4.12, α is the dimensionless length (scaled by channel width of the input channel) of the region of influence of the bifurcation and determines over which distance from the junction the transverse transport in the source channel occurs. Bolla Pittaluga et al. (2003) suggested that α is between 2-3. From physical experiments, Bertoldi and Tubino (2007) suggested that α has an optimum value of

6. However, Redolfi et al. (2019) found that the value of α depends on the Shields stress and friction coefficient. We used α=3. Moreover, the constant r in Eq. 4.11 is a calibration parameter for transverse bedslope effect and according to Baar et al. (2018), r ranges between 0.2-1.5 depending on sediment mobility and bedform characteristics. To keep the computation in the model as simple as possible and focus the study on investigating how tides affect the morphodynamics of bifurcation, a constant α and r are applied (3 and 0.5) as also applied in chapter 2 and in Bolla Pittaluga et al. (2015a). Meanwhile, h_{inp} is the depth of the source channel at the junction and h_{123} is the weighed average depth of the connected channels at the junction, expressed by

$$h_{123} = \frac{w_{inp}h_{inp} + w_{out1}h_{out1} + w_{out2}h_{out2}}{w_{inp} + w_{out1} + w_{out2}}. \tag{4.14}$$

where w_{inp} is the width of the source channel at the junction while w_{out1} and w_{out2} are the widths of the sink channels. In Eq. 4.11, ϑ'_{inp} is the grain-related Shields stress in the input channel at the junction and was calculated by

$$\vartheta' = \mu\vartheta, \tag{4.15}$$

where μ is efficiency factor (van Rijn, 2007) and is calculated as $\mu = (C/C')^2$ in which C' is grain-related Chézy coefficient,

$$C' = 18\log_{10}(12h/2.5D_{50}) \tag{4.16}$$

with D_{50} the median grain size of sediment (van Rijn, 1984a). Furthermore, ϑ is total Shields stress,

$$\vartheta = \frac{(Q/A)^2}{\left(\frac{\rho_s}{\rho_w} - 1\right) C^2 D_{50}} \tag{4.17}$$

in which rho_s and rho_w are the density of sediment and water, respectively. $\frac{\partial\eta}{\partial y}$ in Eq. 4.11 is the transverse bed slope at the bifurcation calculated between the channel centres as:

$$\frac{\partial\eta}{\partial y} = \frac{\eta_{out2} - \eta_{out1}}{0.5w_{inp}}. \tag{4.18}$$

Finally, the morphological change is computed using the sediment continuity equation and assumes a dynamic riverbed while the riverbanks are fixed:

$$w(1-p)\frac{\partial\eta}{\partial t} + \frac{\partial Q_s}{\partial x} = 0. \tag{4.19}$$

Here, p is the sediment porosity, which has a value of 0.35. The numerical scheme to solve Eq. 4.19 was described in chapter 2.

4.2.2 Model set-up

The schematized junction consists of an upstream channel of 80 km length and two downstream channels of 20 km length, discretized with spatial and time steps of 250 m and 5 minutes, respectively. The river discharge was imposed at upstream boundary applying a defined slope to calculate Eq. 4.4 that was constant for all simulations in this study (3x10^{-5}) while a semi-diurnal tidal component with T_k of 12 hours was imposed at downstream boundaries. The location of these boundaries can be seen in Figure 4.1.

To investigate the stability of bifurcations as a function of tidal influence, we defined sets of simulations in which prescribed tidal amplitude and channel width profile were changed (Table 4.1).

The tidal influence is indicated by the ratio of tidal flow amplitude (U_2) over tide-averaged flow (U_0) in the upstream channel at the bifurcation in morphodynamic equilibrium (symmetric condition, not yet perturbed). Note that tidally averaged flow is caused by river discharge and by Stokes return flow and is nonzero for zero river discharge. We simulated conditions from U_2/U_0=0 (river-only/no tide) to U_2/U_0=9. We prescribed the following width profile. The downstream channels are convergent over their entire length, which can be characterized by the e-folding length scale for width (L_w). These converging channels are very typical for tidal systems (e.g. Davies and Woodroffe, 2010; Fagherazzi and Furbish, 2001; Langbein, 1963; Lanzoni and Seminara, 1998). The upstream channel is convergent until $x = -Lc$, after which the channel is straight until the upstream boundary:

$$W_{upstream}(x) = \begin{cases} W_{1;0}e^{x/L_w}, & \text{for} - L_c \leq x \leq 0 \\ W_{1;0}e^{-L_c/L_w}, & \text{for} x \leq -L_c km \end{cases} \qquad (4.20)$$
$$W_{downstream}(x) = W_{2;0}e^{x/L_w} = W_{3;0}e^{x/L_w}.$$

Here, $w_{1;0}$ is width of upstream channel at the junction, and $w_{2;0}$ and $w_{3;0}$ are the widths of both downstream channels at the junction, which in this study were defined as $w_{2;0} = w_{3;0} = 0.5w_{1;0}$. Since $w_{1;0}$ is self-defined, by changing L_c and L_w, $w_{1;ub}$ also changes. This affects the prescribed discharge according to Eq. 4.4 and also the tidally-averaged flow velocity at the bifurcation (U_0). Furthermore, L_c and L_w affect the propagation of tides in the system. Similarly, river discharge (see Eq. 4.4) and tidal propagation are also affected by the prescribed upstream water depth. As a result, beside defining a different tidal amplitude at seaward boundaries, we varied the tidal influence in the system by having different L_c, L_w and initial depth.

For the design of channel shape, the effect of L_w, L_c, river discharge and grain sizes on the equilibrium bed profile was studied. The settings for these simulations are shown in Table 4.2. These runs were also used to estimate conditions for which U_2/U_0 at the bifurcations obtains a certain desired value. After this, two continuous simulations were conducted in which we aimed to simulate, for a certain value of U_2/U_0, the sensitivity of the results to width-to-depth ratio and Shields stress.

Firstly, unperturbed simulations were conducted. We simulated the morphological evolution of a symmetric bifurcation until equilibrium (morphology is constant in time). This was followed by a set of simulations in which a perturbation was imposed on the symmetric equilibrium morphology. One downstream channel was deepened and the other one was made shallower by 1 cm and the perturbed system was simulated until a new equilibrium was achieved. We analysed the depth asymmetry between both channels as a function of time, computed as

$$\Psi_h = \frac{\overline{h_3} - \overline{h_2}}{\overline{h_3} + \overline{h_2}}. \qquad (4.21)$$

where $\overline{h_3}$ and $\overline{h_2}$ are water depth averaged over the tidal cycle and over the entire branch length. A stable symmetric bifurcation is stable when the initially prescribed asymmetry decays, resulting in Ψ_h=0 in final equilibrium, while the symmetric bifurcation is unstable when the asymmetry grows, resulting in a non-zero Ψ_h (asymmetric bifurcation).

The sensitivity of the results to the width-to-depth ratio (w/h) was studied by varying the width of the upstream channel at the bifurcation ($w_{1;0}$), while the sensitivity to the grain related Shields stress was studied by varying the sediment grain size between 0.06-0.5 mm. This range of bed sediment size is within the range of observed values in tide-influenced deltas and estuaries according to observations of several tidal systems (e.g. Buschman et al., 2013; Hoitink et al., 2017; Hu et al., 2009; Sassi et al., 2013; Stephens et al., 2017).

Other model parameters were the morphological acceleration factor and the Chézy bed roughness coefficient. Since morphological development is a long-term process that requires up to thousands of

Table 4.1 Boundary conditions, model settings and some dimensional parameters for two continuous simulations. For each U_2/U_0, the equilibrium bed level was first calculated for a range of widths and grain sizes. Subsequently, this equilibrium was perturbed, and the simulation was continued until it reached the new equilibrium.

U_2/U_0	initial depth (m)	discharge (m^3s^-1)	w_1 at bifurcation (m)	tidal amplitude (m)	L_w (km)	L_c (km)	D_{50} (mm)	MorFac	tide-averaged Froude nr.	tide-averaged Rouse nr.
0 (river-only)	10	2,598 - 12,471	250 - 1,200	0	Inf.	0	0.07 - 0.4	800	0.105	0.48 - 12.63
0.4	10	292.65 - 1,877.85	100 - 1,000	1	15	10	0.07 - 0.5	800 - 2,000	0.096	0.48 - 15.61
1.7	10	125.21 - 1,252.11	100 - 1,000	1.5	15	20	0.07 - 0.4	10 - 2,000	0.052	0.48 - 12.63
3	10	32.3 - 165.03	97 - 500	1.5	15	40	0.07 - 0.4	50 - 2,000	0.042	0.48 - 12.63
5	6	30.80 - 151.82	94 - 500	1.35	15	40	0.06 - 0.2	15 - 1,000	0.020	0.36 - 5.17
9	4.5	27.87 - 132.91	130 - 620	1.5	15	40	0.06 - 0.2	30 - 800	0.012	0.36 - 5.17

Table 4.2 Channel geometry, boundary conditions and MorFac for test simulations to study the sensitivity of equilibrium bed to L_w, L_c ,river discharge and D_{50}.

test case	L_w (km)	L_c (km)	D_{50} (mm)	tidal amplitude (m)	discharge (m^3s^{-1})	initial depth (m)	w_1 at bifurcation (m)	MorFac	U_2/U_0 at equilibrium
Sensitivity of L_w	15 - Inf	20	0.25	1.5	1,252 - 10,392.3	10	1,000	400	0 - 4
Sensitivity of L_c	15	20 - 40	0.25		1,252 - 710.2			220	0 - 3
Sensitivity of Q	15	20	0.25		214.4 - 710.2	4.5 - 10		30 - 400	0 - 9
Sensitivity of D_{50}	15	20	0.1 - 0.4		1,252	10		200	0 - 1.7

years until the bed level achieves a morphological equilibrium, we applied a parameter morphological acceleration factor (MorFac) to accelerate the morphological development (Lesser et al., 2004). The MorFac value applied depended on the model settings as shown in Table 4.1 and Table 4.2. Regarding the bed roughness, a dimensionless Chézy coefficient was applied with the value of 20 (60 $m^0.5s^{-1}$ in dimensional form) as typically applied in tidal systems (Guo et al., 2015; Iwantoro et al., 2020; Xu et al., 2017). The channel configuration, boundary conditions and model settings for each simulation are shown in Table 4.1.

4.2.3 Validation of 1D approach by comparison with 2D model

The 1D model results for hydrodynamics and morphodynamics were compared with a well-established 2D numerical model (Delft3D model). This was done to check whether the 1D model is able to simulate the morphological evolution for cases that flows reverse during a tidal cycle. We therefore compared the 1D model results to a case similar as described in chapter 3. The numerical approach of the Delft3D model can be found in Lesser et al. (2004). The grid schematization to build a bifurcation followed the method of Kleinhans et al. (2008), in which the upstream channel was split by removing one node, or two grid cells, in the middle of the domain, as illustrated in Figure 4.3 (see also chapter 3 for details). For the comparison, we applied settings and forcings from the simulation with U_2/U_0=3, as shown in Table 4.1 applying a w/h of 50 and D_{50} of 0.07 mm. This was a case for which the symmetric bifurcation is unstable and in final equilibrium the bed levels of the two downstream channels are asymmetric.

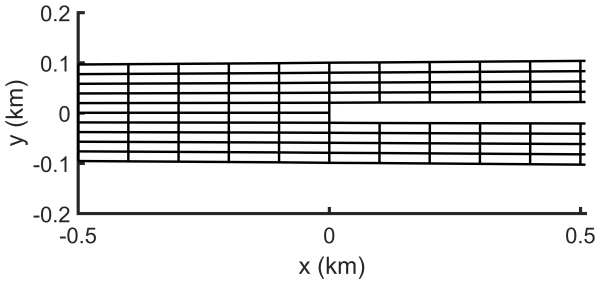

Figure 4.3 Close up of the numerical grid near the bifurcation for Delft3D model setup.

Regarding the hydrodynamics, the tide-averaged, semi-diurnal amplitude and its overtides (quarter- and sixth-diurnal amplitude) of water levels and flow velocities were compared for the symmetric case. No morphological update was included for the hydrodynamics comparison to prevent possible differences caused by different morphological evolution. The 1D results were compared with width-averaged values of the 2D model. The 1D model and 2D model show a fairly high correlation with r^2 values above 0.97 for all tidal constituents, both for along-channel water levels and flow velocities.

Regarding the morphodynamic evolution, the symmetric case without bed perturbation shows a very similar bed level profile in both models, in which a downstream shallowing pattern occurs from the point where the channel starts to widen (Figure 4.4a). The 1D model has a bit deeper lying bed than the

2D model, but the difference is less than 1 meter. The jump in bed level between upstream channel and downstream channels in Delft3D is due to the removal of two grid cells in the middle of the upstream channel, which caused a sudden reduction of channel width, starting at the bifurcation. Therefore, the bed level of the downstream channel compensates this width reduction resulting in a deepening of both downstream channels. As this width reduction was also applied to this 1D model run it likewise shows a sudden deepening after the bifurcation. After the bed levels of the symmetric bifurcation were perturbed and the bed evolution was simulated till a new equilibrium was achieved (Figure 4.4b), both models show similar bed level patterns and bed level asymmetry, in which the shallow downstream channel deepens in seaward direction while the deep shallows, and the depth difference between both channels is smaller downstream. While the model bed levels in the 1D model and 2D model are not exactly the same, the differences are acceptable and are caused by the fact that 2D model allows for variations in flow velocities and depth over the channel width. Because of the nonlinear feedbacks between flow and bed level this results in different width-averaged bed levels in the 1D and Delft3D model. The two models show some differences in the time series of morphological evolution of the downstream channels near the bifurcation (Figure 4.4c). Where Delft3D results show a gradual change until the new equilibrium, the 1D model shows a faster morphological change after 400 years. However, both models show a similar equilibrium depth of around 2.6 m for the shallow channel and 5.8 m for the deep one. Based on the comparison of the 1D and Delft3D model we conclude that the 1D model is able to simulate the morphodynamics of tide-influence bifurcations and can be used for further study.

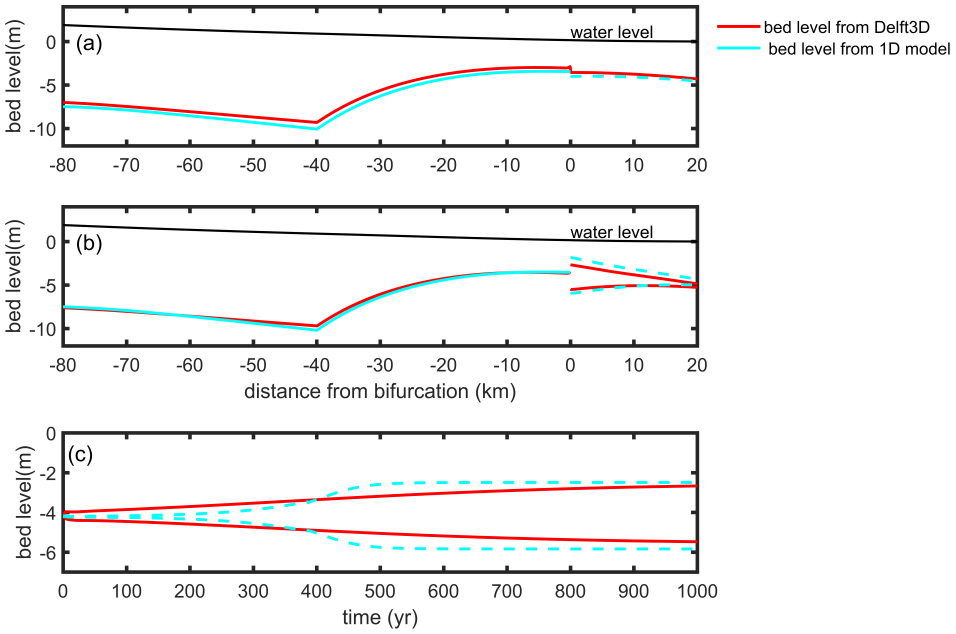

Figure 4.4 (a) Comparison of equilibrium morphology between the results of Delft3D (red line) and 1D model (cyan line) for symmetric bifurcation, Solid line is upstream channel and dashed lines represents morphology in downstream channels. Bifurcation is located at x=0. (b) Same as (a), but now after a bed perturbation in downstream channels was applied. (c) Time series of the morphological development in the downstream channels at bifurcation after bed perturbation.

4.3 Results

4.3.1 Effect of channel width profile on equilibrium morphology of symmetric bifurcations

The sensitivity of the equilibrium channel depth profile to the channel width profiles was simulated for the symmetric conditions (unperturbed) for a system forced by both river flow and tides (S_2 amplitude of 1.5 m). The e-folding length scale for channel width (L_w) and the position where the upstream channel becomes straight (L_c) strongly control the equilibrium morphology of the symmetric bifurcations (Figure 4.5a, b). Regarding the effect of L_w (Figure 4.5a), a straight channel (L_w=inf) results in channel deepening in seaward direction, up to about 25 m at sea. This confirms results of Leuven et al. (2021), Ragno et al. (2020) and Bolla Pittaluga et al. (2015b), who also found that tides in straight channels cause deeper channels compared to river-dominated conditions. The strong tidal flow downstream and river discharge upstream results in an unrealistic deepening of the channels and larger tides result in a deeper equilibrium depth profile. When prescribing a converging channel width profile in the seaward portion of the system, the depth profile at equilibrium has a linear bed profile in the upstream part, until the point where the channel starts widening. The slope has a small dependence on the value of L_w. Seaward from the straight-converging transition point the channel starts shallowing. The converging channel width increases the tidal influence upstream while decreasing the river-induced flow velocities, and a smaller L_w (stronger convergence) results in a stronger tidal influence and a more pronounced shallowing of the channel at the seaward side, as is found in many estuaries. Furthermore, a larger L_c, results in the shallowing part of the system to shift more upstream (Figure 4.5b) while the depth at the mouth seems to be independent of L_c. The value of L_c mainly influences the river-induced flow velocities and thereby the relative strength of tidal currents compared to river flow. Thus, beside defining a smaller L_w, a stronger tidal influence can be achieved by defining a channel width profile with a larger L_c.

The equilibrium bed profile is also sensitive to the prescribed initial depth (Figure 4.5c) because its value influences the prescribed discharge upstream (Eq. 4.4). Though the same tides were imposed for both simulations, the smallest discharge results in largest tidal influence (U_2/U_0 = 9, compared U_2/U_0 = 3 for largest discharge) at the bifurcation and the bed profile is very different.

In contrast to the channel width profile or upstream depth, the equilibrium bed profile is insensitive to the chosen grain size (Figure 4.5d). Thus, for the same tidal and river influence a change in grain sizes and therefore Shields stress will result in a similar equilibrium bed profile. Similarly, the equilibrium bed level of the symmetric bifurcations is also insensitive to the width at the bifurcation ($w_{1;0}$) and therefore width-to-depth ratio. This is because we approximated the wetted perimeter to be equal to width of the channel, as described in Section 4.2.1. By doing this, the morphological equilibrium of a symmetric bifurcation with the same L_w, L_c and initial depth but different channel width will be the same. The insensitivity of the equilibrium bed profiles to $w_{1;0}$ and grain size allows for a systematic study of the stability properties of the symmetric bifurcations as a function of width-to-depth ratio and Shields stress, while the sensitivity of the results to tidal influence can be studied by changing the width profile or depth.

4.3.2 Stability and asymmetry of tide-influenced bifurcations

The stability of symmetric bifurcations is highly sensitive to the tidal influence in the system. Figure 4.6a shows the neutral stability curves, indicating the transition for which symmetric bifurcation are stable to depth perturbations (lower left-hand side of graph) and unstable (upper right-hand side). The neutral stability curves were obtained from the model for a range of tidal influences (indicated by U_2/U_0) as a function of ebb-averaged width-to-depth ratio $< w/h >_{ebb}$ and the ebb-averaged grain-related Shields stress $< \vartheta' >_{ebb}$ averaged over the ebb phase. Figure 4.6b shows the neutral stability curves for different ebb-averaged with-to-depth ratios as a function of tidal

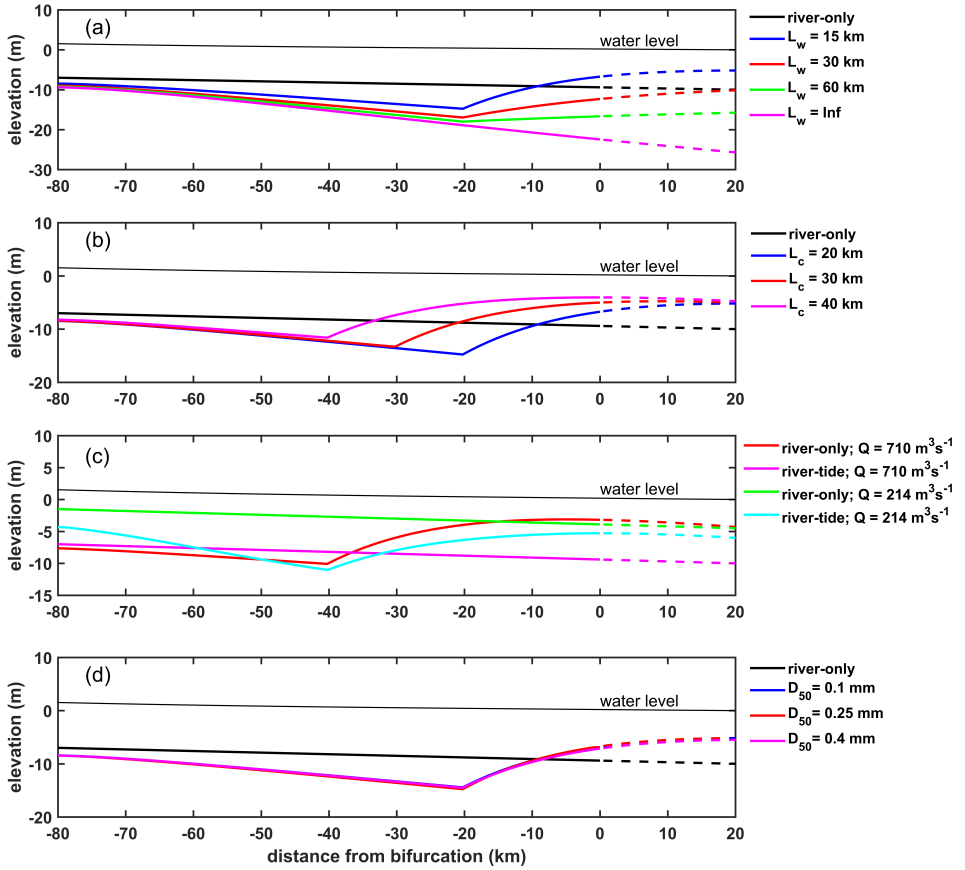

Figure 4.5 Equilibrium depth in all channels for the symmetric bifurcations for (a) different L_w with L_c = 20 km; (b) different L_c with L_w = 15 km and D_{50} = 0.25 mm; (c) different discharge due to different initial depth; and (d) different values of D50 with L_w = 15 km and L_c = 20 km. All simulations applied S_2 tidal amplitude of 1.5 m. The thick solid line indicates bed profile in the upstream channel while the dashed line is in downstream channels. The black (in (a), (b), and (d)); green; and magenta line (in (c)) are the equilibrium bed profile in river-only conditions (without tides and straight channel) and initial condition for simulations with tides.

influence and the ebb-averaged grain-related Shields stress averaged over the ebb phase. The averaging over the ebb phase was considered to be more suitable than tide-averaging because of two reasons. First, ebb flow has the same flow direction as river flow and therefore the results from the set of simulations with U_2/U_0<1 can be more easily compared to river-only bifurcations. Second, for the sets of simulations with low tidal influences (e.g., U_2/U_0=1.7), the Shields stress is nearly zero for several hours during rising tides. This is because the flood flow is counteracted by the river discharge. This would result in a small tide-averaged Shields stress, while it is clear that morphological change mainly takes place during ebb. Without the presence of tides (U_2/U_0=0), symmetric bifurcations are stable in only a limited range of low Shields stress and small w/h. This is consistent with findings in chapter 2 and in the previous studies (Bolla Pittaluga et al., 2003; Bolla Pittaluga et al., 2015a; Redolfi et al., 2019). When forced by small tides, the range of conditions for stable symmetric bifurcations significantly expand to a much larger width-to-depth ratio value (Figure 4.6a). The larger U_2/U_0 also

results in a larger range of ebb-averaged Shields stress conditions with stable symmetric bifurcations, up till a maximum (Figure 4.6b). However, when the system becomes more tide dominated, indicated by the cases of U_2/U_0=5 and 9, the opposite behaviour occurs. The unstable conditions expand to a much lower ebb-averaged values of Shields stress and w/h. As a result, only a limited stable regime exists, as shown for U_2/U_0=5 in Figure 4 6a,b and for U_2/U_0=9 in Figure 4.6b.

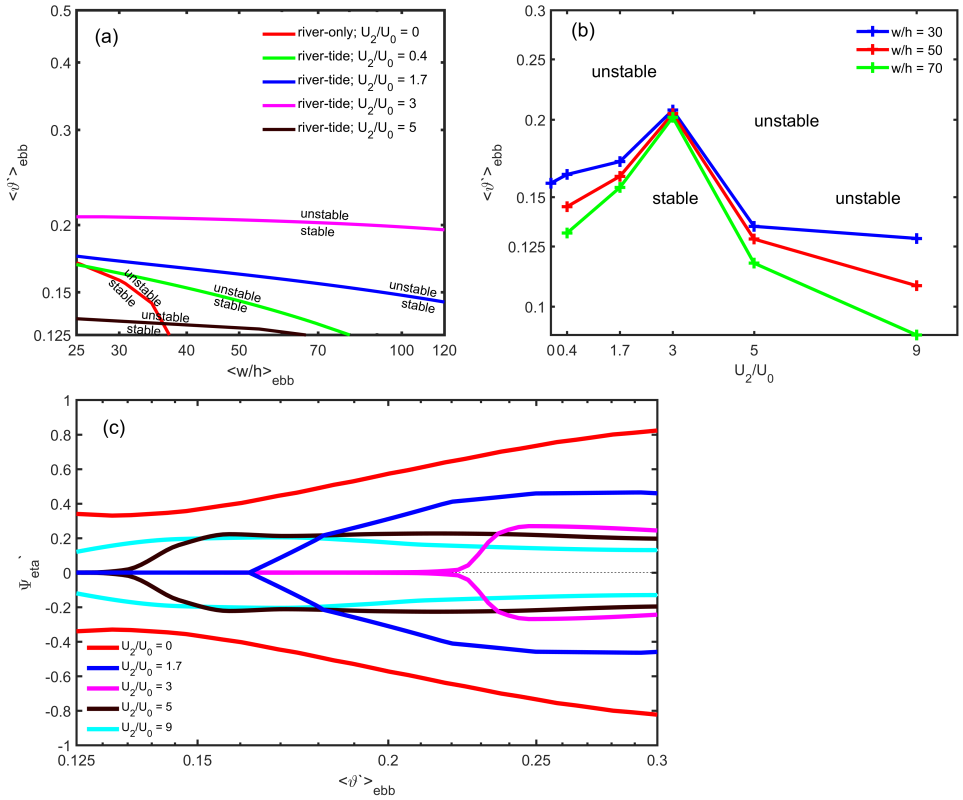

Figure 4.6 Neutral stability curves of symmetric bifurcations for a range of ebb-averaged grain-related Shields stress $< \vartheta' >_{ebb}$: (a) as a function of ebb-averaged width-to-depth ratio (w/h) for U_2/U_0 of 0-5 and (b) as a function of U_2/U_0; and (c) the bed level asymmetry between downstream channels in equilibrium for w/h of 50 and U_2/U_0 of 0-9.

Besides having a strong influence on the range of conditions for which stable symmetric bifurcations occur, tides also reduce the final asymmetry for the unstable conditions. Figure 4.6c shows the asymmetry in equilibrium for a range of Shields stress conditions and tidal dominance, for w/h=50. In the river-only case, asymmetric bifurcations occur for the entire range of Shields stress conditions, where the bed level asymmetry Ψ_h for higher Shields stress is close to 1, indicating a condition in which one of the two downstream channels will be abandoned. For the case of U_2/U_0=1.7, the asymmetry in unstable condition is about 50% smaller than for the river-only situation, and a range of conditions exist in which the bifurcation is stable to depth perturbations. For increasing tidal influence, the final asymmetry for the unstable symmetric conditions becomes increasingly smaller. Therefore, though the unstable symmetric bifurcations expand to a lower ebb-averaged Shields stress conditions for the most tide dominated conditions (U_2/U_0=5 and 9), the final depth asymmetry shows a further reduction, with maximum values around 0.2 This results in

bifurcations where both downstream channels continue to convey significant flow and sediment discharge.

4.3.3 Physical mechanism determining stability of bifurcations

We analysed our simulations to study the intratidal dynamics that determine whether a symmetric bifurcation is stable or unstable. It turned out that during ebb the asymmetry of the bifurcation decays, while it grows during flood, as long as flow velocities during flood are above the threshold value. We analysed the intratidal behaviour of flow, sediment transport and morphological change for two cases that have similar hydrodynamics, but different sediment mobility due to different D_{50}. One case had a stable symmetric bifurcation, while the other was unstable to depth perturbation. For the unstable case the asymmetry decay during ebb could not compensate the asymmetry growth that occurred during flood, while for the stable case it did. Because the asymmetry index based on the most upstream nodes in the downstream channels ($\Psi_{h;0}$) behaves similarly as the asymmetry index based on the spatial average of the bed level in each downstream channel (Ψ_h), focusing on what happens near the bifurcation is sufficient.

Tides cause a time-varying sediment mobility (Figure 4.7a,b), width-to-depth ratio and $\Psi_{h;0}$ (Figure 4.7c,d) when U_2/U_0=5. It can be seen that at flood the asymmetry grows. During ebb the asymmetry change is more variable in time, but it is mainly growing in the first part of the ebb (till 8h) and decreasing during the second part. The bed evolution in both channels $\frac{\partial Q_{s;0}}{\partial x} \approx \frac{\partial \eta_{;0}}{\partial t}$, shows that erosion and deposition (positive $\frac{\partial Q_{s;0}}{\partial x}$ indicates erosion and negative ($\frac{\partial Q_{s;0}}{\partial x}$ indicates deposition) in both downstream channels occur simultaneously during a tidal cycle (Figure 4.7e,f), but at different rates, explaining the change in bed-level asymmetry.

Asymmetry growth during flood

At early flood, deposition occurs in both downstream channels (Figure 4.7e,f). This is because during this phase, flood-directed flow velocities are larger seaward than they are landward resulting in a negative $\frac{\partial Q_{s;0}}{\partial x}$. The bed level asymmetry grows during this phase, because in the shallow channel deposition rate is faster than in the deep channel. Because in the deep channel the tides propagate faster than in the shallow channel, the tides tend to arrive earlier from the deeper channel. This causes spilling of water from the deep channel to the shallow channel (indicated by the interaction term of flow in Figure 4.8a), decreasing the spatial gradient in flow velocities (and thereby sediment transport) in the deep channel and increasing it in the shallow channel. This mechanism is illustrated in Figure 4.8a, where the interaction of flow between downstream channels induces a different spatial gradient of flow in both channels resulting in a development of bed level asymmetry. This asymmetry growth is more pronounced for the unstable symmetric case than for the stable case because the Shields stress is much larger for the unstable case, because of the smaller D_{50}. After the peak flood, the decreasing sediment mobility is followed by a decreasing deposition rate and in the late flood even erosion occurs, followed by a few hours without morphological change because Shields stress is too small to induce sediment transport. The same asymmetry change during flood is also found for U_2/U_0=3, (Figure 4.10 in Appendix 4A) but for U_2/U_0=1.7 the flood flow is too weak to induce sediment transport (Figure 4.10 in Appendix 4A). We conclude that when flood flows are large enough to induce sediment transport, during the flood phase the bed level asymmetry grows.

Asymmetry change during ebb

During ebb, the morphodynamics in the downstream channels are determined by the sediment division at the bifurcation. At early ebb, both downstream channels have an increasing erosion rate. At these moment the ebb-directed flow velocities increase in seaward direction, explaining the erosive trend. This is followed by a decreasing erosion rate and even a phase with deposition, when ebb flow is declining (Figure 4.7e,f). However, the rate of bed level change in both downstream channels is

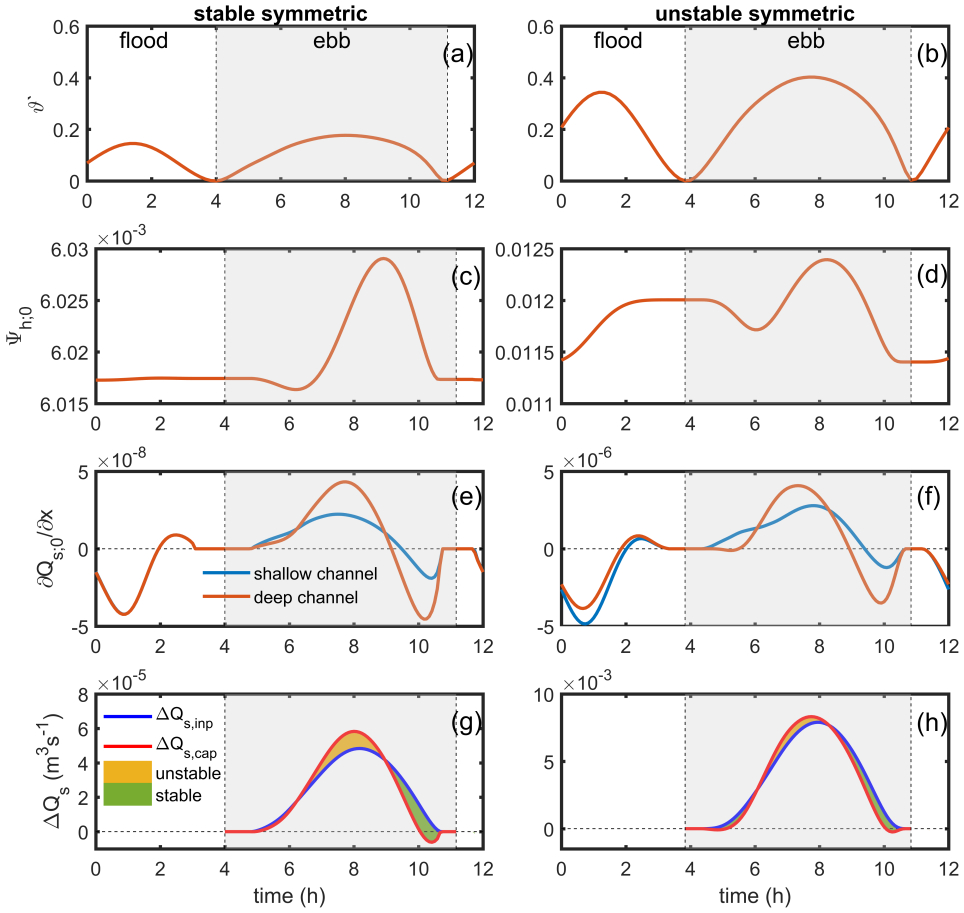

Figure 4.7 A fluctuation in a tidal cycle at the beginning of the simulation after the perturbation was imposed (the first 50 years) for: grainrelated Shields stress (ϑ') ((a) and (b)), bed level asymmetry at the most upstream grid in downstream channels (x=0) ((c) and (d)), sediment transport spatial gradient in downstream channels at x = 0 ((e) and (f)), and sediment supply and capacity difference between downstream channels ((g) and (h)) for simulations with U_2/U_0=5, $< \vartheta' >_{ebb}$=0.12 (left panels), $< \vartheta' >_{ebb}$=0.26 (right panels), and w/h=50.

different, which explains the change in bed level asymmetry in time. The temporal behaviour of $\Psi_{h;0}$ during ebb can be explained by the relation between the sediment transport capacity difference ($\Delta Q_{s,cap}$) between both channels and sediment supply difference ($\Delta Q_{s,inp}$) from upstream channel to both downstream channels (Figure 4.7g,h). $Q_{s,cap}$ is the sediment transport capacity at the most upstream node in the downstream channels while $Q_{s,inp}$ is the sediment supply from the upstream channel to each downstream channel that is computed by the nodal point relationship. When $\Delta Q_{s,inp}$ is higher than $\Delta Q_{s,cap}$ the bed level asymmetry between downstream channels decays, and otherwise it grows (Bolla Pittaluga et al., 2015a; Iwantoro et al., 2021). The differences between sediment supply and sediment transport capacity change in time during the ebb phase. At the beginning of ebb, when Shields stress is small, $\Delta Q_{s,inp}$ compensates $\Delta Q_{s,cap}$ and therefore reduces the asymmetry between downstream channels (Figure 4.7e,f). When the sediment mobility increases,

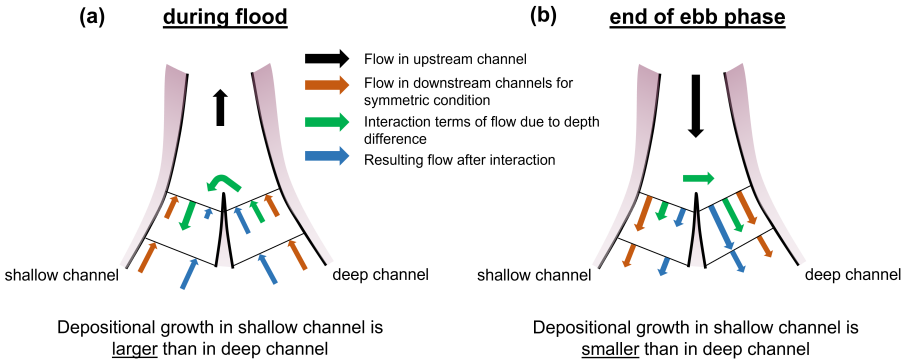

Figure 4.8 Mechanism of flow distribution at a bifurcation due to a depth difference between the downstream channels (defined perturbation) during (a) flood and (b) declining ebb flow, and its effect on the morphological development in the channels. Brown arrow indicates the symmetric flow condition when the bed level in the downstream channels is equal. After imposing bed level asymmetry between downstream channels, flow propagation from one downstream channel to the other (green arrow) occurs and results in a different spatial gradient of flow between downstream channels (blue arrow).

$\Delta Q_{s,cap}$ gradually exceeds $\Delta Q_{s,inp}$. The more rapid increase of $\Delta Q_{s,cap}$ is due to the nonlinear dependence of sediment transport capacity on flow velocity. The flow velocity in deep channel is larger than in the shallow channel, for the same reason as why it is larger during flood. As a result, the erosion rate in deep channel is larger than in shallow channel and therefore the asymmetry between downstream channels increases. When ebb flow declines, $\Delta Q_{s,cap}$ decreases more rapidly than $\Delta Q_{s,inp}$ and at some point the asymmetry starts to decay. During this phase the flow velocity in the upstream channel is larger than in both downstream channels as the declining ebb flow is earlier downstream. Furthermore, there is this interaction flow from the shallow to the deep channel, which causes a relatively large supply of sediment to the deep channel (caused by the cross-channel flow component in the nodal point relation as indicated by the interaction term of flow in Figure 4.8b). This explains the relatively fast deposition occurring in the deep channel during this phase. The same asymmetry change during ebb is also found for the other tidal influence conditions as shown in Figure 4.10 for U_2/U_0=3 and Figure 4.11 for U_2/U_0=1.7 in Appendix 4A.

4.4 Discussion

4.4.1 Applicability of the 1D model

In this study, a 1D morphodynamic model for bifurcations in river-dominated systems was extended to tide-influenced systems. Unlike earlier 1D models for tide-influenced systems (e.g. Jeuken and Wang, 2010; Zhang et al., 2014), the present 1D numerical model incorporates a nodal point relationship for sediment partitioning at bifurcation that considers transverse sediment transport when the sediment divides at the junction. Previous studies that used this approach were limited to river-dominated bifurcations (e.g. Bolla Pittaluga et al., 2015a; Redolfi et al., 2019; Iwantoro et al., 2021), or small tidal influence (Ragno et al., 2020) in which tides induce a changing flow magnitude but no change in direction (U_2/U_0<1). In this study we developed the approach further to allow the nodal point relationship to be applied in tide-influenced systems in which the flow magnitude and direction can differ in each connected channels and change through time. As a result, this model can be applied for a wide range of tide-influenced conditions. We have shown that the outcome of the 1D

model results in a similar morphological development as with a 2D model but requires a much shorter simulation time at less computational cost. Therefore, this model is more suitable to investigate a long-term morphological development at the scale of tidal deltas. Furthermore, in this study we base our conclusions on 800 simulations, while the findings in chapter 3 were based on 13 simulations. By having more simulations, a wider range of sediment mobility, width-to-depth ratio, and tidal influence than in chapter 3 were investigated. As a result, in contrast to the study conducted in chapter 3, this study found stable symmetric bifurcations with considerable tidal influence.

This study applied a new approach to compute sediment distribution at a bifurcation in unsteady flow conditions and can be applied in tide-influenced situations. It was assumed that the bed-slope driven sediment transport component can be scaled by the bed level differences between the different branches that connect at the junction and that it can immediately adapt when flow conditions change. However, in reality it may take time for this bedslope to develop, because it originates from a bar that develops at the junction (Redolfi et al., 2016; Salter et al., 2017). The comparison of the 1D model with the Delft3D simulations shows that this simplified approach works well, but further study is needed whether this is related to the fact that most of the time the flow was in a bifurcation condition in which water was flowing from the upstream channel to the two downstream ones as shown in Figure 4.9. The bifurcation condition at which the water flows from one of the downstream channels to the other two channels occurs when the depth between downstream channels is asymmetric and is limited to the transition between ebb and flood (shaded area in Figure 4.9). In this limited duration, the flow is small and therefore the sediment transport as well. When a situation occurs in which for a large portion of the tidal cycle water and sediment are flowing from one of the downstream channels to the other two channels also 3D flow effects can possibly be important, because the bifurcation angle is then very large. A vertical flow variation (3D effect) as presented, for instance, in Marra et al. (2014) and Lane et al. (1999) could become significant. However, in the 1D numerical model, this 3D effect is not taken into account (e.g. Kleinhans et al., 2012; Bolla Pittaluga et al., 2015a; Ragno et al., 2020). Field data is required for further study of the 3D effects in 1D models for tide-influenced bifurcations.

4.4.2 Comparison with previous findings

The wider range of conditions for stable bifurcations for weak tidal influence systems as shown in this study were also found by Ragno et al. (2020). They proposed that the more stable symmetric condition occurs because fluctuation of tidal flow deepens the downstream channels and therefore reduces the imposed asymmetry between downstream channels. The deepening of the channels also causes the w/h ratio to become smaller, favouring stability. While we also found that channel deepening occurs during ebb flow, we found that the morphological asymmetry development in an ebb cycle is due to the changing dominance of sediment transport capacity and supply difference between the downstream channels. This study also confirms the finding in chapter 3 that the equilibrium asymmetry of bifurcations is lower for systems with more tidal influence. As a result, the unstable symmetric bifurcations would not lead to abandonment of one downstream channel as often found in river-dominated systems, but instead asymmetric bifurcations can exist in a wide range of conditions. This is consistent with observations in tide- influenced deltas, such as by Kästner and Hoitink (2019). It is interesting to note that predicted equilibrium asymmetry for U_2/U_0>5 is in the order of 0.2 or even smaller. This implies that both channels will convey a considerable part of the tidal prism, river discharge and sediment transport, which has long-term ramifications for symmetry of delta progradation. In a purely fluvial situation with full channel avulsions, the delta only prograde around the mouth of active branches, but with tidal flows keeping both branches active, delta progradation would be more widespread and continuous.

The depth difference between downstream channels in the asymmetric bifurcations causes a partial tidal propagation from the deep channel to the shallow channel, as explained in the results section. This mechanism was also observed by Wagner and Mohrig (2019) in Wax Lake Delta where the tidal

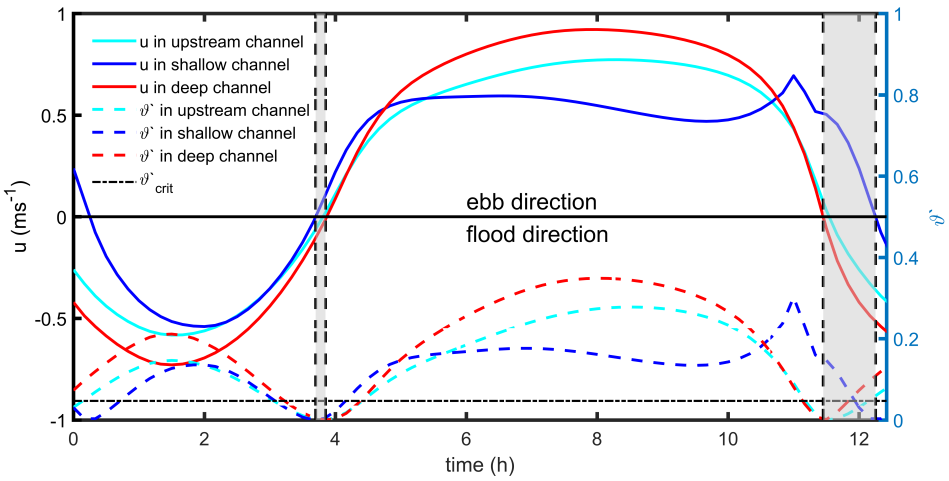

Figure 4.9 Intratidal behaviour of flow (u) and grain-related Shields stress (ϑ') at the bifurcation in all channels for asymmetric equilibrium condition of 1D model and Delft3D comparison. The shaded area indicates the transition period between ebb and flood at which flow (1) merges from the downstream and upstream channel to the other downstream channel (indicated by negative (flood-direction) u in the deep downstream channel, and positive (ebb-direction) u in the upstream and the shallow downstream channel) and (2) divides from one downstream channel to the the other two channels (indicated by positive u in the shallow downstream channel, and negative u in the upstream channel and the deep downstream channel). The dashed-dotted line indicates the critical Shields stress for sediment transport.

phase difference between downstream channels has caused a tidal propagation from one downstream channel to the other. Besides the phase difference they also observed a larger tidal flow amplitude in the channel that has the earlier tides as also shown in our model (Figure 4.12 in Appendix 4A). According to Chapter 3, the tidal propagation from one downstream channel to the other can lead to a development of subtidal trench at the bifurcation that connects the two downstream channels. This deepening at the bifurcation and tendency to keep both downstream channels open has also been observed in the Berau River Delta (Buschman et al., 2013).

While many tide-influenced channel networks exist without significant intertidal areas, many others do have extensive intertidal areas (Bain et al., 2019; Hiatt and Passalacqua, 2015). The presence of tidal flats could significantly change the asymmetry between flood and ebb flow. A larger tidal flat area in tidal systems generally leads to a more ebb-dominated condition (Pethick, 1980). This study has shown that flood flow increases the asymmetrical morphology between downstream channels. Defining tidal flats in the model may therefore reduce the influence of flood flow on the morphological development, which could lead to a broader range of conditions in which symmetric bifurcations are stable and a lower asymmetry between downstream channels for unstable symmetric conditions.

4.4.3 Future directions

This study showed the effects of tides and proposed an explanation of the physical mechanisms that determine the morphological evolution of tide-influenced bifurcations, but future studies are still required to explain other important effects that could be important for the stability and asymmetry of tide-influenced bifurcations. We propose several promising research directions.

First, human interventions can significantly disturb the morphodynamics of tide-influenced bifurcations in deltas. Globally, deltas with their distributary channels have high ecological and

economical values and are the centre of populations (Ericson et al., 2006; Syvitski and Saito, 2007). Engineering works such as dredging-dumping activities for navigation, e.g. in the ebb-flood channels of the Western Scheldt in the Netherlands (Jeuken and Wang, 2010) and the construction of short-cut channel between downstream branches of bifurcations could significantly influence the morphodynamics of these systems. Jeuken and Wang (2010) have, for example, shown that the equilibrium depth asymmetry between downstream channels can depend on the magnitude of the imposed initial perturbation. However, in their study the presence of transverse sediment transport at bifurcations that can compensate the asymmetry growth was not applied yet. This raises the questions whether transverse transport at a bifurcation can compensate the imposed asymmetry and whether there is a critical asymmetry threshold above which it cannot compensate the initial perturbation.

Second, sea level rise is important to the morphodynamics of bifurcations, especially in tide-influenced deltas. It changes tidal amplitude, tidal asymmetry and therefore the morphological response in the estuaries and deltas (Leuven et al., 2019; Prandle and Lane, 2015). Important questions are how and why sea level rise will affect the stability of bifurcations and their asymmetry. The deepening of the channel due to sea level rise increases the flood dominance (Wang et al., 2002) and different deposition rates in both downstream channels during flood, as shown in this study, may increase the asymmetry of the bifurcations. However, the morphological response during flood also depends on the relative importance of flood flow over ebb flow after sea level rises, so the effect is not clear yet.

Third, implementing movable channel banks in the model could further improve our knowledge about the morphodynamics in tide-influenced bifurcations. In tidal systems, tides induce morphological changes of the banks, resulting a converging channel width (as hypothesised in Savenije (2015)). This converging channel width provides feedback to the tidal propagation and affects the deformation of tides along the estuaries. In this study, the converging channel width was imposed. The effect of movable banks on tide-influenced bifurcations is unknown. However, effects of movable river banks in river dominated bifurcations were studied by Kleinhans et al. (2011) and Miori et al. (2006). They found that the unstable conditions for river bifurcations expand when the movable riverbanks are allowed in the model. This raises the question whether such an approach can be implemented in tide-influenced systems and whether this results in the same behaviour as in river-dominated systems.

Fourth, in the model the transverse transport of suspended sediment at bifurcation is only driven by cross-channel flow, while in nature a diffusive transverse suspended load could also occur due to a transverse bed slope (Baar et al., 2018; Hepkema et al., 2019). This transverse suspended sediment transport could oppose the asymmetric morphological development between downstream channels during flood and ebb may lead to a wider range of conditions for where symmetric bifurcations are stable than presented in this paper. Besides, this mechanism may also result in a smaller bed level asymmetry for unstable symmetric bifurcation.

Lastly, many deltas in the world have complex channel networks formed by several junctions, such as in Mahakam Delta, Rhine-Meuse Delta and Mekong River Delta. Our model results suggest that tidal channel networks with two active channels are not ephemeral systems that develop slowly towards asymmetry and abandonment but are in a stable condition. The more complex settings with more than two channels may lead to a significant asymmetric tidal propagation throughout the system. For instance, a length difference between downstream channels would impact the propagation of the tides and will result in differences in tidal flow velocities between channels. Furthermore, while we prescribed the same phase for the tides at the downstream boundaries, in reality both amplitude and phase can be different. We did not study these kind of externally forced asymmetries in this paper. The results in chapter 3 showed that increasing tidal influence will reduce the bed level asymmetry due to a length difference between downstream channels. They also showed

that a larger difference in tidal amplitude or phase prescribed at the two downstream channels results in a less asymmetric bifurcations. Simulating the hydrodynamics in the entire Mahakam Delta, Sassi et al. (2011) found that bifurcations closer to the sea have a higher tidal influence and have a less asymmetric tide-averaged discharge division between downstream channels. In contrast, using a series of simulations with a single, schematic bifurcation, Buschman et al. (2010) showed that tides increase this discharge asymmetry. This indirectly suggests that, beside affecting the flow distribution, the morphodynamics of bifurcations in a complex channel network may influence each other and induce an effect that cannot be captured by studying a single bifurcation. This leads to an open question whether the morphodynamics of an individual bifurcation in tide-influenced channel networks are influenced by the morphodynamic evolution of the other bifurcations.

4.5 Conclusions

Using a schematized bifurcation in a one-dimensional numerical model, this study showed the effects of tides on the stability and asymmetry of bifurcations in the range of river- to tide-dominated conditions and explained the mechanisms behind the effect of tides. We extend previous studies, which either focused on weak tides or were limited to few simulations, to tide-dominated conditions and explored a much larger parameter space. Compared with river-dominated systems, tides extend the conditions for which stable symmetric bifurcations can occur in mixed fluvial-tidal dominated systems, as long as the flood flow hardly drives morphological change. For these systems, the asymmetry change is determined by the ebb flows. For increasing tidal dominance, the smaller river discharge relative to the tidal discharge results in smaller peak ebb velocities and longer periods with low sediment mobility, and thereby cause symmetric systems to be stable. When tidal influence is increased above a certain optimum, the range of conditions for which symmetric bifurcations are stable becomes smaller again. We find that during flood the asymmetry grows. When the flood flow magnitude becomes comparable to the ebb flow magnitude, the asymmetry growth that occurs during flood cannot be compensated anymore during the ebb phase, and the bifurcation becomes unstable. However, although stronger tidal influence results in a more likely asymmetric development of the bifurcation, the final morphodynamic equilibrium becomes increasingly less asymmetric, confirming earlier findings. This keeps both downstream channels open and therefore prevents the tendency of abandonment of a downstream channel in tide-influenced bifurcations.

4.6 Appendix 4A

4.6.1 Additional figures: Mechanisms that induce morphological development in downstream channel

Figure 4.10 and Figure 4.11 shows that the asymmetric development between downstream channels depends on the sediment transport fluctuation in the downstream channels for simulations with U_2/U_0=3 and U_2/U_0=1.7, respectively. For the different tidal influence the most significant difference is during flood where the sediment mobility is larger for larger tidal influence (Figure 4.10a,b and Figure 4.11a,b). This also causes a larger asymmetric development during this phase (Figure 4.10c,d and Figure 4.11c,d) due to a larger morphological change (Figure 4.10e,f and Figure 4.11e,f). Meanwhile during ebb a similar asymmetry development occurs for different tidal influence that is mainly due to the relation between $\Delta Q_{s,inp}$ than $\Delta Q_{s,cap}$ (Figure 4.11g,h) where $\Delta Q_{s,cap}$ is dominantly due to the asymmetry of tidal flow (Figure 4.12).

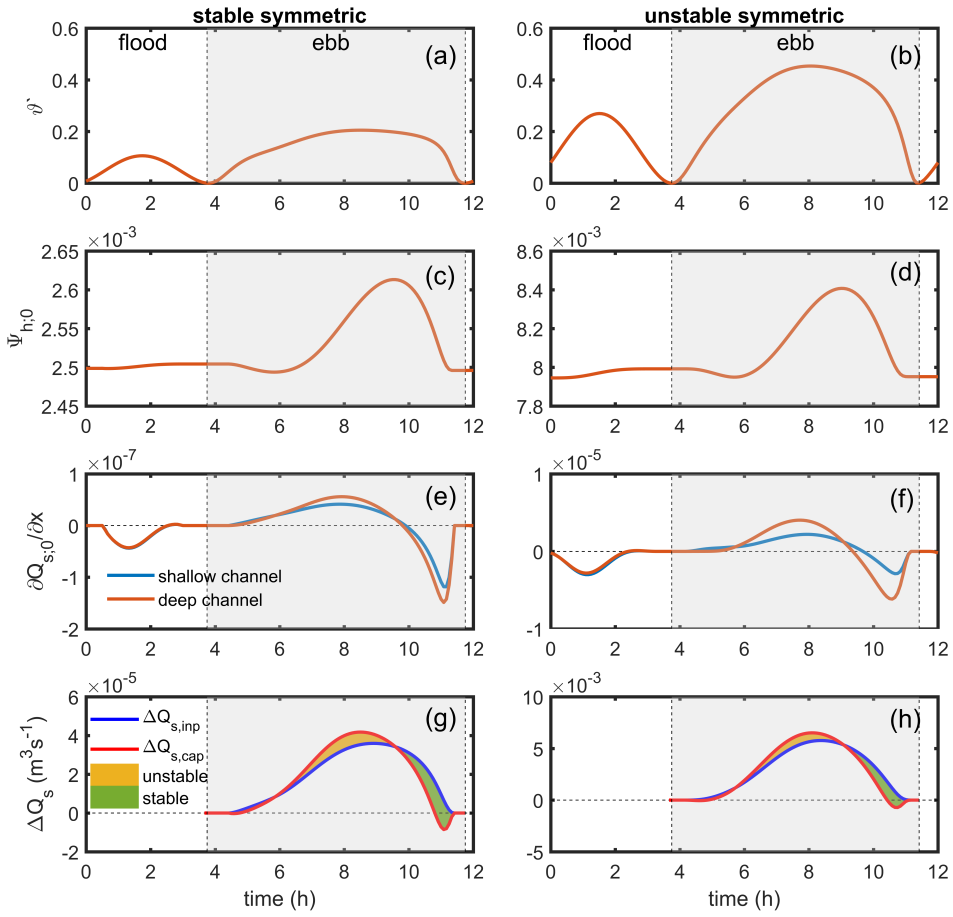

Figure 4.10 Same figure as Figure 4.7 for U_2/U_0=3 at $< \vartheta' >_{ebb}$=0.15 (right panels), and $< \vartheta' >_{ebb}$=0.25 (left panels).

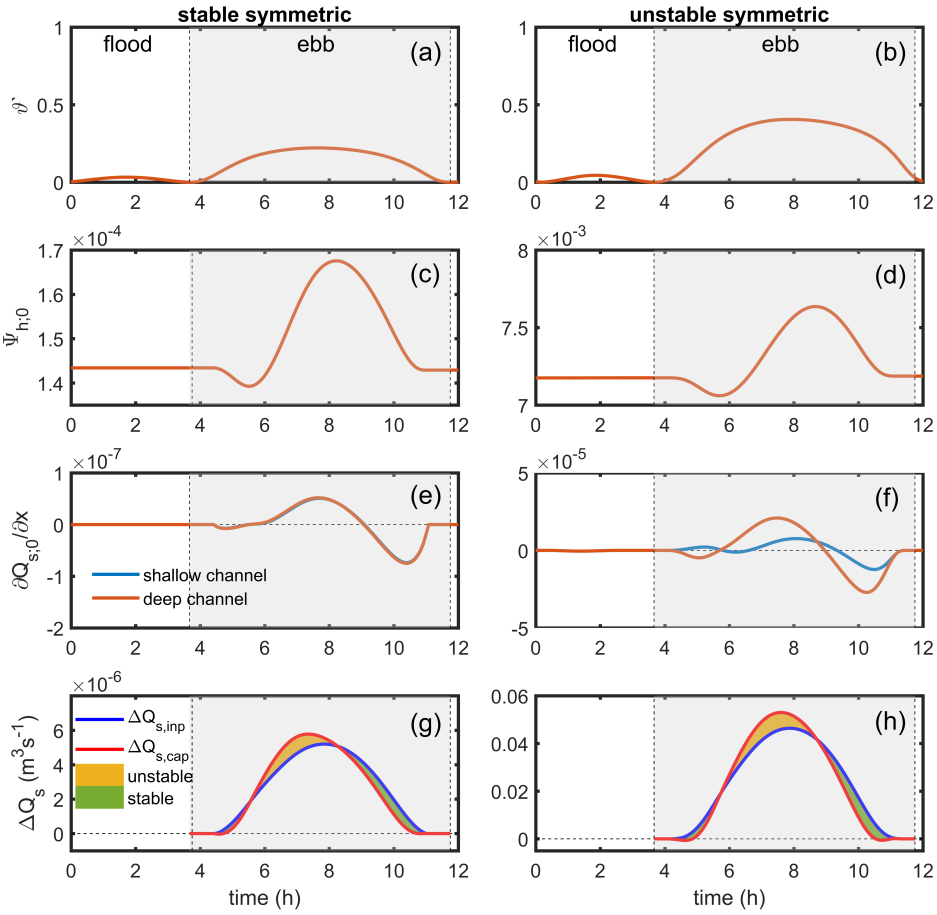

Figure 4.11 Same figure as Figure 4.7 for U_2/U_0=1.7 at $< \vartheta' >_{ebb}$=0.15 (right panels), and $< \vartheta' >_{ebb}$=0.45 (left panels).

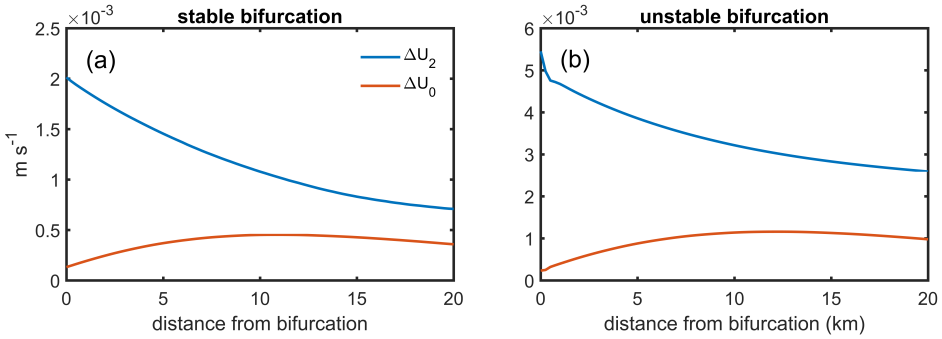

Figure 4.12 Tidal amplitude and tide-averaged flow velocity difference between deep and shallow downstream channel (ΔU_2 and ΔU_0, respectively) along the channels for (a) stable and (b) unstable symmetric bifurcation at the beginning of simulation after perturbation was imposed (the first 50 years with U_2/U_0=5, $< \vartheta' >_{ebb}$=0.12 (left panels), $< \vartheta' >_{ebb}$=0.26 (right panels), and w/h of 50.

4.6.2 Notation

$< \vartheta' >_{ebb}$	ebb-averaged grain-related Shields stress at bifurcation in upstream channel
$< w/h >_{ebb}$	ebb-averaged width-to-depth ratio at bifurcation in upstream channel
A	cross section area of the channel
a_k	tidal amplitude
C	total Chézy coefficient
C	grain-related Chézy coefficient
D_{50}	median diameter of sediment
g	gravitational acceleration
h	water depth
L_c	upstream distance from bifurcation where upstream channel width is funneling
L_w	e-folding length scale for width
P	wetted perimeter of the channel cross section
p	sediment porosity
Q	water discharge
Q_{bedl}	bedload flux
$Q_{bedl,y}$	transverse bedload flux at bifurcation
Q_s	total sediment load
$Q_{s,cap}$	sediment transport capacity
$Q_{s,inp}$	sediment supply from upstream channel to downstream channels
Q_{susp}	suspended load flux
$Q_{susp,y}$	transverse suspended load flux at bifurcation
Q_y	transverse water discharge
r	empirical constant for transverse bed slope effect
S	channel slope
T_k	tidal period
t	time
U_0	tide-averaged flow
U_2	tidal flow amplitude
w	channel width
w_s	sediment settling velocity
x	spatial coordinate in streamwise direction
y	spatial coordinate in transverse direction
z	water level
α	dimensionless length of the region under bifurcation influence
$\Delta Q_{s,cap}$	sediment transport capacity difference between downstream channels
$\Delta Q_{s,inp}$	sediment supply difference between downstream channels
η	bed level
ϑ	total Shields stress
ϑ'	grain-related Shields stress
μ	efficiency factor for grain-related Shields stress
ξ	Nikuradse roughness length related to the bedform
ρ_s	sediment density
ρ_w	water density
φ_k	tidal phase
Ψ_h	asymmetry index of along channel- and tide-averaged depth between downstream channels
$\Psi_{h,0}$	asymmetry index of tide-averaged depth between downstream channels at bifurcation
ω_k	tidal frequency

Chapter 5 | Morphodynamics of the Mahakam Delta: a channel network consisting of multiple bifurcations

Abstract

Abstract Mahakam River Delta in Indonesia is a typical example of a mixed fluvio- and tide-influenced river delta with a distributary channel network. The channels are connected at bifurcations where each upstream channel splits into two downstream channels. In such systems, the sediment distribution at the bifurcations determines the morphological development in the downstream channels. Furthermore, the tides, that drive unsteady flows in the network, induce a periodically changing sediment distribution at the bifurcations. This makes the morphological development of the delta more complicated than of river-dominated deltas. This study investigates how multiple tide-influenced bifurcations in the channel network affect the morphodynamics of the delta and whether the number of channels in the delta affects the morphological equilibrium of the entire delta. A channel network, inspired by the Mahakam Delta, was set up in a one-dimensional numerical model and simulations with different complexity of channel network were conducted. We found that, for a uniform initial bed level in convergent channels, the number of channels in the delta networks does not affect equilibrium channel morphology. We also found that in the case where the system has multiple bifurcations, imposing an initially different bed level in channel pairs downstream of bifurcations affect the morphological development of the entire delta and triggers asymmetric development of other bifurcations. Moreover, this enlarges the channels: the asymmetric condition increases the summed cross-sectional area of the channels along the delta. Unlike is common in river-dominated deltas, tides prevent channel abandonment in the shallowing channels while the other channels deepen, because tides reduce the difference between downstream bed elevations and keep both channels open. Since the morphological equilibrium of delta networks depends on the interaction among the channels, the more channels in a delta increase the possible equilibrium conditions that will occur due to the different initial conditions of the morphology.

5.1 Introduction

5.1.1 Background

Tide-influenced river deltas tend to be characterized by distributary channel networks with increasing numbers of downstream channels. The morphodynamics of tide-influence river deltas are mainly driven by the upstream river flow and by tidal propagation from the sea. In these systems, river flow and sediment transport through the delta are distributed mainly by bifurcations. Hence, bifurcations are the main factor determining morphodynamic development of each channel. As the studies in chapter 3 and chapter 4 showed, tides can have a stabilizing influence on bifurcations and induce less asymmetry, i.e. less of a difference in bed levels between the two downstream channels. However, these studies were based on a river network with one bifurcation only: one upstream channel that splits off into two downstream channels. However, many tide-influenced deltas have channel networks with multiple bifurcations, which begs the question whether tides influence a multi-channel network differently than a single bifurcation. Using the Mahakam Delta as a case study, we studied how the asymmetric evolution of one bifurcation system in a delta influences the other bifurcations. In terms of hydrodynamics, Sassi et al. (2011) found that in the Mahakam Delta the tide-averaged discharge asymmetry is smaller at the bifurcations further downstream, where tidal influence is bigger. These findings contradict Buschman et al. (2010)'s two-dimensional, idealised-model results of a single-bifurcation system, which showed that the tide-averaged discharge asymmetry at the bifurcation increases with increasing tidal influence. This raises the question whether the contradictory results are caused by the presence of multiple bifurcations in the channel network.

In this chapter we investigate how multiple tide-influenced bifurcations affect the morphodynamics within a delta and whether the number of channels in a delta influences the morphological equilibrium of the entire delta. We applied the one-dimensional (1D) numerical model from chapter 2 and chapter 4 to the Mahakam Delta (Figure 5.1). Although a 1D model will not yield detailed hydrodynamic and morphological features, as 2D and 3D models do, applying a 1D model has proven useful for systematically investigating complex channel networks, such as braided rivers (Howard et al., 1970), anastomosing rivers (Kleinhans et al., 2012) and river-dominated deltas (Salter et al., 2020), especially for studying morphodynamics at centennial or millennial time scales.

5.1.2 Study area

The Mahakam Delta was formed by alluvial deposits from the Mahakam River into the Makassar Strait. The Mahakam is one of the largest rivers in Indonesia with a catchment area of 77,100 km^2 (Hidayat et al., 2011) and a total channel length of about 900 km (Sassi et al., 2011). The delta has a very mild slope, allowing for tidal water level fluctuations up to 150 kilometres inland from the river mouth (Hidayat et al., 2011). In this tidal limit area, the river is connected to a lake which acts as a buffer for the river flooding upstream from the delta region (Hidayat et al., 2012). Kalimantan Island has a tropical climate with a dry season (May to September) and a wet season (October to April), which affect the river discharge in the delta, but the variation in discharge is reduced by the buffering lake. The annual mean discharge is estimated at about 3,000 m^3s^{-1} (Allen and Chambers, 1998) with the peak discharge during the wet season at around 5,000 m^3s^{-1} (Sassi et al., 2011). Two kilometres upstream from the delta apex (red star in Figure 5.1) is the Port of Samarinda, one of the biggest ports in Kalimantan for both container and passenger transport. The southern channels of the Mahakam Delta are dredged every year to maintain the depth of the shipping fairways that connect the port to the sea. These dredged channels are represented by solid white lines in Figure 5.1.

The Mahakam Delta has a fan-shaped distributary network and can be classified as a mixed fluvial-tidal delta (Galloway, 1975). The typical tidal regime in this delta is mixed, mainly semidiurnal (Indonesian Ministry of Transportation, 2021). During spring tides, the tidal range is between 1.8 and 2 m, while during neap tides, it ranges from 0.6 to 0.7 m (Indonesian Ministry of Transportation,

Figure 5.1 The Mahakam Delta in Kalimantan Island, Indonesia. The red dot in the inset shows where in Indonesia the delta is located. The solid white line indicates the shipping fairways through the Mahakam Delta. (Source: Google Earth©)

2021). At the delta apex, which is currently located about 35 km from the coastline, the river splits into two main distributary systems. One of these runs northeast and the other southeast. The southeastern distributary has a more complex channel network than the northeastern branch (see Figure 5.1). All the channels have diverging width downstream, as is common in tide-influenced channels (Friedrichs, 2010; Savenije, 2005). The channels are typically between 2 and 15 m deep, with the deepest end near bifurcations and the shallowest end near the river mouth. Neither channel migration (Allen et al., 1976) nor avulsion (Storms et al., 2005) occur in this delta, so the channel network has remained fixated for millennia. Channel sediment deposits in the Mahakam Delta consist of medium to fine sand with sediment sizes ranging from 0.2 to 0.3 mm, and of mud with sediment sizes smaller than 0.062 mm Gastaldo et al., 1995; Pham Van et al., 2016; Sassi et al., 2011.

5.2 Methodology

To study the multiple bifurcations in this delta, we used the 1D model presented in chapter 4. This model solves the Saint-Venant equations for hydrodynamics, van Rijn (1984a) and van Rijn (1984b) for sediment transport, the Iwantoro et al. (2021) and Iwantoro et al. (2022) approach for sediment division at the junctions under bifurcation conditions and the Exner equation for morphological development. chapter 2 and chapter 4 describe this model in more detail. Below is a description of the model set-up and schematizations for this chapter's study.

5.2.1 Defined cases

The Mahakam Delta channel network was simplified into three cases, based on the number of bifurcations in the channel network system. First, a 0-bifurcation case simulated a single channel estuary by merging all the channels of the Mahakam Delta into one channel. Second, a 1-bifurcation

case simulated a system with a single bifurcation, where the Mahakam River split into two downstream channels at the delta apex (Figure 5.2a). The width of each distributary was based on the summed width of the channels at a certain distance from the apex, which is the same as the 0-bifurcation channel's width. Each downstream channel was simplified based on the distributaries divided at the delta apex (represented by a red and white line in Figure 5.2b). Third, a 3-bifurcation case simulated a channel network with three bifurcations (Figure 5.2c). The approach was similar to the 1-bifurcation case, but here another downstream bifurcation was added to each channel. Figure 5.2d shows the steps by which the Mahakam distributaries were simplified into the channels used in the model. The 3-bifurcation case was included to investigate how one bifurcation in a large network can influence the morphological development of other bifurcations and therefore the entire system.

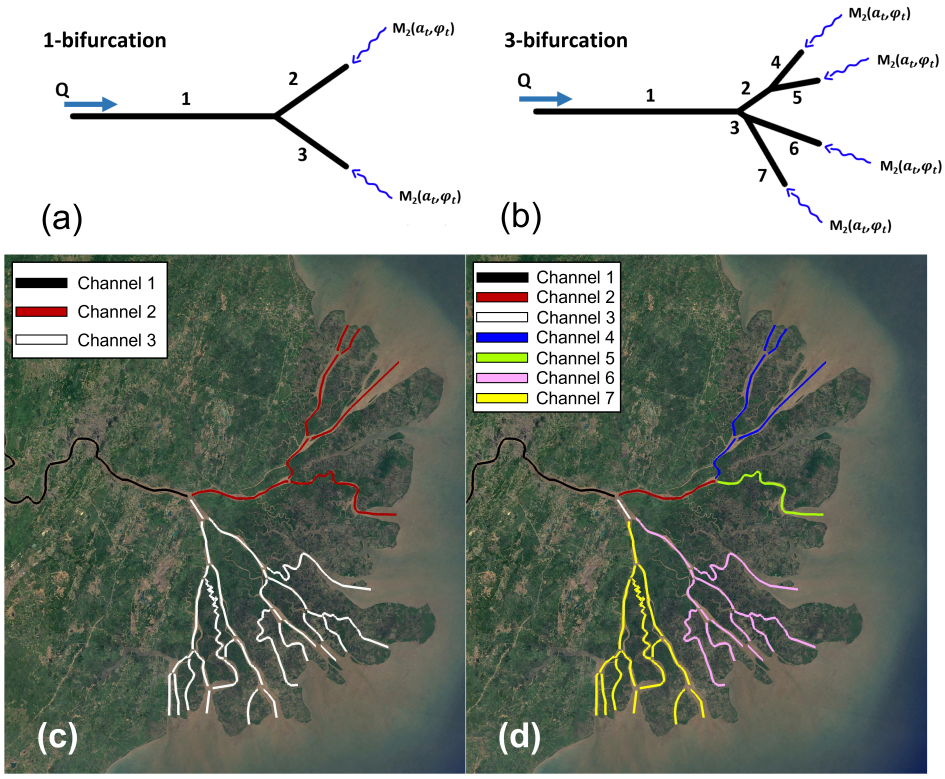

Figure 5.2 Schematization of the Mahakam Delta and the forces applied at open boundaries for (a) the 1-bifurcation case and (b) the 3-bifurcation case. The channels were defined based on the simplification of colorized channels for (c) the 1-bifurcation case and (d) the 3-bifurcation case.

5.2.2 Channel schematization

In the 0-bifurcation case, the width of the channel was assumed to remain constant for the upper 80 km, and widen along the lower 34.5 km. The transition from straight to widening channel is assumed to take place at the delta apex. The upstream section was defined as 1,240 m wide, based on the width of the Mahakam River near the apex at mean sea level as derived from a dataset collected by the Indonesian Navy (Pusat Hidro-Oseanografi Angkatan Laut (Pushidrosal)). The channel is assumed to widen exponentially downstream by applying the following expression

$$w(x) = w_0 e^{x/L_w} \tag{5.1}$$

where w_0 is upstream channel width and x is the local coordinate along the channel, where $x = 0$ at the apex and positive downstream. L_w is the e-folding length scale for width with a value of 10.6 km. The L_w value was obtained by measuring and fitting the summed width of all main channels from the river mouth to the apex based on the Pushidrosal dataset. The main channels that were included in the measurement are coloured in Figure 5.2c,d. The river mouths in which the width measurement was started are shown in red in Figure 5.3a. In defining the channel length from sea to apex, we needed to take into account that each river mouth in the delta is at a different distance from the apex and that there are many channel pathways whose distances needed to be measured. We therefore defined a polar coordinate system with its centre at the delta apex and its perimeter running along the distal of the delta as shown in Figure 5.3b. The channel length was defined as the radial distance from the centre to the perimeter. By taking this approach, we neglected any channel meandering and length differences between channels. This could be another variable to be investigated in a different study. Table 5.1 shows a summary of the channel configuration for the 0-bifurcation case.

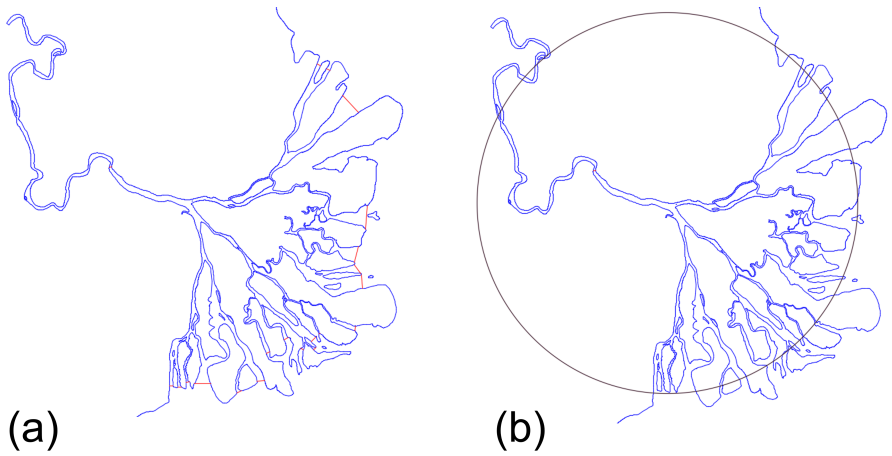

Figure 5.3 The Mahakam Delta overlaid by (a) the sea boundary locations (solid red line) and (b) a virtual circle (solid black line) with the delta apex at the centre and the delta's distal zone as the edge for measuring the distance from the apex to the sea, for the settings with symmetric length.

In both the 1-bifurcation case and the 3-bifurcation case, the upstream channel (Channel 1 in Figure 5.2) was defined to be the same as the upstream part of the channel in the 0-bifurcation case: straight, 1,240 m wide, 80 km long. The differences were in the distributaries only. In the 1- and 3-bifurcation cases, the channel divides flux equally at all bifurcations. Hence, the width of the bifurcates is half of their upstream channel width. This simplification was applied to avoid any effect of channel width difference between bifurcates on the morphological development of each bifurcation. Except for the upstream channel, all channels widen exponentially downstream from the apex to the sea by applying Eq. 5.1. For each channel, w_0 in Eq. 5.1 is the channel width furthest upstream. By applying these settings, the summed width of the channels along the delta and the distance from the apex to the sea are identical to the 0-bifurcation case. This means that the morphological development in the different cases can only be affected by the number of channels in the system, which is what this study was designed to investigate.

Table 5.1 The boundary conditions and parameter settings for all simulations.

case	channel name	length (km)	width at bifurcation (at apex for Case 0) (m)	e-folding length scale (km)	tidal amplitude (m)	river discharge (m^3s^{-1})	channel slope
0-bifurcation	channel 1	114.5	1,239.66	10.76	0.55	3,500	$1x10^{-5}$
1-bifurcation	channel 1	80	1,239.66	Inf.			
	channel 2	34.5	619.83	10.76			
	channel 3	34.5	619.83	10.76			
3-bifurcation	channel 1	80	1928.53	Inf.			
	channel 2	15.5	619.83	10.76			
	channel 3	3.75	619.83	10.76			
	channel 4	19	1,308.7	10.76			
	channel 5	19	1,308.7	10.76			
	channel 6	30.75	439.14	10.76			
	channel 7	30.75	439.14	10.76			

For the 1- and 3-bifurcation cases, two types of runs were performed. The first run was performed by initializing a uniform depth profile for all the channels (symmetric condition) and running the model until the equilibrium morphology was achieved. The final bed level from the first run was applied to simulate the second run. For this run, the equilibrium morphology was perturbed. In the 1-bifurcation case, the symmetric condition was perturbed by shallowing Channel 2 and deepening Channel 3 by 10 cm. In the 3-bifurcation case, the perturbation was applied in three different ways: by shallowing Channel 6 and deepening Channel 7 (hereafter: south perturbation), by shallowing Channel 4 and deepening Channel 5 (hereafter: north perturbation), and by combining both perturbations (hereafter: north-south perturbation). All deepening and shallowing had an amplitude of 10 cm. The perturbations were used to study the stability of the symmetric cases and possible interactions between the bifurcations.

5.2.3 Boundary conditions and parameterizations

The model was driven by river discharge from the upstream boundary and tides from the sea boundaries. The river discharge was based on the upstream channel properties.

$$Q = wCh\sqrt{ghS} \tag{5.2}$$

where w is channel width, h is channel depth, g is gravity and S is the initial channel slope. C is the nondimensional Chézy coefficient with a value of 20 (equivalent to about 60 $m^{0.5}s^{-1}$ for the dimensional Chézy), which is a typical value for tidal systems (e.g. Davies and Woodroffe, 2010; Fagherazzi and Furbish, 2001; Lanzoni and Seminara, 1998). In all simulations, the channel had an initial slope of $1x10^{-5}$ (Sassi et al., 2011). Using Eq. 5.2, the river discharge was 3,500 m^3s^{-1} which is within the range of the Mahakam Delta's annually averaged discharge and its wet period discharge (3,000-5,000 m^3s^{-1}) (Allen and Chambers, 1998; Sassi et al., 2011). Hence, the upstream depth was 6 meters. To define tides, the model requires the amplitude and phase data of the tidal components at the sea boundaries. In this study, we only imposed the most dominant tidal component in the Mahakam Delta, namely the semidiurnal tide M_2, in order to isolate the system from the effect of periodic tidal range variation on the morphological development caused by multiple tidal components. The M_2 amplitude at the downstream boundaries was set at 0.55 meters (Sassi et al., 2011) and the tidal phase was assumed to be equal at all downstream boundaries. Table 5.1. shows the boundary conditions.

Regarding sediment properties, Sassi et al. (2011) observed that the Mahakam riverbed mainly consists of fine to medium sand (0.2-0.3 mm). This sediment size is transported mainly as bedload, while the fine-grained sediment in the system (<0.062 mm) is transported largely as suspended load

(Pham Van et al., 2016). Since the model can only define a single medium grain size (D_{50}), we ran all simulations in Table 5.1 twice, each with a different sediment size. These two sets of simulations were defined to analyse whether the coarse and fine sediment contributed to the system's morphodynamics and if so, how. We first applied a medium grain size D_{50} of 0.25 mm, since this is within the range of sand sizes observed by (Sassi et al., 2011) in the Mahakam Delta. Then we applied a finer grain size than observed in the Mahakam Delta (D_{50} = 0.1 mm) to analyse the effect of finer-grained sediment on the morphodynamics in the system.

The channels were discretized with a 250-meter spatial step (Δx) and a 5-minute time step (Δt). Since morphological time scales are much longer than hydrodynamic time scales, we used an acceleration factor of 50 (Lesser et al., 2004) for morphological change (MorFac). This value is in the range used in our other 1D model studies (see chapter 2 and chapter 4 as well as in Delft3D simulations (e.g. Iwantoro et al., 2020; Roelvink, 2006; Van Der Wegen and Roelvink, 2008). We checked numerical stability and we checked that the results were not sensitive to the MorFac value. For all simulations, the bed levels of all channels and the morphological asymmetry of all bifurcations were analysed (calculated by Eq. 4.21 in chapter 4), and simulations were continued until a morphodynamic equilibrium was achieved. Morphological equilibrium is reached when morphological development ceases. The morphological time scale required to achieve an equilibrium is different for each simulation, depending on how much the initial morphology differs from the equilibrium morphology.

5.3 Results

5.3.1 Unperturbed runs

Figure 5.4 shows the equilibrium bed levels for all unperturbed cases. All cases showed very similar bed level profiles. In the upstream channel (or the upstream section of the channel in the 0-bifurcation case) where the channel is straight, the bed level gradually deepened downstream, and the equilibrium bed level was deeper than the initial bed level. The downstream widening of the channel, from the delta apex toward the sea, resulted in a shallowing of the downstream bed level profile. This profile is consistent with the available bed level data from the Mahakam Delta's north distributary, which is unperturbed by engineering activities, and shows the shallowest depths near the river mouths and a gradual increase of bed level upstream. The measured bed levels were obtained from Indonesian Ministry of Transportation (2021) and were averaged over the width. Compared to the north distributary data, the bed level dataset from the south distributary shows a more uniform depth, because the main channels of this distributary are regularly dredged to maintain the shipping fairways (Indonesian Ministry of Transportation, 2021). The measurements also show much more spatial variability and the presence of deep sections near the bifurcations (Sassi et al., 2011). Still, the modelled bed levels were within the range of the observed bed levels, with the exception of the most seaward 20 km of the estuary where the observed bed levels tended to be a bit deeper than the modelled ones. Given the simplified width profile compared to the real situation, we concluded that the comparison was satisfactory and usable for the second set of models.

The modelled M_2 water level profile along the channel in the unperturbed equilibrium for the 3-bifurcation case was compared with the dataset obtained from Indonesian Ministry of Transportation (2021) (Figure 5.5a). This dataset was based on a fortnightly water level measurement at four locations in the delta on 17-31 August 2014, as shown in Figure 5.5b. Table 5.2 shows the M_2 water level amplitude values from the dataset and the model results. Without an imposed morphological asymmetry or perturbation, the spatial pattern of the modelled M_2 water level amplitude looks similar to the observed water levels and ranges from 0.4 to 0.5 m. The model generally captures the gradual decreasing trend upstream also visible in the observations, but

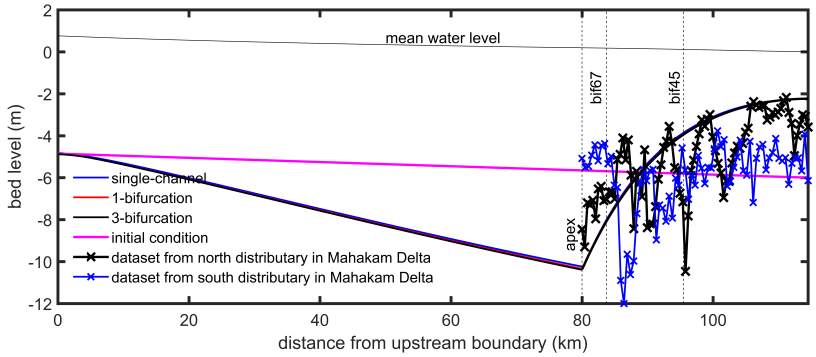

Figure 5.4 Equilibrium bed level profile along the channel for all unperturbed cases; their initial bed level; and the observed width-averaged bed level from the Mahakam Delta's north and south distributaries. The bifurcation locations are represented by a dashed line, where bif45 is the bifurcation that splits Channel 2 into Channels 4 and 5 and bif67 is where Channel 3 splits into Channels 6 and 7.

underestimates the M_2 water level amplitude at Samarinda and Tanjung Dewa. This could be caused by the friction coefficient variation along the channel in the Mahakam River and the simplification of the channel geometry applied in the model, such as width variations, too shallow water depths at the river mouth and the absence of stratification effects due to salinity differences.

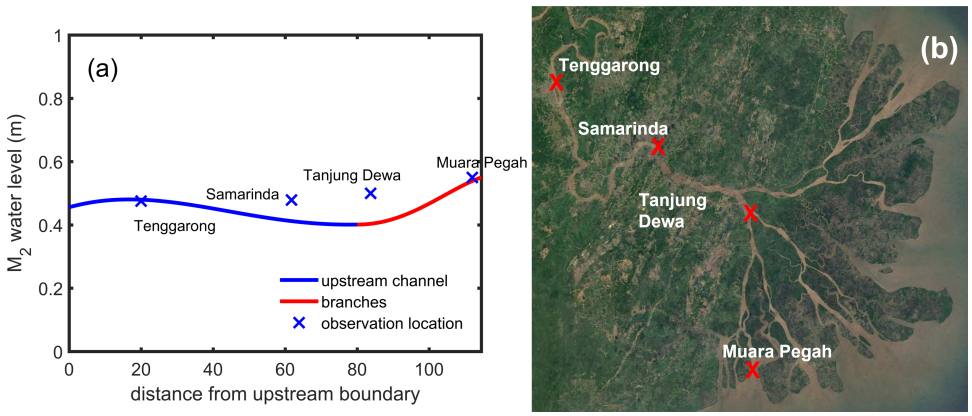

Figure 5.5 (a) Comparison of M_2 water level amplitude in the 3-bifurcation case at symmetric (unperturbed) equilibrium morphology with the data obtained by observation at four locations in the Mahakam Delta (Indonesian Ministry of Transportation, 2021) and (b) the locations of the measurements.

5.3.2 Equilibrium bed level for perturbed runs

The equilibrium bed level in the 1-bifurcation case was perturbed by shallowing one downstream channel and deepening the other one. The simulation was continued until a morphodynamic equilibrium was reached. The initial asymmetry increased, and the final bed level asymmetry was much greater than the initial perturbation. This indicates that the symmetric bifurcation is unstable. Furthermore, the final equilibrium morphology was asymmetric for both grain sizes studied (Figure 5.6). The initially shallow channel (Channel 2) became much shallower than 5 meters, while Channel 3 became deeper, and deepest at the apex (almost 20 m deep). Although the bed level was

Table 5.2 M_2 water level amplitude at four locations in the Mahakam Delta, shown in Figure 5.5b, from the dataset provided by Indonesian Ministry of Transportation (2021) and model results.

locations	M_2 water level amplitude (m)	
	measured	model results (unperturbed)
Muara Pegah	0.55	0.54
Tanjung dewa	0.51	0.40
Samarinda	0.48	0.41
Tenggarong	0.48	0.48

asymmetric, both channels showed maximum depth near the bifurcation and gradually shallowed downstream. Interestingly, the bed level in both channels became more similar near the sea boundaries and similar to the depths in the unperturbed simulation. This is because the hydrodynamic conditions near the sea boundaries are strongly tide-influenced and the tidal amplitude in both channels is the same. This results in a similar morphological equilibrium which is insensitive to the initial condition. Also note that the upstream channel is deeper in the asymmetric equilibrium than in the unperturbed, symmetric case.

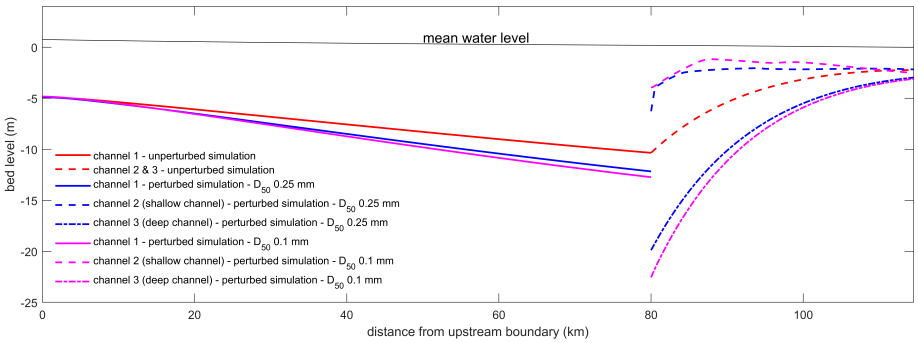

Figure 5.6 Equilibrium bed level for 1-bifurcation case in unperturbed (solid and dashed red lines) and perturbed simulations, for the coarse (0.25 mm) grain size run (solid and dashed blue lines) and the fine (0.1 mm) grain size run (solid and dashed magenta lines).

Figure 5.7 shows the equilibrium bed level for the 3-bifurcation case in which the branches furthest downstream were perturbed. In all variations of this case, the asymmetry increased, and the symmetric case turned out to be unstable. The growing asymmetry between the two downstream branches also induced asymmetry of the bifurcation at the delta apex and caused the equilibrium bed level in the upstream channel (Channel 1) to deepen. Similar to the 1-bifurcation case, the bed level asymmetry between each bifurcation's channels was greatest close to the bifurcation and significantly less downstream, particularly near the sea boundaries.

The initial depth difference between Channel 6 and Channel 7 (south perturbation in Figure 5.7a) resulted in a growing asymmetry between the two channels. The deep channel (Channel 7) overdeepened, to a maximum of about 30 m near the bifurcation, while the equilibrium depth in the shallow channel (Channel 6) was about 5 m. Furthermore, Channel 3, which is directly connected to the perturbed south branches, became much deeper than Channel 2 (north branch), while the shallowing occurred through the entire north distributary. However, although Channels 4 and 5 both shallowed, their bed levels were the same, because in this case there was no trigger that would induce

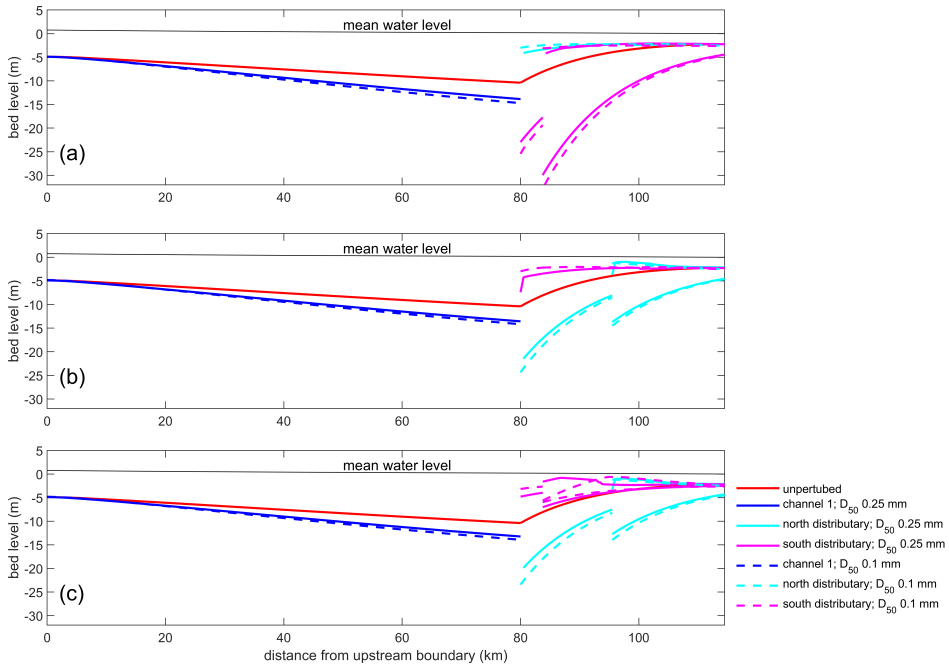

Figure 5.7 Equilibrium morphology of the 3-bifurcation case in perturbed simulations after imposing an initial depth difference between: (a) the south branches (Channel 6 (shallow branch) and Channel 7 (deep branch)), (b) the north branches (Channel 4 (shallow branch) and Channel 5 (deep branch)), and (c) both the north and south branches. Simulations are shown for a 0.25 mm D_{50} (solid lines) and a 0.1 mm D_{50} (dashed lines). The unperturbed equilibrium bed level (solid red line) is also plotted in each panel for assessment of the asymmetry.

asymmetry. Interestingly, the north branch bed levels ended up very similar to the bed level in Channel 6 (shallow south branch).

Similar results were obtained when the north branch bifurcation was perturbed (imposed depth difference between Channel 4 and Channel 5). The development was a mirror image of the south perturbation: the asymmetric development between Channels 4 and 5 resulted in asymmetric bed levels in Channels 2 and 3, but in this simulation, Channel 2 became deeper than Channel 3 and the shallowing occurred along the entire south distributary (Figure 5.7b).

Figure 5.7c shows the equilibrium bed level in the simulation in which both the north and south branches were perturbed. The north bifurcation's final asymmetry is similar to the asymmetry resulting from the simulation in which north perturbation was imposed. The south bifurcation ended up less asymmetrical than in the simulation in which only south perturbation was imposed. The asymmetry between Channels 4 and 5 was larger than the asymmetry between Channels 6 and 7. Furthermore, the perturbation in the downstream bifurcations also caused Channel 2 to become deeper than Channel 3.

Sediment grain size mildly affected the equilibrium bed level and the bifurcations' asymmetry, but the general patterns did not change. In the upstream channel, using a finer grain size caused a slightly deeper channel and the bifurcations tended to become more asymmetrical. A noticeable exception was the bifurcation of Channel 6 and Channel 7 in the simulation with both north and south perturbation. In the fine-sediment simulation, this bifurcation's branches were nearly symmetrical near the south bifurcation, while in the course-sediment simulation, they ended up asymmetrical.

5.3.3 Temporal evolution of bed level asymmetry

Asymmetric development of the delta apex bifurcation's branches is driven by the asymmetrical development of the bifurcations furthest downstream. The depth perturbation propagates upstream. Figure 5.8a and Figure 5.8b show bed level asymmetry of the bifurcation at the delta apex compared to the asymmetry at the bifurcation furthest downstream for all time steps, in the simulation with south perturbation (Figure 5.8a) and north perturbation (Figure 5.8b) respectively. The asymmetry between branches in the downstream bifurcation increased much earlier and faster than asymmetry at the delta apex, because the perturbation was initially imposed in the downstream bifurcation. As the asymmetric growth in the downstream bifurcation slowed down, the asymmetry in the delta apex bifurcation started to grow faster. This delayed growth in asymmetry at the delta apex bifurcation indicates that perturbation of the channels further downstream propagates upstream.

In the simulation with north and south perturbation combined (Figure 5.8c), the bifurcations also interact, but their interaction is less straightforward. The north bifurcation and the delta apex bifurcation interact in a way that is similar to the interaction in the north-only perturbation. However, the interaction between the south bifurcation and the delta apex bifurcation differs from the interaction in the south-only perturbation. In the combined perturbation, the asymmetry in the south bifurcation increases at the beginning of the simulation, but starts decreasing again when the asymmetry of the delta apex bifurcation exceeds 0.7. This indicates that the interaction between bifurcations is not just a one-way interaction, with the perturbed bifurcation affecting the others, but that it is a two-way process. This reduction in asymmetry only occurred close to the bifurcation, as shown in Figure 5.9. At the beginning of the simulation, the shallow channel (Channel 6) silted up due the presence of a sand bar that propagates downstream. This was followed by an increase in depth near the bifurcation, resulting in a depth that was more similar to the deep channel (Channel 7) that continued to deepen over time. However, this increase in depth in Channel 6 occurred only near the bifurcation, while in the middle of the channel, a sand bar caused a very shallow depth (less than 1 meter) and barely moved during 8,000 years of simulation. This very shallow depth in the middle of the branch indicates near-abandonment of Channel 6 and therefore weakens the tidal flow in this channel. The extreme shallowness of the shallow channel and the presence of tides that propagate from Channel 7 induce tidal propagation from Channel 7 to Channel 6 resulting in a strong tidal flows near the bifurcation in both channels. In accordance with chapter 3, this results in channel deepening at the bifurcation and development of a transverse subtidal trench that connects the branches. This process explains the sudden deepening at the bifurcation in Channels 6 and 7 in the fine-sediment simulation in Figure 5.7.

5.4 Discussion

5.4.1 Equilibrium depth in tide-influenced channel networks

This study showed that river deltas with multiple junctions and channels have the same bed level profile as a single channel estuary in which the width equals the summed width of all channels, as long as the bifurcations are symmetric (Figure 5.4). This supports the idea that simplifying delta channel networks into a single estuary is a plausible approach to study estuarine hydrodynamics and processes. This is because the single channel has almost the same total cross-sectional area and tidal prism as the delta with multiple channels and junctions (Figure 5.10). This approach has been used before, for example by Nguyen and Savenije (2006). In this study, the researchers simplified parts of the multi-channel Mekong Delta into a single channel to investigate salt intrusion.

The bed level profile of the Mahakam Delta in an unperturbed condition deepens in the straight, river-dominated section, attains maximum depth at the apex, and becomes shallower seaward in the section of the diverging channel width. Hence, the modelled bed level profile for the Mahakam Delta

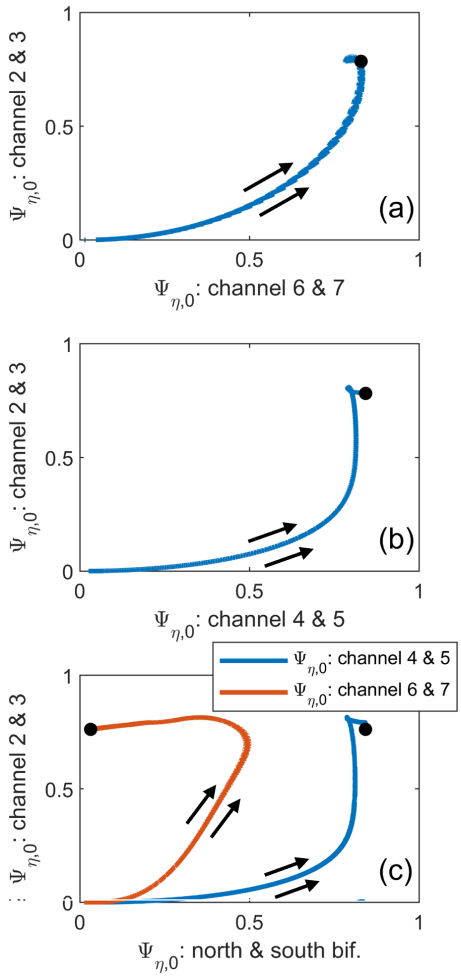

Figure 5.8 Bed level asymmetry over time (indicated by arrows) for the 3-bifurcation case; (a) delta apex bifurcation (y-axes) compared to south bifurcation in the simulation with south perturbation, (b) delta apex bifurcation compared to north bifurcation in the simulation with north perturbation, and (c) delta apex bifurcation compared to both bifurcations furthest downstream (north bifurcation in solid blue and south bifurcation in solid red). Black dots represent the asymmetry in which the compared bifurcations are in morphological equilibrium. Asymmetry is calculated for the upstream node in the branches. Results are shown for the simulation with D_{50}=0.1 mm.

has a 'large-scale scour hole', as Leuven et al. (2021) showed. They also found that for these systems the maximum depth occurs at the transition between the section that has a constant width and the section that has a diverging channel width. Furthermore, they found that this 'scour hole' is deeper for systems with a larger tidal amplitude and stronger channel divergence and is absent when the divergence is not strong enough.

A second main finding of this study is that when the bifurcations in a delta develop asymmetrically, the depth profile and summed cross-sectional area of all channels differ from those in the symmetric system. We perturbed the depth of different channels in the delta and found that in the Mahakam

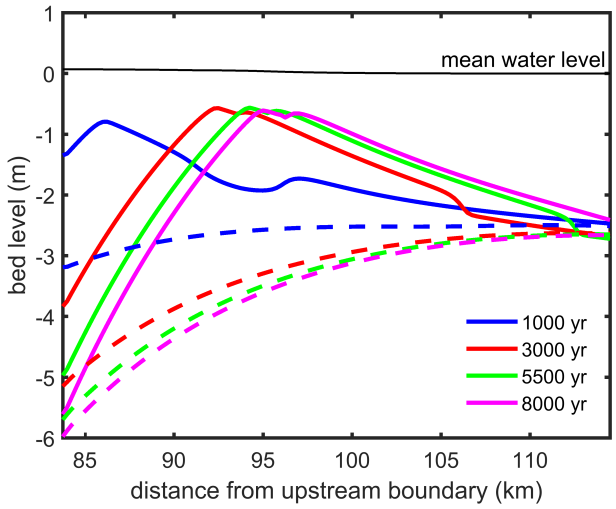

Figure 5.9 Bed level evolution along Channel 6 (solid lines) and Channel 7 (dashed lines) for the 3-bifurcation case (north and south perturbation) and simulation with D_{50} of 0.1 mm.

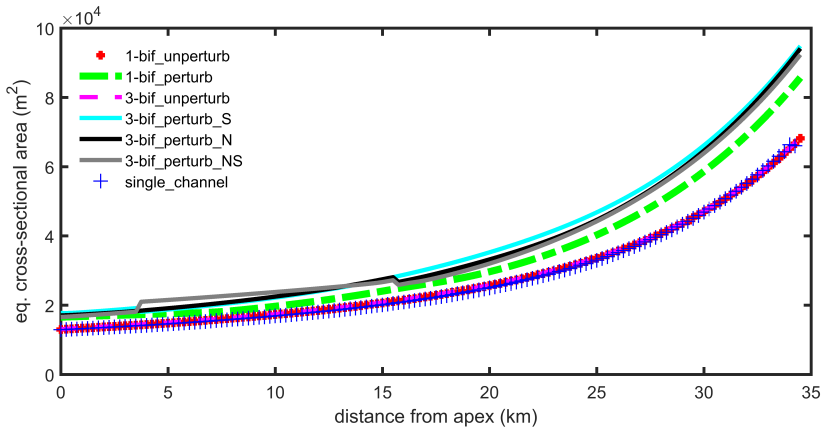

Figure 5.10 Total cross-sectional area for all simulations in the equilibrium morphology condition. See text for explanation.

model, this asymmetry increased, and new equilibrium bed level profiles were reached. As a result, the total cross-sectional area of all channels along the delta becomes larger than in the symmetric system and the presence of more bifurcations in a delta leads to a larger cross-sectional area (Figure 5.10). This is because tides keep the shallow channels open. Even though the deep branch of a bifurcation overdeepens, the shallow branch is not abandoned, which results in an increase in the total cross-sectional area. In addition, tides also cause less asymmetric bifurcations compared to river-dominated bifurcations, as we showed in chapter 3 and chapter 4. Asymmetric bifurcations in tide-influenced systems have been observed in many natural systems, such as in the Yangtze Estuary (Chen et al., 1982; Jiang et al., 2012) and in the Kapuas River Delta (Kästner et al., 2017; Kästner and Hoitink, 2019). In the Kapuas River Delta, there are three main bifurcations, whose depth asymmetry

Table 5.3 Comparison between the results of this study and those in chapter 4 regarding the stability of the bifurcations in the symmetric condition.

case	bifurcation	U_2/U_0	ebb-averaged Shields $(< \vartheta >_{ebb})$		$<w/h>_{ebb}$	model		stability plot	
			fine grain	coarse grain		fine grain	coarse grain	fine grain	coarse grain
1-bif	apex	1.61	0.14	0.062	117.70	unstable	unstable	Shields too low	Shields too low
3-bif	apex	1.63	0.144	0.064	119.296	unstable	unstable	unstable	Shields too low
	bif45 (north perturbation)	2.002	0.094	0.044	664.102	unstable	unstable	unstable	unstable
	bif67 (south perturbation)	1.68	0.164	0.058	108.828	unstable; stable for combined perturbation	unstable	unstable	Shields too low

index (Eq. 4.21 in chapter 4) ranges from 0.25 to 0.45 and whose downstream channels differ more than 50% in width (Kästner et al., 2017). However, this asymmetric condition seems to have been in a steady state for centuries (Kästner et al., 2017), suggesting a stable asymmetric situation.

5.4.2 Comparison of bifurcation asymmetries in chapter 4 (Iwantoro et al., 2022)

We determined the ebb-averaged Shields stress and width-to-depth ratio for all junctions in the Mahakam Delta's modelled configurations and compared the values to our findings in chapter 4 (Table 5.3). The results in this chapter are consistent with the stability conditions in the single bifurcation system we studied in chapter 4. The large width-to-depth ratios (above 117) and the moderate Shields stress conditions in the Mahakam Delta favour asymmetric bifurcations.

Most of the coarse-sediment simulations showed a lower sediment mobility (close to the beginning of sediment motion) than studied in chapter 4. However, we know from river-dominated bifurcations that such low mobility bifurcations tend to grow asymmetrically (Bolla Pittaluga et al., 2003; Bolla Pittaluga et al., 2015a). This tendency to have asymmetric bifurcations is even more pronounced in systems with gentle channel slopes (chapter 2). Hence, we conclude that the asymmetry of the bifurcations in the Mahakam model are fully in line with the findings of previous studies, for both the fine and coarse sediment fractions.

5.4.3 Comparison with the real condition in the Mahakam Delta

The results from the symmetric bifurcation simulation compared favourably to the bed levels observed in the Mahakam Delta. However, these symmetric bifurcations are unstable and turn into asymmetric bifurcations. While the modelled bed levels in the dominant channels are much deeper than the observed levels, observations in the delta also suggest that bifurcations are asymmetric. For example, in the north distributary, the asymmetry index for tidal-averaged flow (that has the same expression as Eq. 2.26 in chapter 2) between Channels 4 and 5 (see Figure 5.2d) is presently 0.15 (Sassi et al., 2012), with Channel 4 showing larger flow velocities than Channel 5. This asymmetry is also reflected in the channels' respective width, with Channel 4 being wider than Channel 5 (Figure 5.2d). In addition, the fact that the south distributary (Channel 7 in Figure 5.2d) serves as the navigational channel from the Port of Samarinda to the sea (Figure 5.1) because it is deeper than Channel 6, also suggests the existence of bed level asymmetries in the Mahakam Delta. However, modelled channel depths of more than 20 m have not been observed in the delta.

There are several possible causes for this lack of correspondence between model and observations. The first cause could be the presence of fine sediment in the Mahakam Delta (Pham Van et al., 2016). In this study, the possible effects of multi-sediment conditions were assessed by conducting two sets of simulations with different grain sizes. The effect of fine sediment on the morphodynamics in the delta was studied by parameterising fine sand (D_{50} = 0.1 mm). However, these simulations show a

similar asymmetry for two reasons. First, the shallow equilibrium bed level results in a large width-to-depth ratio causing a very limited range for stable symmetric bifurcations. Second, the model did not account for the cohesiveness of fine sediment. Braat et al. (2017) found that estuaries with a larger fine sediment fraction have shallower and narrower channels due to the cohesiveness of fine sediment. This cohesiveness reduces the erodibility of the riverbed and could thus counteract the deep channel's overdeepening that the model computed. Because the Mahakam Delta sediment is dominated by two fractions, namely sand (Sassi et al., 2011) and fine (cohesive) sediment (Pham Van et al., 2016), and because we focused solely on the sand fraction here, the omittance of the cohesive fraction could have resulted in too deep channels. Therefore, the model needs to be developed further to include multiple sediment grain sizes, as Braat et al. (2017) and Franz et al. (2017) did. Furthermore, when cohesive sediment is involved, the saltwater intrusion and stratification become significant to the morphodynamic processes in the delta and need to be considered as well, because density-driven currents have been observed to play an important part in driving sediment transport in deep channels (Allen et al., 1980; Friedrichs, 2009).

A second possible cause for the differences between modelled and observed results is the simplified hydrodynamic forcing from the sea. The spring-neap variation affects sediment transport (Li et al., 2015), because at spring tide the larger tidal range could enhance the generation of higher harmonics, resulting in a stronger tidal asymmetry and larger net sediment transport in the flood direction (Dronkers, 1986; Friedrichs and Aubrey, 1988; Speer et al., 1991). In addition, subtidal waves caused by river-tide interaction (Buschman et al., 2010) could influence morphological development.

A third possible cause for the differences between the model and the real condition is that we assumed a constant river discharge, while seasonal variations in river discharge causes variations in sediment input from upstream. During the wet season, the increased river discharge (Sassi et al., 2011) and sediment input into the delta could compensate for the erosional processes in the delta. Although the presence of the lake dampens the peak discharges and hence also the seasonal discharge variation (Hidayat et al., 2012), deforestation in the Mahakam catchment has increased the sediment input into the delta over the past decades (Prayoga, 2016; Tambunan, 2014). This could increase the disequilibrium deposition rate in the delta, including in the deepened channels.

A fourth possible cause are the simplifications we used to define the model. The reduced complexity of the system could affect the morphodynamics of the systems. In the Mahakam Delta, there are several small channel networks that were neglected in the model, especially in the south distributary. Channels 6 and 7 are simplifications of these complex channel networks, as seen in Figure 5.2d. Based on the model results, we showed that asymmetric development of a bifurcation in a channel network system could affect other bifurcations' asymmetry, which was corroborated by observations in river-dominated channel networks (Kleinhans et al., 2012; Salter et al., 2020). Based on these modelled and observed interactions, we could argue that if we set up a more complex channel network with more junctions, the morphodynamics in the smaller Mahakam Delta bifurcations might also affect the asymmetric development of the main bifurcations in the model.

A fifth and last possible cause is that we simulated the perturbed conditions until morphological equilibrium was achieved. This took thousands of years, because the gently sloping landscape in the Mahakam Delta and the relatively small tidal amplitudes offshore create a low-energy condition. This in turn results in low sediment mobility and slower morphological change than in river systems with steeper channel slopes. Therefore, today's Mahakam Delta might still be in a non-equilibrium state and might develop into a more asymmetric delta over the next centuries. Morphological change in the delta is also slowed down by the presence of cohesive sediment that reduces the erodibility of the riverbed.

5.4.4 Implications of the results for the Mahakam Delta

Human activity in the Mahakam River catchment could be regarded as a given perturbation that might induce asymmetric development of the bifurcations in the Mahakam Delta. Increasingly intensive agriculture, coal mining and palm oil plantations (Carlson et al., 2013) have led to massive infrastructural development to accommodate cargo shipping in Kalimantan (Indonesia), and particularly in the river deltas there. Kalimantan's river deltas play a vital role in the transportation and distribution of natural resources and in the transportation of people between islands. This is because water transportation is the most effective mode of transportation in the region (Mahmudah et al., 2010). To maintain the navigational channels between port and sea, regular dredging is required in high-traffic deltas, such as the Mahakam Delta, the Kapuas River Delta, the Barito River Delta, and the Berau River Delta. In this study, we have shown that a slight deepening of one channel in the delta will also perturb the morphology of other channels when the bifurcations are unstable, and will result in morphological changes such as silting up (3-bifurcation case for the distributary of Channel 2). The dredging works in the Mahakam Delta represented in Figure 5.1 act as a perturbation to the system that could shift the morphological equilibrium of the entire river delta. According to the model simulations, this perturbation could cause asymmetric development of all bifurcations in the delta. Though avulsion is less likely to occur, the other channels could silt up, which would disrupt the ecosystem in the delta. This merits further investigation in future studies.

5.5 Conclusion

In this study we used a 1D model whose settings were based on the current condition of the Mahakam Delta in Indonesia to investigate the morphodynamics of a tide-influenced river delta as a function of the number of bifurcations in the delta. The channel pattern of this delta was simplified to three levels of complexity, ranging from a system without bifurcations to a channel network with three bifurcations.

First, we investigated whether simplifying the delta system in terms of its number of channels and bifurcations would affect the morphological equilibrium of symmetrically shaped, unperturbed networks, where the equilibrium is expressed as the collective cross-sectional area along the channels. We found that the number of channels and bifurcations does not affect the depth profile and summed cross-sectional area along the delta in a symmetric, unperturbed condition. All studied channel network cases resulted in the same bed level profile as the single-channel estuary without bifurcations.

Subsequently, we perturbed the symmetric equilibrium by deepening one channel and shallowing the other channel downstream of a bifurcation. We ran simulations until morphodynamic equilibrium was achieved and studied how perturbations of the bifurcations furthest downstream affect the dynamics of the entire delta. When the morphodynamic equilibria were perturbed, asymmetric bed level profiles developed. The perturbed simulations showed that morphological development among the channels depended strongly on the number of bifurcations. For three bifurcations, all bed level profiles in the delta became asymmetric at the bifurcations. However, tides prevent complete abandonment of the shallow channels while the deep channels become quite deep in the cases with one and three bifurcations. This results in a larger total cross-sectional area in an asymmetric, perturbed delta than in a symmetric delta.

Based on the results of this study, we conclude that the morphological equilibrium of river deltas depends on the system's initial condition. In multi-channel systems, the channels' strong interdependent morphological development results in more possible equilibrium conditions depending on which channels were perturbed in the initial condition. In the case of the Mahakam Delta, anthropogenic interference with the morphology of the delta, such as new dredging works in other channels, will shift the morphological development from the existing situation to a new equilibrium.

Chapter 6 | Synthesis

The main objective of this research is to improve our understanding of the morphodynamics of tide-influenced bifurcation in river deltas. Based on this objective, four research questions were defined in chapter 1:

1. *How do channel slope and sediment size affect the morphological stability of river bifurcations?*
2. *How do tidal and fluvial influences affect the morphological asymmetry of bifurcations that have asymmetric downstream geometries or different tides in their downstream channels?*
3. *How does the relative importance of river and tidal influence affect the morphological stability of river bifurcations with a symmetric downstream geometry?*
4. *How do multiple bifurcations in tide-influenced delta networks affect the equilibrium of the entire deltaic channel network?*

The detailed results, discussions and conclusions of the research can be found in chapter 2 through chapter 5. This chapter summarizes and discusses the main findings and ends with suggestions for future research, aimed at further application and development of the 1D model for morphodynamic studies.

6.1 Summary of the main findings

From this research we conclude that, despite the fact that in tidal systems asymmetric bifurcations occur in a wider range of conditions than in river-dominated systems, tides counteract the avulsion and channel abandonment that often occur at river-dominated bifurcations. The detailed findings from chapter 2 through chapter 5 are summarized below:

1. Channel slopes and sediment sizes significantly influence the morphological stability of river bifurcations. Given a range of sediment mobility and width-to-depth ratio conditions, bifurcations with lower channel slopes and finer sediment sizes will have wider ranges of conditions that may lead to asymmetric bifurcations and a higher chance of avulsion.

2. For bifurcations with limited tidal influence, where no or only minor flood flows occur, increased tidal influence results in a wider range of conditions in which symmetric bifurcations are stable. However, in tide-dominated bifurcations where flood flow is considerable, increased tidal influence results in a narrower range of conditions in which symmetric bifurcations are stable.

3. In conditions where symmetric bifurcations are unstable, tides reduce the asymmetry between downstream channels compared to river-dominated conditions. At the same ebb-averaged width-to-depth ratio and sediment mobility, bifurcations with more tidal influence will show less depth asymmetry between downstream channels.

4. In distributary delta networks with multiple bifurcations, the number of channels does not affect the morphological equilibrium nor therefore the summed cross-sectional area of all channels along the symmetric geometry deltas, assuming negligible bank friction. However, the depth asymmetry imposed on a bifurcation furthest downstream of a distributary in the river delta can induce asymmetry of the apex bifurcation and reshape the morphological equilibrium of the entire delta. This asymmetric equilibrium depth will increase the total cross-sectional area and therefore tidal prism along the delta compared to the symmetric delta network. Hence, the morphological equilibrium of delta networks strongly depends on their initial conditions. The more channels there are in a delta, the greater the possibility of an ultimate equilibrium.

6.2 Stability of bifurcations in tide-influenced river deltas

Our first finding shows that small channel slopes and fine sediment increase the chances of abandonment of a downstream channel in river-dominated bifurcations. Hence, avulsion will occur in a wider range of conditions in lowland rivers, including river deltas, than suggested by previous studies (e.g. Bolla Pittaluga et al., 2015a; Redolfi et al., 2019). This is because lower channel slopes are observed further downstream in river systems (Pitlick and Cress, 2002) which, according to the relationship in Figure 2.3 (chapter 2), are also more likely to have finer sediment compositions.

The presence of tides in river deltas significantly affects the stability of bifurcations. Although we found a different explanation, part of our results confirms the findings of Ragno et al. (2020) for limited tidal influence, where increased tidal influences result in a broader range of conditions in which symmetric bifurcations are stable. While Ragno et al. (2020) suggested that the increase in the range of conditions in which symmetric bifurcations are stable is caused by the downstream channel deepening due to tide-induced flow fluctuation, our study shows that this increase is due to intratidal flow, and hence sediment mobility fluctuation, which causes the changing regime for bifurcation asymmetry in a tidal cycle as explained in chapter 4. This study also shows that this range of conditions for stable symmetric bifurcations peaks at a certain tidal influence condition. In more tide-dominated conditions, increased tidal influence leads to a wider range of conditions in which symmetric bifurcations are unstable. This is because there is more flood flow, which drives morphological change in the initially perturbed downstream channels. During flood, the asymmetry between downstream channels grows and this reduces the range of conditions for stable symmetric bifurcations. Though the conditions that foster unstable symmetric bifurcations increase, we found that increased tidal influence will have a dampening effect on a downstream channel's abandonment processes. In the conditions that favour unstable symmetric bifurcations, increased tidal influence also results in smaller asymmetries, as described in chapter 3 and chapter 4. This implies that the instability of a symmetric bifurcation will not lead to channel abandonment as observed in the Kapuas River Delta for bifurcations with large planform asymmetry (Kästner and Hoitink, 2019). The insights gained by this modelling explain the occurrence of nearly symmetric bifurcations in tide-influenced river deltas such as in the Berau River Delta (Buschman et al., 2013) and the Mahakam River Delta (Sassi et al., 2011) in conditions that would be conducive to avulsion in river-dominated deltas.

The stability of a single distributary with multiple bifurcations in tide-influenced distributaries such as the Mahakam Delta is not only affected by tides, but it is also determined by the morphological development of other bifurcations. In general, we found a strong interaction between the bifurcations in distributary delta networks. The bed level and asymmetry of bifurcations evolves in response to a perturbation imposed by a slight depth asymmetry in another bifurcation. Furthermore, in this new asymmetric equilibrium, a distributary system with more channels results in a larger summed cross-sectional area of all channels along the delta and therefore a larger tidal prism. This is because tides maintain all channels to keep conveying the water, which prevents the channels from silting up and being abandoned as they would in river-dominated distributaries. The perturbation that drives asymmetric development might be induced by sand mining or navigational dredging and dumping activities in estuaries and river deltas (e.g. Jeuken and Wang, 2010). Dredging-dumping activities in deltas and estuaries are required to maintain the depth of the shipping fairways. Navigation-related channel deepening is often conducted in response to anthropogenic activities upstream (e.g. Carlson et al., 2013) that require massive infrastructure development to accommodate transportation activities. The findings in chapter 5 suggest that dredging-dumping activities in a particular channel in a complex delta network will change the geomorphological equilibrium of the entire delta by inducing an asymmetrical development and a change in hydrodynamic conditions through an increase in tidal prism.

6.3 Future studies

6.3.1 Future advancement of 1D numerical model

In this study, we developed a 1D numerical model to simulate morphodynamics in tide-influenced channel networks. Using this model we showed and explained how the morphology of river bifurcations in river- and tide-dominated bifurcations evolves under a range of sediment mobilities, width-to-depth ratios, sediment grain sizes, channel slopes and tidal influences. The 1D model has confirmed the findings of a study that used a well-established 2D model (Delft3D). Future improvement of the 1D model is required to explain other important effects on the morphodynamics of bifurcations in river deltas. I propose several research directions.

First, naturally formed downstream channels of bifurcations have various and time-varying angles. The 1D model has ignored this. For bifurcations whose downstream channels are at a wide angle, the effect of non-uniform vertical flow structures (3D effect) at bifurcation could be important to the channels' morphodynamics (Kästner and Hoitink, 2019; Van der Mark and Mosselman, 2013). Although the downstream channels in tide-influenced systems have a narrow angle, tidal flows that result in flow and therefore sediment division from a downstream channel to another downstream channel and upstream channel could have great 3D flow effects, such as flow separation, on the sediment division at bifurcations. Further studies involving field measurement (e.g. Buschman et al., 2013; Kästner and Hoitink, 2019) and physical modelling (e.g. Marra et al., 2014) would be useful to quantify and parameterize this effect by adapting the nodal point relationship for implementation in the 1D model .

Second, diffusive, transverse, suspended load transport was observed in suspended load-dominated rivers (Biswas et al., 2015; Hepkema et al., 2019). In this study, the 1D model assumed that the transverse suspended load transport at bifurcation was caused only by transverse flow induced by asymmetric discharge division. At bifurcations, diffusion-induced sediment transport could also occur, due to a lateral variation in bed level and sediment concentration (Biswas et al., 2015; Hepkema et al., 2019). According to Hepkema et al. (2019), it has a similar direction as the transverse bedslope effect. Therefore, it also counteracts the asymmetrical development of bifurcations. This could result in a wider range of conditions that foster stable symmetric bifurcations and decreased asymmetry of unstable symmetric bifurcations.

Third, while many tide-influenced delta networks have limited intertidal areas that act as flood storage, others have been observed to have extensive intertidal areas (Bain et al., 2019; Hiatt and Passalacqua, 2015). In chapter 4, we showed that the morphological asymmetry of bifurcations is highly dependent on the dynamics of flood and ebb flow. Pethick (1980) suggested that a larger tidal flat leads to more ebb-dominated conditions. Thus, the presence of tidal flats could reduce the effect of flood flow on the morphodynamics of bifurcations. According to chapter 4, this could lead to a wider range of conditions that are conducive to stable symmetric bifurcations, and, for unstable symmetric bifurcations, to less asymmetry between downstream channels. The 1D model needs to be improved to include tidal flats, like Hepkema et al. (2018) did, and their effects on the stability of bifurcations needs to be studied.

Fourth, while previous studies have included river bank evolution in 1D models (Kleinhans et al., 2011; Miori et al., 2006), these have been limited to river-dominated bifurcations and are not readily applicable to tide-influenced bifurcations where flow direction regularly and systematically changes much more rapidly than the morphology. Including river bank development is not only relevant for the morphology. Anthropogenic activities such as aquaculture (Aslan et al., 2021; Setiawan et al., 2015), tourism Rahmawan et al., 2017 and agriculture (Nelson and Gunma, 2015; Yuen et al., 2021) have required land conversion, resulting in a significant reduction of mangrove forests in many river deltas (Alongi, 2002; Aslan et al., 2021; Webb et al., 2014). This land conversion has been observed, for

instance, in the Mahakam Delta as shown in Figure 6.1 (Fawzi and Husna, 2021). This deforestation not only damages and removes valuable ecosystems, but it also increases the erodibility of river banks and so could change the geomorphological equilibrium in deltas (Braat et al., 2017; Emberson, 2017).

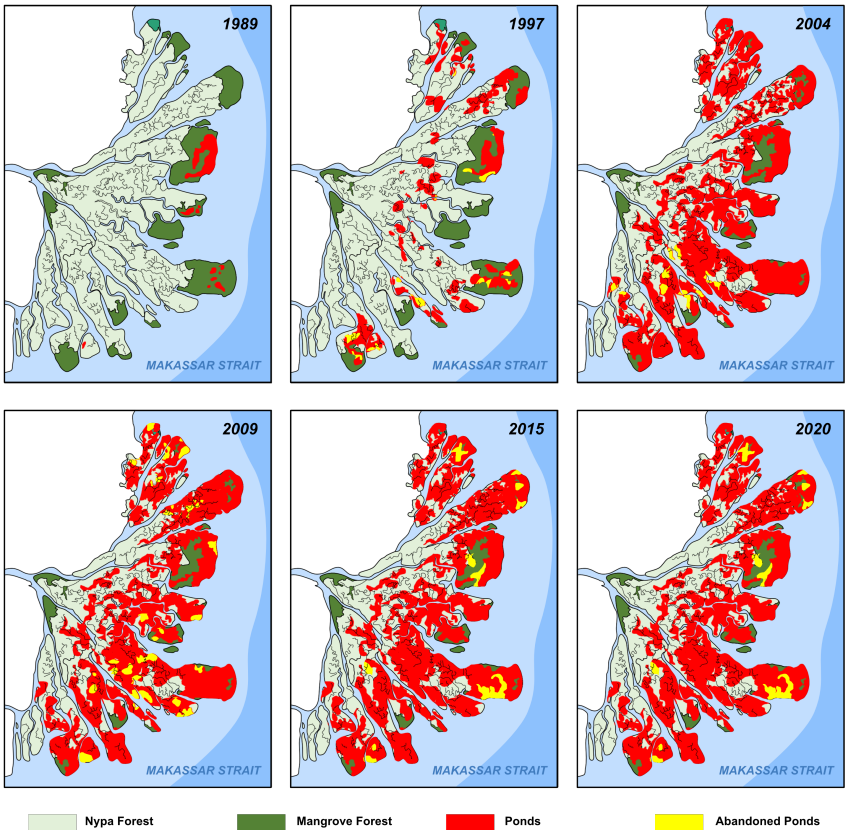

Figure 6.1 Land conversion from mangrove (*Avicennia* and *Rhizophora*) (dark green) and nypa palm (light green) forests to aquaculture ponds (red and yellow) in the Mahakam Delta, Indonesia over the last 30 years (after Fawzi and Husna, 2021).

6.3.2 Prospective applications of the 1D numerical model for river deltas

Although several improvements are needed to explore more morphodynamic processes in river deltas, the 1D model developed in this study is ready to be applied for studying important phenomena that significantly influence the development of river deltas all over the world. We mention two possible studies that could be conducted using the 1D model.

One is a study into the reduction of sediment flux from upstream that has been seen to occur in many river deltas. This is caused by land use change and extensive engineering works upstream over the past decades, such as upstream damming and levee hardening (Day et al., 2007; Syvitski et al., 2009;

Syvitski and Saito, 2007). As a result, many river deltas have lost land and have become more vulnerable to flooding due to storms, high river discharge and heavy rainfall (Day et al., 2007; Syvitski et al., 2009). However, the effect of sediment flux reduction on the morphodynamics of bifurcations in river deltas is unknown. Bifurcation stability may be affected by both channel shortening due to coastal erosion and channel deepening due to reduced upstream sediment supply. The 1D model developed in this study could be a useful tool to investigate this anthropogenic effect on river deltas. Instead of applying an equilibrium sediment transport condition at the upstream boundary as presented in this study, a reducing sediment input can be defined at the upstream boundary to study whether, how and why the upstream sediment reduction affects the morphological stability of tide-influenced bifurcations.

The second study that we propose is a study into the effect of climate change-driven sea level rise on the morphodynamics of tide-influenced bifurcations in river deltas. Sea level rise changes the tidal propagation into the channels (Ensing et al., 2015; Leuven et al., 2019) and therefore reshapes the delta's morphology (Van De Lageweg and Slangen, 2017). In systems with deep estuaries, sea level rise leads to sediment starvation and channel deepening (Leuven et al., 2019). Channel deepening increases flood dominance (Wang et al., 2002). During flood, a different deposition rate leads to an increase in downstream channel asymmetry as shown in chapter 4, so sea level rise may increase the range of conditions for unstable symmetric bifurcations and increase their asymmetry. However, morphological development during flood also depends on the relative importance of flood flow over ebb flow. In other words, the effects of sea level rise on tide-influenced bifurcations is still unknown, but could be investigated with the 1D model.

References

Alebregtse, N. & de Swart, H. (2016). Effect of river discharge and geometry on tides and net water transport in an estuarine network, an idealized model applied to the Yangtze Estuary. *Continental Shelf Research*, 123, pp. 29–49. DOI:HTTPS://DOI.ORG/10.1016/J.CSR.2016.03.028.

Allen, G.P., Salomon, J.C., Bassoullet, P., Du Penhoat, Y. & de Grandpré, C. (1980). Effects of tides on mixing and suspended sediment transport in macrotidal estuaries. *Sedimentary Geology*, 26 (1-3). DOI:HTTPS://DOI.ORG/10.1016/0037-0738(80)90006-8.

Allen, G. & Chambers, J. (1998). Sedimentation in the Modern and Miocene Mahakam Delta. *Indonesian Petroleum Association*.

Allen, G., Laurier, D. & Thouvenin, J. (1976). Sediment Distribution Patterns in the Modern Mahakam Delta. *Proceeding Indonesian Petroleum Association, Fifth Annual Convention*, (June 1976), pp. 159–178.

Alongi, D.M. (2002). *Present state and future of the world's mangrove forests*. DOI:HTTPS://DOI.ORG/10.1017/S0376892902000231.

Ashmore, P.E. (1982). Laboratory modelling of gravel braided stream morphology. *Earth Surface Processes and Landforms*, 7 (3), pp. 201–225. DOI:HTTPS://DOI.ORG/10.1002/ESP.3290070301.

Ashworth, P.J., Best, J.L. & Jones, M. (2004). Relationship between sediment supply and avulsion frequency in braided rivers. *Geology*, 32 (1), pp. 21–24. DOI:HTTPS://DOI.ORG/10.1130/G19919.1.

Aslan, A., Autin, W.J. & Blum, M.D. (2005). Causes of River Avulsion: Insights from the Late Holocene Avulsion History of the Mississippi River, U.S.A. *Journal of Sedimentary Research*, 75 (4), pp. 650–664. DOI:HTTPS://DOI.ORG/10.2110/JSR.2005.053.

Aslan, A., Rahman, A.F., Robeson, S.M. & Ilman, M. (2021). Land-use dynamics associated with mangrove deforestation for aquaculture and the subsequent abandonment of ponds. *Science of the Total Environment*, 791, pp. 148–320. DOI:HTTPS://DOI.ORG/10.1016/J.SCITOTENV.2021.148320.

Assine, M.L. (2005). River avulsions on the Taquari megafan, Pantanal wetland, Brazil. *Geomorphology*, 70 (3-4 SPEC. ISS.), pp. 357–371. DOI:HTTPS://DOI.ORG/10.1016/J.GEOMORPH.2005.02.013.

Baar, A.W., Boechat Albernaz, M., van Dijk, W.M. & Kleinhans, M.G. (2019). Critical dependence of morphodynamic models of fluvial and tidal systems on empirical downslope sediment transport. *Nature Communications*, 10 (1). DOI:HTTPS://DOI.ORG/10.1038/S41467-019-12753-X.

Baar, A.W., de Smit, J., Uijttewaal, W.S.J. & Kleinhans, M.G. (2018). Sediment Transport of Fine Sand to Fine Gravel on Transverse Bed Slopes in Rotating Annular Flume Experiments. *Water Resources Research*, 54 (1), pp. 19–45. DOI:HTTPS://DOI.ORG/10.1002/2017WR020604.

Bain, R.L., Hale, R.P. & Goodbred, S.L. (2019). Flow Reorganization in an Anthropogenically Modified Tidal Channel Network: An Example From the Southwestern Ganges-Brahmaputra-Meghna Delta. *Journal of Geophysical Research: Earth Surface*, 124 (8), pp. 2141–2159. DOI:HTTPS://DOI.ORG/10.1029/2018JF004996.

Bertoldi, W. & Tubino, M. (2007). River bifurcations: Experimental observations on equilibrium configurations. *Water Resources Research*, 43 (10). DOI:HTTPS://DOI.ORG/10.1029/2007WR005907.

Bertoldi, W., Zanoni, L., Miori, S., Repetto, R. & Tubino, M. (2009). Interaction between migrating bars and bifurcations in gravel bed rivers. *Water Resources Research*, 45 (6). DOI:HTTPS://DOI.ORG/10.1029/2008WR007086.

Biswas, R.K., Egashira, S. & Yorozuya, A. (2015). Influence of lateral bed slope on erosion-deposition processes in suspended-sediment dominated rivers. *Journal of Japan Society of Civil Engineers, Ser. B1 (Hydraulic Engineering)*, 71 (4), I$_8$71*I*$_8$76. DOI:HTTPS://DOI.ORG/10.2208/JSCEJHE.71.I_871.

Blondeaux, P. & Seminara, G. (1985). A unified bar–bend theory of river meanders. *Journal of Fluid Mechanics*, 157 (HY11), pp. 449–470. DOI:HTTPS://DOI.ORG/10.1017/S0022112085002440.

Bolla Pittaluga, M., Coco, G. & Kleinhans, M.G. (2015a). A unified framework for stability of channel bifurcations in gravel and sand fluvial systems. *Geophysical Research Letters*, 42 (18), pp. 7521–7536. DOI:HTTPS://DOI.ORG/10.1002/2015GL065175.

Bolla Pittaluga, M., Repetto, R. & Tubino, M. (2003). Channel bifurcation in braided rivers: Equilibrium configurations and stability. *Water Resources Research*, 39 (3), p. 1046. DOI:HTTPS://DOI.ORG/10.1029/2001WR001112.

Bolla Pittaluga, M., Tambroni, N., Canestrelli, A., Slingerland, R., Lanzoni, S. & Seminara, G. (2015b). Where river and tide meet: The morphodynamic equilibrium of alluvial estuaries. *Journal of Geophysical Research: Earth Surface*, 120 (1), pp. 75–94. DOI:HTTPS://DOI.ORG/10.1002/2014JF003233.

Braat, L., van Kessel, T., Leuven, J.R.F.W. & Kleinhans, M.G. (2017). Effects of mud supply on large-scale estuary morphology and development over centuries to millennia. *Earth Surface Dynamics*, 5 (4), pp. 617–652. DOI:10.5194/ESURF-5-617-2017.

Burge, L.M. (2006). Stability, morphology and surface grain size patterns of channel bifurcation in gravel–cobble bedded anabranching rivers. *Earth Surface Processes and Landforms*, 31 (10), pp. 1211–1226. DOI:HTTPS://DOI.ORG/10.1002/ESP.1325.

Buschman, F.A., Hoitink, A.J.F., van der Vegt, M. & Hoekstra, P. (2010). Subtidal flow division at a shallow tidal junction. *Water Resources Research*, 46 (12), W12515. DOI:HTTPS://DOI.ORG/10.1029/2010WR009266.

Buschman, F.A., van der Vegt, M., Hoitink, A.J.F. & Hoekstra, P. (2013). Water and suspended sediment division at a stratified tidal junction. *Journal of Geophysical Research: Oceans*, 118 (3), pp. 1459–1472. DOI:HTTPS://DOI.ORG/10.1002/JGRC.20124.

Carlson, K.M., Curran, L.M., Asner, G.P., Pittman, A.M., Trigg, S.N. & Marion Adeney, J. (2013). Carbon emissions from forest conversion by Kalimantan oil palm plantations. *Nature Climate Change*. DOI:HTTPS://DOI.ORG/10.1038/NCLIMATE1702.

Chau, K.W. (Jan. 1990). Application of the Preissmann scheme on flood propagation in river systems in difficult terrain. English. *Hydrology in mountainous regions I*, pp. 535–543.

Chen, J.Y., Yun, C. & Xu, H. (1982). The model of development of the Changjiang estuary during the last 2000 years. In: *Proceedings of the Sixth Biennial International Estuarine Research Conference*, pp. 655–666.

Cunge, J.A., Holly, F.M. & Verwey, A. (1980). *Practical aspects of computational river hydraulics*. Pitman: London.

Dalrymple, R.W., Zaitlin, B.A. & Boyd, R. (1992). Estuarine facies models : conceptual basis and stratigraphic implications. *Journal of Sedimentary Petrology*, 62 (6), p. 1130. DOI:HTTPS://DOI.ORG/10.1306/D4267A69-2B26-11D7-8648000102C1865D.

Daniel, G., Brad, H., Miodrag, S., Forrest, H., Hasan, P. & Nolan, R. (1999). Application of 3D Mobile Bed, Hydrodynamic Model. *Journal of Hydraulic Engineering*, 125 (7), pp. 737–749. DOI:HTTPS://DOI.ORG/10.1061/(ASCE)0733-9429(1999)125:7(737).

Davies, G. & Woodroffe, C.D. (2010). Tidal Estuary width convergence: Theory and form in North Australian estuaries. *Earth Surface Processes and Landforms*. DOI:HTTPS://DOI.ORG/10.1002/ESP.1864.

Day, J.W., Boesch, D.F., Clairain, E.J., Kemp, G.P., Laska, S.D., Mitsch, W.J., Orth, K., Mashriqui, H., Reed, D.J., Shabman, L., Simenstad, C.A., Streever, B.J., Twilley, R.R., Watson, C.C., Wells, J.T. & Whigham, D.F. (2007). *Restoration of the Mississippi Delta: Lessons from Hurricanes Katrina and Rita*. DOI:HTTPS://DOI.ORG/10.1126/SCIENCE.1137030.

Dissanayake, D.M.P.K., Roelvink, J.A. & van der Wegen, M. (2009). *Modelled channel patterns in a schematized tidal inlet*. DOI:HTTPS://DOI.ORG/10.1016/J.COASTALENG.2009.08.008.

Dronkers, J. (1986). Tidal asymmetry and estuarine morphology. *Netherlands Journal of Sea Research*, 20 (2-3). DOI:HTTPS://DOI.ORG/10.1016/0077-7579(86)90036-0.

Dyer, K.R. (1997). *Estuaries: a physical introduction. 2nd edition*. John Wiley & Sons.

Dyer, K.R. (1995). Sediment transport processes in estuaries. *Developments in Sedimentology*, 53 (C). DOI:10.1016/S0070-4571(05)80034-2.

Edmonds, D.A. & Slingerland, R.L. (2007). Mechanics of river mouth bar formation: Implications for the morphodynamics of delta distributary networks. *Journal of Geophysical Research: Earth Surface*, 112 (F2). DOI:HTTPS://DOI.ORG/10.1029/2006JF000574.

Edmonds, D.A. & Slingerland, R.L. (2008). Stability of delta distributary networks and their bifurcations. *Water Resources Research*, 44 (9). DOI:HTTPS://DOI.ORG/10.1029/2008WR006992.

Emberson, R. (2017). Accelerating riverbank erosion. *Nature Geoscience*, 10 (5). DOI:HTTPS://DOI.ORG/10.1038/NGEO2948.

Engelund, F. & Hansen, E. (1967). A monograph on sediment transport in alluvial streams. *Monografia*.

Ensing, E., de Swart, H.E. & Schuttelaars, H.M. (2015). Sensitivity of tidal motion in well-mixed estuaries to cross-sectional shape, deepening, and sea level rise: An analytical study. *Ocean Dynamics*, 65 (7), pp. 933–950. DOI:HTTPS://DOI.ORG/10.1007/S10236-015-0844-8.

Ericson, J.P., Vörösmarty, C.J., Dingman, S.L., Ward, L.G. & Meybeck, M. (2006). Effective sea-level rise and deltas: Causes of change and human dimension implications. *Global and Planetary Change*, 50, pp. 63–82. DOI:HTTPS://DOI.ORG/10.1016/J.GLOPLACHA.2005.07.004.

Fagherazzi, S. & Furbish, D.J. (2001). On the shape and widening of salt marsh creeks. *Journal of Geophysical Research: Oceans*, 106 (C1), pp. 991–1003. DOI:HTTPS://DOI.ORG/10.1029/1999JC000115.

Fawzi, N.I. & Husna, V.N. (2021). Aquaculture Development Monitoring on Mangrove Forest in Mahakam Delta, East Kalimantan. In: *IOP Conference Series: Earth and Environmental Science*. Vol. 750. 1. DOI:HTTPS://DOI.ORG/10.1088/1755-1315/750/1/012002.

Fokkink, R.J., Wang, Z.B. & Schropp, M.H.I. (1995). On 1D morphodynamic network models. In: *Proceedings of the Congress International Association for Hydraulic Research*. Vol. 3. Local Organizing Committee of the XXV Congress, pp. 104–109.

Franz, G., Leitão, P., Pinto, L., Jauch, E., Fernandes, L. & Neves, R. (2017). Development and validation of a morphological model for multiple sediment classes. *International Journal of Sediment Research*, 32 (4). DOI:HTTPS://DOI.ORG/10.1016/J.IJSRC.2017.05.002.

Friedrichs, C.T. (2009). York River Physical Oceanography and Sediment Transport. *Journal of Coastal Research*, 10057. DOI:HTTPS://DOI.ORG/10.2112/1551-5036-57.SP1.17.

Friedrichs, C.T. (2010). *Barotropic tides in channelized estuaries*. Ed. by A. Valle-Levinson. Cambridge University Press: Cambridge, pp. 27–61. DOI:10.1017/CBO9780511676567.

Friedrichs, C.T. & Aubrey, D.G. (1988). Non-linear tidal distortion in shallow well-mixed estuaries: a synthesis. *Estuarine, Coastal and Shelf Science*, 27 (5). DOI:HTTPS://DOI.ORG/10.1016/0272-7714(88)90082-0.

Frings, R.M. & Kleinhans, M.G. (2008). Complex variations in sediment transport at three large river bifurcations during discharge waves in the river Rhine. *Sedimentology*, 55 (5), pp. 1145–1171. DOI:HTTPS://DOI.ORG/10.1111/J.1365-3091.2007.00940.X.

Galloway, W.E. (1975). Process framework for describing the morphologic and stratigraphic evolution of deltaic depositional systems. In: *Deltas: Models for Exploration*. Ed. by M. Broussard. Houston Geological Society: Houston, pp. 87–98.

Gastaldo, R.A., Allen, G.P. & Huc, A.Y. (1995). The tidal character of fluvial sediments of the modern Mahakam River delta, Kalimantan, Indonesia. *Tidal signatures in modern and ancient sediments*. DOI:HTTPS://DOI.ORG/10.1002/9781444304138.CH11.

Geleynse, N., Storms, J.E.A., R., W.D.J., Jagers, H.R.A, Wang, Z.B. & Stive, M.J.F. (2011). Controls on river delta formation; insights from numerical modelling. *Earth and Planetary Science Letters*, 302 (1), pp. 217–226. DOI:HTTPS://DOI.ORG/10.1016/J.EPSL.2010.12.013.

Giosan, L., Constantinescu, S., Filip, F. & Deng, B. (2013). Maintenance of large deltas through channelization: Nature vs. humans in the Danube delta. *Anthropocene*, 1, pp. 35–45. DOI:HTTPS://DOI.ORG/10.1016/J.ANCENE.2013.09.001.

Groen, P. (1967). On the residual transport of suspended matter by an alternating tidal current. *Netherlands Journal of Sea Research*, 3 (4), pp. 564–574. DOI:HTTPS://DOI.ORG/10.1016/0077-7579(67)90004-X.

Guo, L., van der Wegen, M., Roelvink, J.A., Wang, Z.B. & He, Q. (2015). Long-term, process-based morphodynamic modeling of a fluvio-deltaic system, part I: The role of river discharge. *Continental Shelf Research*, 109, pp. 95–111. DOI:HTTPS://DOI.ORG/10.1016/J.CSR.2015.09.002.

Gurram, S.K., Karki, K.S. & Hager, W.H. (1997). Subcritical Junction Flow. *Journal of Hydraulic Engineering*, 123 (5), pp. 447–455. DOI:HTTPS://DOI.ORG/10.1061/(ASCE)0733-9429(1997)123:5(447).

Hepkema, T.M., de Swart, H.E. & Schuttelaars, H.M. (2019). Sensitivity of Tidal Bar Wavelength to Channel Width. *Journal of Geophysical Research: Earth Surface*, 124 (10), pp. 2417–2436. DOI:HTTPS://DOI.ORG/10.1029/2019JF005032.

Hepkema, T.M., de Swart, H.E., Zagaris, A. & Duran–Matute, M. (2018). Sensitivity of tidal characteristics in double inlet systems to momentum dissipation on tidal flats: a perturbation analysis. *Ocean Dynamics*, 68 (4-5). DOI:HTTPS://DOI.ORG/10.1007/S10236-018-1142-Z.

Hiatt, M. & Passalacqua, P. (2015). Hydrological connectivity in river deltas: The first-order importance of channel-island exchange. *Water Resources Research*, 51 (4), pp. 2264–2282. DOI:HTTPS://DOI.ORG/10.1002/2014WR016149.

Hibma, A., Stive, M.J.F. & Wang, Z.B. (2004). Estuarine morphodynamics. *Coastal Engineering*, 51 (8). Coastal Morphodynamic Modeling, pp. 765–778. DOI:HTTPS://DOI.ORG/10.1016/J.COASTALENG.2004.07.008.

Hidayat, H., Hoekman, D.H., Vissers, M.A.M. & Hoitink, A.J.F. (2012). Flood occurrence mapping of the middle Mahakam lowland area using satellite radar. *Hydrology and Earth System Sciences*, 16 (7), pp. 1805–1816. DOI:HTTPS://DOI.ORG/10.5194/HESS-16-1805-2012.

Hidayat, H., Vermeulen, B., Sassi, M.G., Torfs, P.J.J.F. & Hoitink, A.J.F. (2011). Discharge estimation in a backwater affected meandering river. *Hydrology and Earth System Sciences*, 15 (8), pp. 2717–2728. DOI:HTTPS://DOI.ORG/10.5194/HESS-15-2717-2011.

Hoitink, A.J., Wang, Z.B., Vermeulen, B., Huismans, Y. & Kästner, K. (2017). *Tidal controls on river delta morphology*. DOI:HTTPS://DOI.ORG/10.1038/NGEO3000.

Howard, A.D., Keetch, M.E. & Vincent, C.L. (1970). Topological and Geometrical Properties of Braided Streams. *Water Resources Research*, 6 (6), pp. 1674–1688. DOI:HTTPS://DOI.ORG/10.1029/WR006I006P01674.

Hoyal, D.C.J.D. & Sheets, B.A. (2009). Morphodynamic evolution of experimental cohesive deltas. *Journal of Geophysical Research: Earth Surface*, 114 (F2). DOI:HTTPS://DOI.ORG/10.1029/2007JF000882.

Hu, K., Ding, P., Wang, Z. & Yang, S. (2009). A 2D/3D hydrodynamic and sediment transport model for the Yangtze Estuary, China. *Journal of Marine Systems*, 77 (1-2), pp. 114–136. DOI:HTTPS://DOI.ORG/10.1016/J.JMARSYS.2008.11.014.

Ikeda, S. (1982). Incipient Motion of Sand Particles on Side Slopes. *Journal of the Hydraulics Division*, 108 (1), pp. 95–114.

Ikeda, S., Parker, G. & Sawai, K. (1981). Bend theory of river meanders. Part 1. Linear development. *Journal of Fluid Mechanics*, 112, pp. 363–377. DOI:HTTPS://DOI.ORG/10.1017/S0022112081000451.

Indonesian Ministry of Transportation (2021). *Survei Investigasi Dan Desain (SID) Alur Pelayaran/Kolam Pelabuhan Samarinda Provinsi Kalimantan Timur*. Tech. rep. Unpublished Report.

Islam, A, Sighn, R & Raghuwanshi, N. (2003). Numerical Techniques in Canal Hydraulic Modeling: A Review. In: *Water Resource System Operation: proceedings of the International Conference on Water and Environment (WE-2003)*. Ed. by V. Singh & R. Yadava. Allied Publishers: Mumbai, pp. 401–411.

Iwantoro, A.P., van der Vegt, M. & Kleinhans, M.G. (2020). Morphological evolution of bifurcations in tide-influenced deltas. *Earth Surface Dynamics*, 8 (2), pp. 413–429. DOI:HTTPS://DOI.ORG/10.5194/ESURF-8-413-2020.

Iwantoro, A.P., van der Vegt, M. & Kleinhans, M.G. (2021). Effects of sediment grain size and channel slope on the stability of river bifurcations. *Earth Surface Processes and Landforms*, 46 (10), pp. 2004–2018. DOI:HTTPS://DOI.ORG/10.1002/ESP.5141.

Iwantoro, A.P., van der Vegt, M. & Kleinhans, M.G. (2022). Stability and Asymmetry of Tide-Influenced River Bifurcations. *Journal of Geophysical Research: Earth Surface*, 127 (6), e2021JF006282. DOI:HTTPS://DOI.ORG/10.1029/2021JF006282.

Jerolmack, D.J. (2009). Conceptual framework for assessing the response of delta channel networks to Holocene sea level rise. *Quaternary Science Reviews*, 28 (17). Quaternary Ice Sheet-Ocean Interactions and Landscape Responses, pp. 1786–1800. DOI:HTTPS://DOI.ORG/10.1016/J.QUASCIREV.2009.02.015.

Jerolmack, D.J. & Mohrig, D. (May 2007). Conditions for branching in depositional rivers. *Geology*, 35 (5), pp. 463–466. DOI:HTTPS://DOI.ORG/10.1130/G23308A.1.

Jerolmack, D.J. & Swenson, J.B. (2007). Scaling relationships and evolution of distributary networks on wave-influenced deltas. *Geophysical Research Letters*, 34 (23). DOI:HTTPS://DOI.ORG/10.1029/2007GL031823.

Jeuken, M.C.J.L. & Wang, Z.B. (2010). Impact of dredging and dumping on the stability of ebb–flood channel systems. *Coastal Engineering*, 57 (6), pp. 553–566. DOI:HTTPS://DOI.ORG/10.1016/J.COASTALENG.2009.12.004.

Jiang, C., Li, J. & de Swart, H.E. (2012). Effects of navigational works on morphological changes in the bar area of the Yangtze Estuary. *Geomorphology*, 139-140, pp. 205–219. DOI:HTTPS://DOI.ORG/10.1016/J.GEOMORPH.2011.10.020.

Jones, L.S. & Harper, J.T. (Apr. 1998). Channel avulsions and related processes, and large-scale sedimentation patterns since 1875, Rio Grande, San Luis Valley, Colorado. *GSA Bulletin*, 110 (4), pp. 411–421. DOI:HTTPS://DOI.ORG/10.1130/0016-7606(1998)110<0411:CAARPA>2.3.CO;2.

Kästner, K. & Hoitink, A.J.F. (2019). Flow and Suspended Sediment Division at Two Highly Asymmetric Bifurcations in a River Delta: Implications for Channel Stability. *Journal of Geophysical Research: Earth Surface*, 124 (10), pp. 2358–2380. DOI:HTTPS://DOI.ORG/10.1029/2018JF004994.

Kästner, K., Hoitink, A.J.F., Vermeulen, B., Geertsema, T.J. & Ningsih, N.S. (2017). Distributary channels in the fluvial to tidal transition zone. *Journal of Geophysical Research: Earth Surface*, 122 (3), pp. 696–710. DOI:HTTPS://DOI.ORG/10.1002/2016JF004075.

Kleinhans, M.G., Cohen, K.M., Hoekstra, J. & Ijmker, J.M. (2011). Evolution of a bifurcation in a meandering river with adjustable channel widths, Rhine delta apex, The Netherlands. *Earth Surface Processes and Landforms*, 36 (15), pp. 2011–2027. DOI:10.1002/ESP.2222.

Kleinhans, M.G., de Haas, T., Lavooi, E. & Makaske, B. (2012). Evaluating competing hypotheses for the origin and dynamics of river anastomosis. *Earth Surface Processes and Landforms*, 37 (12), pp. 1337–1351. DOI:HTTPS://DOI.ORG/10.1002/ESP.3282.

Kleinhans, M.G., Ferguson, R.I., Lane, S.N. & Hardy, R.J. (2013). Splitting rivers at their seams: Bifurcations and avulsion. *Earth Surface Processes and Landforms*, 38 (1), pp. 47–61. DOI:HTTPS://DOI.ORG/10.1002/ESP.3268.

Kleinhans, M.G., Jagers, H.R.A., Mosselman, E. & Sloff, C.J. (2008). Bifurcation dynamics and avulsion duration in meandering rivers by one-dimensional and three-dimensional models. *Water Resources Research*, 44 (8), pp. 1–31. DOI:HTTPS://DOI.ORG/10.1029/2007WR005912.

Kleinhans, M.G. & van den Berg, J.H. (2011). River channel and bar patterns explained and predicted by an empirical and a physics-based method. *Earth Surface Processes and Landforms*, 36 (6), pp. 721–738. DOI:HTTPS://DOI.ORG/10.1002/ESP.2090.

Kleinhans, M.G., Weerts, H.J. & Cohen, K.M. (2010). Avulsion in action: Reconstruction and modelling sedimentation pace and upstream flood water levels following a Medieval tidal-river diversion catastrophe

(Biesbosch, The Netherlands, 1421-1750AD). *Geomorphology*, 118 (1-2), pp. 65–79. DOI:HTTPS://DOI.ORG/10.1016/J.GEOMORPH.2009.12.009.

Lane, S.N., Bradbrook, K.F., Richards, K.S., Biron, P.A. & Roy, A.G. (1999). The application of computational fluid dynamics to natural river channels: three-dimensional versus two-dimensional approaches. *Geomorphology*, 29 (1), pp. 1–20. DOI:HTTPS://DOI.ORG/10.1016/S0169-555X(99)00003-3.

Lane, S.N., Westaway, R.M. & Hicks, D.M. (2003). Estimation of erosion and deposition volumes in a large, gravel-bed, braided river using synoptic remote sensing. *Earth Surface Processes and Landforms*, 28 (3), pp. 249–271. DOI:HTTPS://DOI.ORG/10.1002/ESP.483.

Langbein, W.B. (1963). The Hydraulic Geometry of a Shallow Estuary. *International Association of Scientific Hydrology. Bulletin*, 8 (3), pp. 84–94. DOI:10.1080/02626666309493340.

Lanzoni, S. & Seminara, G. (1998). On tide propagation in convergent estuaries. *Journal of Geophysical Research: Oceans*, 103 (C13), pp. 30793–30812. DOI:HTTPS://DOI.ORG/10.1029/1998JC900015.

Leddy, J.O., Ashworth, P.J. & Best, J.L. (1993). Mechanisms of anabranch avulsion within gravel-bed braided rivers: Observations from a scaled physical model. *Geological Society Special Publication*, 75, pp. 119–127. DOI:HTTPS://DOI.ORG/10.1144/GSL.SP.1993.075.01.07.

Lentsch, N., Finotello, A. & Paola, C. (June 2018). Reduction of deltaic channel mobility by tidal action under rising relative sea level. *Geology*, 46 (7), pp. 599–602. DOI:HTTPS://DOI.ORG/10.1130/G45087.1.

Leonardi, N., Canestrelli, A., Sun, T. & Fagherazzi, S. (2013). Effect of tides on mouth bar morphology and hydrodynamics. *Journal of Geophysical Research: Oceans*, 118 (9), pp. 4169–4183. DOI:HTTPS://DOI.ORG/10.1002/JGRC.20302.

Lesser, G.R., Roelvink, J.A., van Kester, J.A.T.M. & Stelling, G.S. (2004). Development and validation of a three-dimensional morphological model. *Coastal Engineering*, 51 (8-9), pp. 883–915. DOI:HTTPS://DOI.ORG/10.1016/J.COASTALENG.2004.07.014.

Leuven, J.R.F.W., Pierik, H.J., van der Vegt, M., Bouma, T.J. & Kleinhans, M.G. (2019). Sea-level-rise-induced threats depend on the size of tide-influenced estuaries worldwide. *Nature Climate Change*. DOI:10.1038/S41558-019-0608-4.

Leuven, J.R.F.W., van Keulen, D., Nienhuis, J.H., Canestrelli, A. & Hoitink, A.J.F. (2021). Large-Scale Scour in Response to Tidal Dominance in Estuaries. *Journal of Geophysical Research: Earth Surface*, 126 (5). e2020JF006048 2020JF006048, e2020JF006048. DOI:HTTPS://DOI.ORG/10.1029/2020JF006048.

Li, Z., Li, M.Z., Dai, Z., Zhao, F. & Li, J. (2015). Intratidal and neap-spring variations of suspended sediment concentrations and sediment transport processes in the North Branch of the Changjiang Estuary. *Acta Oceanologica Sinica*, 34 (1). DOI:HTTPS://DOI.ORG/10.1007/S13131-015-0605-Z.

Luo, X.L., Zeng, E.Y., Ji, R.Y. & Wang, C.P. (2007). Effects of in-channel sand excavation on the hydrology of the Pearl River Delta, China. *Journal of Hydrology*, 343 (3-4). DOI:HTTPS://DOI.ORG/10.1016/J.JHYDROL.2007.06.019.

Mahmudah, N., Parikesit, D., Malkhamah, S. & Priyanto, S. (2010). Regional freight transportation model for crude palm oil in Central Kalimantan. *Jurnal Transportasi*.

Marra, W.A., Parsons, D.R., Kleinhans, M.G., Keevil, G.M. & Thomas, R.E. (2014). Near-bed and surface flow division patterns in experimental river bifurcations. *Water Resources Research*, 50 (2), pp. 1506–1530. DOI:HTTPS://DOI.ORG/10.1002/2013WR014215.

Miori, S., Repetto, R. & Tubino, M. (2006). A one-dimensional model of bifurcations in gravel bed channels with erodible banks. *Water Resources Research*, 42 (11). DOI:HTTPS://DOI.ORG/10.1029/2006WR004863.

Nelson, A. & Gunma, M.K. (2015). *A map of lowland rice extent in the major rice growing countries of Asia*.

Nguyen, A.D. & Savenije, H.H.G. (2006). Salt intrusion in multi-channel estuaries: A case study in the Mekong Delta, Vietnam. *Hydrology and Earth System Sciences*, 10 (5), pp. 743–754. DOI:HTTPS://DOI.ORG/10.5194/HESS-10-743-2006.

Nienhuis, J.H. & van de Wal, R.S.W. (2021). Projections of Global Delta Land Loss From Sea-Level Rise in the 21st Century. *Geophysical Research Letters*, 48 (14). DOI:HTTPS://DOI.ORG/10.1029/2021GL093368.

Nnafie, A., Van Oyen, T., De Maerschalck, B., van der Vegt, M. & Wegen, M.v.d. (2018). Estuarine Channel Evolution in Response to Closure of Secondary Basins: An Observational and Morphodynamic Modeling Study of the Western Scheldt Estuary. *Journal of Geophysical Research: Earth Surface*, 123 (1), pp. 167–186. DOI:HTTPS://DOI.ORG/10.1002/2017JF004364.

North, C.P. & Warwick, G.L. (2007). Fluvial Fans: Myths, Misconceptions, and the End of the Terminal-Fan Model. *Journal of Sedimentary Research*, 77 (9), pp. 693–701. DOI:HTTPS://DOI.ORG/10.2110/JSR.2007.072.

Novico, F., Ali, A., Saputro, E., Sinaga, A. & Egon, A. (2018). Morfodinamika Jangka Pendek Pendangkalan di Alur Pelayaran Barito, Kalimantan Selatan. *Jurnal geologi Kelautan*. DOI:HTTPS://DOI.ORG/10.32693/JGK.15.2.2017.402.

Orton, G.J. & Reading, H.G. (1993). Variability of deltaic processes in terms of sediment supply, with particular emphasis on grain size. *Sedimentology*, 40 (3), pp. 475–512. DOI:HTTPS://DOI.ORG/10.1111/J.1365-3091.1993.TB01347.X.

Pethick, J. (1980). Velocity surges and asymmetry in tidal channels. *Estuarine and Coastal Marine Science*, 11 (3), pp. 331–345. DOI:HTTPS://DOI.ORG/10.1016/S0302-3524(80)80087-9.
Pham Van, C., Gourgue, O., Sassi, M., Hoitink, A.J.F., Deleersnijder, E. & Soares-Frazão, S. (2016). Modelling fine-grained sediment transport in the Mahakam land–sea continuum, Indonesia. *Journal of Hydro-environment Research*, 13, pp. 103–120. DOI:HTTPS://DOI.ORG/10.1016/J.JHER.2015.04.005.
Pinter, N., Miller, K., Wlosinski, J.H. & Van Der Ploeg, R.R. (2004). Recurrent shoaling and channel dredging, Middle and Upper Mississippi River, USA. *Journal of Hydrology*, 290 (3-4). DOI:HTTPS://DOI.ORG/10.1016/J.JHYDROL.2003.12.021.
Pitlick, J. & Cress, R. (2002). Downstream changes in the channel geometry of a large gravel bed river. *Water Resources Research*, 38 (10). DOI:HTTPS://DOI.ORG/10.1029/2001WR000898.
Postma, G. (1961). Transport and accumulation of suspended matter in the Dutch Wadden Sea. *Netherlands Journal of Sea Research*, 1 (1), pp. 148–190. DOI:HTTPS://DOI.ORG/10.1016/0077-7579(61)90004-7.
Postma, G. (1995). Sea-level-related architectural trends in coarse-grained delta complexes. *Sedimentary Geology*, 98 (1), pp. 3–12. DOI:HTTPS://DOI.ORG/10.1016/0037-0738(95)00024-3.
Prandle, D. & Lane, A. (2015). Sensitivity of estuaries to sea level rise: Vulnerability indices. *Estuarine, Coastal and Shelf Science*, 160, pp. 60–68. DOI:HTTPS://DOI.ORG/10.1016/J.ECSS.2015.04.001.
Prayoga, A. (2016). Bertumpu pada hutan di DAS Mahakam. *Intip Hutan*, pp. 6–11.
Pritchard, D. & Hogg, A.J. (2003). Cross-shore sediment transport and the equilibrium morphology of mudflats under tidal currents. *Journal of Geophysical Research: Oceans*, 108 (C10). DOI:HTTPS://DOI.ORG/10.1029/2002JC001570.
Ragno, N., Redolfi, M. & Tubino, M. (2021). Coupled Morphodynamics of River Bifurcations and Confluences. *Water Resources Research*, 57 (1). e2020WR028515 2020WR028515, e2020WR028515. DOI:HTTPS://DOI.ORG/10.1029/2020WR028515.
Ragno, N., Tambroni, N. & Bolla Pittaluga, M. (2020). Effect of Small Tidal Fluctuations on the Stability and Equilibrium Configurations of Bifurcations. *Journal of Geophysical Research: Earth Surface*, 125 (8), e2020JF005584. DOI:HTTPS://DOI.ORG/10.1029/2020JF005584.
Rahmawan, G.A., Wisha, U.J., Husrin, S. & Ilham, I. (2017). Analisis Batimetri dan Pasang Surut di Muara Sungai Kampar: Pembangkit Penjalaran Gelombang Pasang Surut "Undular Bore Bono". *Jurnal Ilmiah Geomatika*. DOI:HTTPS://DOI.ORG/10.24895/JIG.2016.22-2.573.
Ranasinghe, R., Swinkels, C., Luijendijk, A., Roelvink, J.A., Bosboom, J., Stive, M. & Walstra, D.J. (2011). Morphodynamic upscaling with the MORFAC approach: Dependencies and sensitivities. *Coastal Engineering*, 58 (8), pp. 806–811. DOI:10.1016/J.COASTALENG.2011.03.010.
Redolfi, M., Zolezzi, G. & Tubino, M. (2016). Free instability of channel bifurcations and morphodynamic influence. *Journal of Fluid Mechanics*, 799, pp. 476–504. DOI:HTTPS://DOI.ORG/10.1017/JFM.2016.389.
Redolfi, M., Zolezzi, G. & Tubino, M. (2019). Free and forced morphodynamics of river bifurcations. *Earth Surface Processes and Landforms*, 44 (4), pp. 973–987. DOI:HTTPS://DOI.ORG/10.1002/ESP.4561.
Roelvink, J.A. (2006). Coastal morphodynamic evolution techniques. *Coastal Engineering*, 53 (2-3), pp. 277–287. DOI:HTTPS://DOI.ORG/10.1016/J.COASTALENG.2005.10.015.
Rossi, V.M., Kim, W., López, J.L., Edmonds, D., Geleynse, N., Olariu, C., Steel, R.J., Hiatt, M. & Passalacqua, P. (2016). Impact of tidal currents on delta-channel deepening, stratigraphic architecture, and sediment bypass beyond the shoreline. *Geology*, 44 (11), pp. 927–930. DOI:HTTPS://DOI.ORG/10.1130/G38334.1.
Salter, G., Paola, C. & Voller, V.R. (2017). Control of Delta Avulsion by Downstream Sediment Sinks. *Journal of Geophysical Research: Earth Surface*, 123 (1), pp. 142–166. DOI:HTTPS://DOI.ORG/10.1002/2017JF004350.
Salter, G., Voller, V.R. & C., P. (2020). Chaos in a simple model of a delta network. *Proceedings of the National Academy of Sciences*, 117 (44), pp. 27179–27187. DOI:HTTPS://DOI.ORG/10.1073/PNAS.2010416117.
Sassi, M.G., Hoitink, A.J.F., de Brye, B. & Deleersnijder, E. (2012). Downstream hydraulic geometry of a tidally influenced river delta. *Journal of Geophysical Research: Earth Surface*, 117 (F4). DOI:HTTPS://DOI.ORG/10.1029/2012JF002448.
Sassi, M.G., Hoitink, A.J.F., De Brye, B., Vermeulen, B. & Deleersnijder, E. (2011). Tidal impact on the division of river discharge over distributary channels in the Mahakam Delta. *Ocean Dynamics*, 61 (12), pp. 2211–2228. DOI:HTTPS://DOI.ORG/10.1007/S10236-011-0473-9.
Sassi, M., Hoitink, A., Vermeulen, B. & Hidayat, H. (2013). Sediment discharge division at two tidally influenced river bifurcations. *Water Resources Research*, 49, pp. 2119–2134. DOI:HTTPS://DOI.ORG/10.1002/WRCR.20216.
Savenije, H.H.G. (2015). Prediction in ungauged estuaries: An integrated theory. *Water Resources Research*, 51 (4), pp. 2464–2476. DOI:HTTPS://DOI.ORG/10.1002/2015WR016936.
Savenije, H.H. (2005). Tide and estuary shape. In: *Salinity and Tides in Alluvial Estuaries*. Ed. by H.H.G. Savenije. Elsevier Science Ltd: Amsterdam, pp. 23–68. DOI:HTTPS://DOI.ORG/10.1016/B978-044452107-1/50003-4.

Schuurman, F., Marra, W.A. & Kleinhans, M.G. (2013). Physics-based modeling of large braided sand-bed rivers: Bar pattern formation, dynamics, and sensitivity. *Journal of Geophysical Research: Earth Surface*, 118 (4), pp. 2509–2527. DOI:HTTPS://DOI.ORG/10.1002/2013JF002896.

Setiawan, Y., Bengen, D.G., Kusmana, C. & Pertiwi, S. (2015). Estimasi nilai eksternalitas konversi hutan mangrove menjadi pertambakan di Delta Mahakam Kabupaten Kutai Kertanegara. *Jurnal Penelitian Hutan Tanaman*. DOI:HTTPS://DOI.ORG/10.20886/JPHT.2015.12.3.201-210.

Shaw, J.B. & Mohrig, D. (Jan. 2014). The importance of erosion in distributary channel network growth, Wax Lake Delta, Louisiana, USA. *Geology*, 42 (1), pp. 31–34. DOI:HTTPS://DOI.ORG/10.1130/G34751.1.

Slingerland, R. & Smith, N.D. (1998). Necessary conditions for a meandering-river avulsion. *Geology*, 26 (5), pp. 435–438. DOI:HTTPS://DOI.ORG/10.1130/0091-7613(1998)026<0435:NCFAMR>2.3.CO;2.

Smith, N.D., Cross, T.A., Dufficy, J.P. & Clough, S.R. (1989). Anatomy of an avulsion. *Sedimentology*, 36 (1), pp. 1–23. DOI:HTTPS://DOI.ORG/10.1111/J.1365-3091.1989.TB00817.X.

Soulsby, R.L. (1997). Dynamics of marine sands: a manual for practical applications. *Oceanographic Literature Review*, 9 (44), p. 947.

Speer, P.E., Aubrey, D.G & Friedrichs, C.T. (1991). Nonlinear hydrodynamics of shallow tidal inlet/bay systems. *Tidal hydrodynamics*, 321, p. 339.

Stephens, J.D., Allison, M.A., Di Leonardo, D.R., Weathers, H.D., Ogston, A.S., McLachlan, R.L., Xing, F. & Meselhe, E.A. (2017). Sand dynamics in the Mekong River channel and export to the coastal ocean. *Continental Shelf Research*, 147, pp. 38–50. DOI:HTTPS://DOI.ORG/10.1016/J.CSR.2017.08.004.

Storms, J.E.A., Hoogendoorn, R.M, Dam, R.A.C., Hoitink, A. & Kroonenberg, S.B. (2005). Late-Holocene evolution of the Mahakam delta, East Kalimantan, Indonesia. *Sedimentary Geology*, 180 (3), pp. 149–166. DOI:HTTPS://DOI.ORG/10.1016/J.SEDGEO.2005.08.003.

Stouthamer, E. & Berendsen, H.J. (2001). Avulsion frequency, avulsion duration, and intervulsion period of holocene channel belts in the rhine-meuse delta, the Netherlands. *Nederlandse Geografische Studies*, (283), pp. 105–126. DOI:HTTPS://DOI.ORG/10.1306/112100710589.

Struiksma, N., Olesen, K.W., Flokstra, C. & De Vriend, H.J. (1985). Bed deformation in curved alluvial channels. *Journal of Hydraulic Research*, 23 (1), pp. 57–79. DOI:HTTPS://DOI.ORG/10.1080/00221688509499377.

Syvitski, J.P.M. & Kettner, A. (2011). Sediment flux and the Anthropocene. *Philosophical Transactions of the Royal Society A: Mathematical, Physical and Engineering Sciences*, 369 (1938), pp. 957–975. DOI:HTTPS://DOI.ORG/10.1098/RSTA.2010.0329.

Syvitski, J.P.M. & Saito, Y. (2007). Morphodynamics of deltas under the influence of humans. *Global and Planetary Change*, 57 (3), pp. 261–282. DOI:HTTPS://DOI.ORG/10.1016/J.GLOPLACHA.2006.12.001.

Syvitski, J.P., Kettner, A.J., Overeem, I., Hutton, E.W., Hannon, M.T., Brakenridge, G.R., Day, J., Vörösmarty, C., Saito, Y., Giosan, L. & Nicholls, R.J. (2009). Sinking deltas due to human activities. *Nature Geoscience*, 2 (10). DOI:HTTPS://DOI.ORG/10.1038/NGEO629.

Talmon, A.M., Struiksma, N. & van Mierlo, M.C.L.M. (1995). Laboratory measurements of the direction of sediment transport on transverse alluvial-bed slopes. *Journal of Hydraulic Research*, 33 (4), pp. 495–517. DOI:HTTPS://DOI.ORG/10.1080/00221689509498657.

Tambunan, E. (2014). Dampak degradasi lingkungan terhadap transportasi sungai mahakam. *The 17th FSTPT International Symposium*.

Tarya, A., van der Vegt, M. & Hoitink, A.J.F. (2015). Wind forcing controls on river plume spreading on a tropical continental shelf. *Journal of Geophysical Research: Oceans*, 120 (1), pp. 16–35. DOI:HTTPS://DOI.ORG/10.1002/2014JC010456.

Van Rijn, L.C. (2007). Unified View of Sediment Transport by Currents and Waves. II: Suspended Transport. *Journal of Hydraulic Engineering*, 133 (6), pp. 668–689. DOI:HTTPS://DOI.ORG/10.1061/(ASCE)0733-9429(2007)133:6(668).

Van De Lageweg, W.I. & Slangen, A.B.A. (2017). Predicting Dynamic Coastal Delta Change in Response to Sea-Level Rise. *Journal of Marine Science and Engineering*, 5 (2). DOI:HTTPS://DOI.ORG/10.3390/JMSE5020024.

van den Berg, J.H. (1995). Prediction of alluvial channel pattern of perennial rivers. *Geomorphology*, 12 (4), pp. 259–279. DOI:HTTPS://DOI.ORG/10.1016/0169-555X(95)00014-V.

Van der Mark, C.F. & Mosselman, E. (2013). Effects of helical flow in one-dimensional modelling of sediment distribution at river bifurcations. *Earth Surface Processes and Landforms*, 38 (5), pp. 502–511. DOI:HTTPS://DOI.ORG/10.1002/ESP.3335.

Van Der Wegen, M. & Roelvink, J.A. (2008). Long-term morphodynamic evolution of a tidal embayment using a two-dimensional, process-based model. *Journal of Geophysical Research: Oceans*, 113 (3), pp. 1–23. DOI:10.1029/2006JC003983.

van der Wegen, M. & Roelvink, J.A. (2012). Reproduction of estuarine bathymetry by means of a process-based model: Western Scheldt case study, the Netherlands. *Geomorphology*, 179, pp. 152–167. DOI:HTTPS://DOI.ORG/10.1016/J.GEOMORPH.2012.08.007.

van der Wegen, M., Wang, Z.B., Savenije, H.H.G. & Roelvink, J.A. (2008). Long-term morphodynamic evoluation and energy dissipation in a coastal plain, tidal embayment. *Journal of Geophysical Research: Earth Surface*, 113 (3). DOI:HTTPS://DOI.ORG/10.1029/2007JF000898.

van Katwijk, M.M., van der Welle, M.E., Lucassen, E.C., Vonk, J.A., Christianen, M.J., Kiswara, W., Inayat al Hakim, I., Arifin, A., Bouma, T.J., Roelofs, J.G. & Lamers, L.P. (2011). Early warning indicators for river nutrient and sediment loads in tropical seagrass beds: A benchmark from a near-pristine archipelago in Indonesia. *Marine Pollution Bulletin*, 62 (7). DOI:HTTPS://DOI.ORG/10.1016/J.MARPOLBUL.2011.04.007.

van Rijn, L.C. (1984a). Sediment transport, part I: Bed load transport. *Journal of Hydraulic Engineering*, 110 (10), pp. 1431–1456. DOI:HTTPS://DOI.ORG/10.1061/(ASCE)0733-9429(1984)110:10(1431).

van Rijn, L.C. (1984b). Sediment transport, part II: Suspended load transport. *Journal of Hydraulic Engineering*, 110 (11), pp. 1613–1641. DOI:HTTPS://DOI.ORG/10.1061/(ASCE)0733-9429(1984)110:11(1613).

Van Rijn, L.C. (1993). *Principles of sediment transport in rivers, estuaries and coastal seas*. Vol. 1006. Aqua publications Amsterdam.

van Straaten, L.M.J.U. & Kuenen, P.H. (Dec. 1958). Tidal action as a cause of clay accumulation. *Journal of Sedimentary Research*, 28 (4), pp. 406–413. DOI:HTTPS://DOI.ORG/10.1306/74D70826-2B21-11D7-8648000102C1865D.

Ve, N.D., Fan, D., Van Vuong, B. & Lan, T.D. (2021). Sediment budget and morphological change in the Red River Delta under increasing human interferences. *Marine Geology*, 431, p. 106379. DOI:HTTPS://DOI.ORG/10.1016/J.MARGEO.2020.106379.

Wagner, W. & Mohrig, D. (2019). Flow and Sediment Flux Asymmetry in a Branching Channel Delta. *Water Resources Research*, 55 (11), pp. 9563–9577. DOI:HTTPS : / / DOI . ORG / 10 . 1029 / 2019WR026050. eprint: https://agupubs.onlinelibrary.wiley.com/doi/pdf/10.1029/2019WR026050.

Wang, Z.B., de Vries, M., Fokkink, R.J. & Langerak, A (1995). Stability of river bifurcations in ID morphodynamic models. *Journal of Hydraulic Research*, 33 (6), pp. 739–750. DOI:HTTPS://DOI.ORG/10.1080/00221689509498549.

Wang, Z.B., Jeuken, M.C.J.L., Gerritsen, H., de Vriend, H. & Kornman, B. (2002). Morphology and asymmetry of the vertical tide in the Westerschelde estuary. *Continental Shelf Research*, 22 (17), pp. 2599–2609. DOI:HTTPS://DOI.ORG/10.1016/S0278-4343(02)00134-6.

Webb, E.L., Jachowski, N.R.A., Phelps, J., Friess, D.A., Than, M.M. & Ziegler, A.D. (2014). Deforestation in the Ayeyarwady Delta and the conservation implications of an internationally-engaged Myanmar. *Global Environmental Change*, 24 (1). DOI:HTTPS://DOI.ORG/10.1016/J.GLOENVCHA.2013.10.007.

Xu, F., Coco, G., Zhou, Z., Tao, J. & Zhang, C. (2017). A numerical study of equilibrium states in tidal network morphodynamics. *Ocean Dynamics*, 67, pp. 1593–1607. DOI:HTTPS://DOI.ORG/10.1007/S10236-017-1101-0.

Yang, Z., Wang, H., Saito, Y., Milliman, J.D., Xu, K., Qiao, S. & Shi, G. (2006). Dam impacts on the Changjiang (Yangtze) River sediment discharge to the sea: The past 55 years and after the Three Gorges Dam. *Water Resources Research*, 42 (4). DOI:HTTPS://DOI.ORG/10.1029/2005WR003970.

Yuanita, N. & Tingsanchali, T. (2008). Development of a river delta: a case study of Cimanuk river mouth, Indonesia. *Hydrological Processes*, 22 (18), pp. 3785–3801. DOI:HTTPS://DOI.ORG/10.1002/HYP.6987.

Yuen, K.W., Hanh, T.T., Quynh, V.D., Switzer, A.D., Teng, P. & Lee, J.S.H. (2021). Interacting effects of land-use change and natural hazards on rice agriculture in the Mekong and Red River deltas in Vietnam. *Natural Hazards and Earth System Sciences*, 21 (5), pp. 1473–1493. DOI:HTTPS://DOI.ORG/10.5194/NHESS-21-1473-2021.

Zhang, E.F., Savenije, H.H.G., Chen, S.L. & Mao, X.H. (2012). An analytical solution for tidal propagation in the Yangtze Estuary, China. *Hydrology and Earth System Sciences*, 16 (9), pp. 3327–3339. DOI:HTTPS://DOI.ORG/10.5194/HESS-16-3327-2012.

Zhang, W., Jia, Q. & Chen, X. (2014). Numerical simulation of flow and suspended sediment transport in the distributary channel networks. *Journal of Applied Mathematics*. DOI:HTTPS://DOI.ORG/10.1155/2014/948731.

List of publications

Refereed journal articles

Iwantoro, A.P., van der Vegt, M., & Kleinhans, M. G. (2020). Morphological evolution of bifurcations in tide-influenced deltas. *Earth Surface Dynamics*, 8(2), pp. 413-429. https://doi.org/10.5194/esurf-8-413-2020

Iwantoro, A. P, van der Vegt, M., & Kleinhans, M. G. (2021). Effects of sediment grain size and channel slope on the stability of river bifurcations. *Earth Surface Processes and Landforms*, 46(10),pp. 2004–2018. https://doi.org/10.1002/esp.5141

Iwantoro, A.P., van der Vegt, M., & Kleinhans, M. G. (2022). Stability and Asymmetry of Tide-Influenced River Bifurcations. *Journal of Geophysical Research: Earth Surface*, 127 (6), pp. e2021JF006282. https://doi.org/10.1029/2021JF006282

Conference proceeding

Iwantoro, A.P., van der Vegt, M., & Kleinhans, M. G. (2022). Effect of tides on stability of bifurcations in river deltas. In *River Flow 2020*, pp. 464-468. CRC Press. https://doi.org/10.1201/b22619-66

Conference abstracts

Iwantoro, A.P., van der Vegt, M., & Kleinhans, M. G. (2019). Determining morphological stability of tidally-influenced bifurcations. *11th RCEM Symposium 2019, Auckland, New Zealand.*

Iwantoro, A.P., van der Vegt, M., & Kleinhans, M. G. (2016). Morphodynamics of estuarine channel network. *EGU 2016, Vienna, Austria.*

Outreach

Best Oral Presentation in the 11th River, Coastal and Estuarine Morphodynamics (RCEM) Symposium, Auckland, New Zealand, 2019.

Acknowledgement

First of all, my promotor and supervisor are the best teacher I have ever had in my life. I knew them from their class during my MSc in Earth Surface and Water programme at Utrecht University and I decided to choose them as my supervisors for my master thesis. I never regret my decision because I could extend my master thesis project to be my PhD project under their supervision. Their teaching style is always the same for me: They pushed me and motivated me at the same time. Thus, I would like to express my gratitude to Prof. Maarten Kleinhans for his patience and trust in giving me the opportunity and supports to conduct this research project. I am grateful to have him as my promotor. Maarten is the person who introduced me to coding and numerical modelling world in my first lesson during my master programme. In fact, before I attended his class I really hate to learn about coding and modelling. But he has successfully changed my mind and somehow has made me very passionate to learn about coding and develop my own numerical model. I would also like to express my sincere appreciation and deepest gratitude to Dr. Maarten van der Vegt for his patience, excellence guidance and critical science as my daily supervisor. He has been a source of idea, support, and encouragement. He introduced me to the wonderful phenomena so-called tidal waves. I did not know tides can be so interesting before. Under his guidance, my understanding in math and physics has been improved hundreds-fold!

I thank Indonesia Endowment Fund for Education (LPDP) for financial supports for my MSc and PhD. Since my PhD project is the extension of my master thesis project, without LPDP financial support for my MSc this PhD project has never existed. At first, I achieved LPDP scholarship for my master. After graduation, I achieved "beasiswa lanjutan" programme from LPDP to pursue my PhD where I extended my master thesis project into PhD research project.

Special thanks for my former officemate: Jasper Leuven for your suggestion to survive as a PhD in my first year; Danghan and Jacob for the good talks and sharing during our overtime evening; Muriel, Jana, Steven, Marcio, Anne, Lisanne, Sepehr, Jude, Joeri, Mas Edwin and to all colleagues in Physical Geography Department and secretariat (Marina and Ruth) for all your supports, talks and drinks. Even though I am a quite person, I learnt a lot from you guys.

Thanks to all wonderful friend who supported me in my early time in The Netherlands: Dr. Richo Andi Wibowo who allowed me to stay in his apartment in my first months in The Netherlands and taught me how to survive in the Netherlands as cheap as possible; Stefan Pluis, Sara, Maartje, Jaco, Yudistira, Bang Isal who taught me on how to be a bit more European.

Saya juga ucapkan banyak terimakasih untuk orang tua asuh saya di Belanda, Oma Nanda dan Opa Richard yang selalu membukakan pintu rumahnya untuk saya selama saya PhD. Kebaikan dan masakan kalian tidak dapat saya bayar dengan apapun dan akan selalu saya ingat. Terimakasih juga untuk kakak saya di Belanda Kang Ade Sudjana dan Anita serta anak-anaknya (Gilang dan Nuri) atas motivasi yang membuat saya betah hidup di Belanda.

Tidak lupa terima Kasih banyak untuk Spartan: Mas Lukman, Mas Fauzi, Mas Aris, Mas Iwan untuk obrol-obrol, rokok-rokok dan makan-makan yang menghibur. Ucapan terimakasih juga saya sampaikan kepada PhD candidate yang sudah berkepala empat Mas Sidiq atas obrol-obrol malam, minum-minuman gula dan list film horror yang tidak ada habisnya. Juga untuk para PhD yang bisa dikategorikan senior: Mas Erlis, Mbak Erda, Uwak Andi, Mas Sidna, Mas Muchlis untuk obrol-obrol, musik-musik dan makan-makannya. Untuk golongan muda, om Zaki atas tur keliling kampung Tanah Abangnya. Untuk anggota SGB yang telah memberikan pencerahan spiritual kepada saya (Kang Pardi, Ancek, Cewin, Kang Yana, Kang Afiel, Mas Raymond). I also have to thank my

colleagues from Ocean Engineering ITB: Rajin Sihombing, Farid Putra Bakti, Deboy Faradino, Mas Nunu, Andra Patria, Ibu Nita Yuanita for your jokes and insight to keep me sane during my PhD.

Saya sangat berterima kasih kepada orang tua dan kakak yang tidak kenal Lelah memotivasi dan mensuport saya untuk bermimpi setinggi-tingginya. Untuk mama, Siti Kurnia Nurlela, guru pertama saya yang selalu mengajarkan saya dan kakak untuk tidak hanya bekerja keras tapi juga bekerja cerdas dan bersiasat. Apa yang mama ajarkan benar-benar bermanfaat untuk Arya dalam menghadapai kesulitan dan keterbatasan terutama selama PhD. Terima kasih untuk kesabaran mama dalam mendidik Arya sejak kecil. Untuk papa, Syukur Iwantoro, yang telah mengajarkan saya untuk selalu memilih bidang pendidikan dan pekerjaan yang sesuai dengan apa yang saya sukai. Terima kasih untuk obrolan-obrolan tentang mimpi-mimpi yang tinggi, buku-buku dari seluruh dunia serta cerita-cerita tentang gambaran negara-negara lain yang telah membuat penasaran dan memotivasi Arya untuk mencoba hidup di negara orang. Kerja keras dan kejujuran papa agar Arya dan kaka bisa mendapatkan Pendidikan terbaik memotivasi Arya untuk terus menghantam dan tidak menyerah dengan kelemahan Arya. Terimakasih juga untuk kaka, Dr. Astari Apriantini, panutan dan tolak ukur Arya. Terima kasih untuk saran dan support moralnya menghadapi masalah di negara orang. Your struggle during your PhD motivated me to finish my PhD.

Special thanks for my small family. My wife, Dwi Sasetyaningtyas, inspired me to be brave to leave my comfort zone. You helped me to improve my weakness in communication. You are the best friend, *juragan*, travel partner, scuba diving buddy, colleague, and business partner I have ever had. I thank you for the talks, tea, vinyl 420time that we spent in the evening after my stressful day. I am looking forward to exploring new things in the different parts of the world with you in the future. For my daughter, Malahayati Arungbhumi Iwantoro, you are my source of happiness. You came to the world in the early stage of my PhD and accelerate my lesson on how to be a fully grown-up man. Even though sometimes nobody understands what we talk about (even your mom!), our weirdly funny chat always makes me laugh even in the most stressful day. I learnt a lot from your honesty and critical thinking as a kid. I hope you can be anything you want to be.

All in all, your kind support and encouragement made me reach this point at the end of a long journey. This thesis is dedicated to you all! *Alhamdulillahi rabbil alamin*. \m/

Djakarta, October 2022

Arya Pamungkas Iwantoro

About author

Arya Pamungkas Iwantoro was born in Djakarta, Indonesia. In 2009, He took his bachelor at Department of Ocean Engineering, Institut Teknologi Bandung in Indonesia. He found his interest in morphodynamic-related studies using computational modelling approach after he saw beautiful figures of his numerical model results when he worked on his bachelor thesis. He considered those results as a beautiful piece of art. Thus, after he obtained his bachelor's degree in 2013 and he intended to learn more about his interest. A year later he applied LPDP grant and finally won the grant that allowed him to continue his study in Physical Geography Department at Utrecht University, The Netherlands where he focused his study in morphodynamics of coastal, tidal, and fluvial systems. He conducted MSc research project about morphodynamics of tide-influenced river bifurcations using numerical modelling approach. After doing this project, he gained his interest in morphodynamics in tidal systems and wanted to do a PhD project to learn more about it. Finally, in 2017, he obtained the opportunity to continue his grant and extended his master thesis project for his PhD research where he can build his own numerical model for the first time! After finishing his PhD, he decided to keep trying to find out what kind arts that water can create using sediments. In his free time, he loves to go scuba diving, paddling, surfing, and hiking. He is also a full-time father and private teacher for his child(ren).